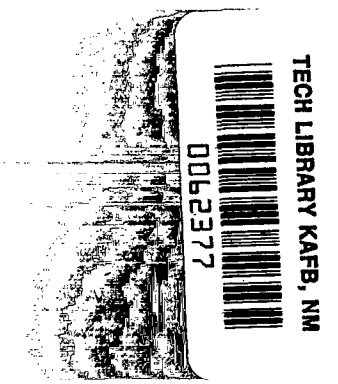

NASA Contractor Report 3754

Prediction of Vortex Shedding From Circular and Noncircular Bodies in Supersonic Flow

M. R. Mendenhall and S. C. Perkins, Jr.

CONTRACT NAS1-17027
JANUARY 1984

NASA

NASA Contractor Report 3754

Prediction of Vortex Shedding From Circular and Noncircular Bodies in Supersonic Flow

M. R. Mendenhall and S. C. Perkins, Jr.
Nielsen Engineering & Research, Inc.
Mountain View, California

Prepared for
Langley Research Center
under Contract NAS1-17027

National Aeronautics
and Space Administration

Scientific and Technical Information Branch

1983

TABLE OF CONTENTS

LIST OF SYMBOLS

a	semi-major or horizontal axis of elliptic cross section
A_ℓ	coefficients of conformal transformation, Eq. (9)
b	semi-minor or vertical axis of elliptic cross section
c_n	normal-force coefficient per unit length, Eq. (39)
c_y	side-force coefficient per unit length, Eq. (43)
C_ℓ	rolling-moment coefficient, Eq. (47)
C_m	pitching-moment coefficient, Eq. (41)
C_n	yawing-moment coefficient, Eq. (45)
C_p	pressure coefficient, Eq. (29)
C_{p_I}	incompressible pressure coefficient, Eq. (31)
C_y	side-force coefficient, Eq. (44)
C_N	normal-force coefficient, Eq. (40)
D	diameter of circular body, or equivalent diameter of noncircular body
G	complex velocity component, Eq. (18)
ℓ_{ref}	reference length
L	total number of Fourier coefficients used to describe transformation, Eq. (9), also model length
M_x	rolling moment about the x-axis
M_y	pitching moment about the y-axis
M_z	yawing moment about the z-axis

M_∞	free-stream Mach number
p	local static pressure
p_∞	free-stream static pressure
q_∞	free-stream dynamic pressure, $\frac{1}{2}\rho V_\infty^2$
r	radial distance from a vortex to a field point
r'	radial distance to a point on a noncircular body, Fig. 4
r_c	vortex core radius, Eqs. (50) and (51)
r_o	radius of circle
Re_ξ	Reynolds number based on boundary layer run length and minimum pressure conditions, $U_m\xi/\nu$, Eq. (37)
S	reference area
u_e	surface velocity in crossflow plane
u_r	axial perturbation velocity
U	local velocity
v_θ	vortex induced velocity
v,w	velocity components in real plane
V_∞	free-stream velocity
W	complex potential, Eq. (16)
x,y,z	body coordinate system with origin at the nose: x positive aft along the model axis, y positive to starboard, and z positive up
x_m	axial location of center of moments
α	angle of attack
α_c	angle between free-stream velocity vector and body axis
β	angle of sideslip; also polar angle in σ-plane, Fig. 2

β'	local slope of body surface, Fig. 4
γ	ratio of specific heats
γ_r	exterior angles of body segment for numerical mapping, Eq. (7)
Γ	vortex strength
Δx	axial length increment
ζ	complex coordinate in an intermediate plane, Fig. 2(b)
η	vertical coordinate in an intermediate plane, Fig. 2(b)
θ	polar angle in ν-plane, Fig. 2(a)
ν	complex coordinate in circle plane, Fig. 2(a); also kinematic viscosity
ξ	run length, Eqs. (36) and (37); or lateral coordinate in an intermediate plane, Fig. 2(b)
ρ	free-stream density
σ	complex coordinate in real plane, Fig. 2(a)
τ, λ	lateral and vertical coordinates in circle plane, Fig. 2(a)
ϕ	roll angle
Φ	velocity potential in real plane
ψ	stream function in real plane

Subscripts

$(\bar{})$	conjugate of complex quantity
$(\,)_m$	vortex m
$(\,)_{cp}$	center of pressure

SUMMARY

An engineering prediction method and associated computer code NOZVTX to predict nose vortex shedding from circular and noncircular bodies in supersonic flow at angles of attack and roll are presented. The body is represented by either a supersonic panel method for noncircular cross sections or line sources and doublets for circular cross sections, and the lee side vortex wake is modeled by discrete vortices in crossflow planes. The three-dimensional steady flow problem is reduced to a two-dimensional, unsteady, separated flow problem for solution. Comparison of measured and predicted surface pressure distributions, flow field surveys, and aerodynamic characteristics are presented for bodies with circular and noncircular cross sectional shapes.

INTRODUCTION

Current missile applications requiring high aerodynamic performance can involve noncircular body shapes in supersonic flow at high angles of attack and nonzero roll angles. The angle of attack range may be sufficiently high to cause formation of body separation vortices, and the body vortex shedding characteristics are directly influenced by the body cross-sectional shape and the flow conditions. It is desirable to model the body vortex wake by means of a rational method capable of considering a variety of body shapes over a wide range of flow conditions. It is important that the separation vortex wake induced effects on the nonlinear aerodynamic characteristics of the body be handled properly.

The phenomena of interest are the sheets of vorticity formed on the lee side of the body at high angles of attack. The vorticity is formed by boundary-layer fluid leaving the

body surface from separation points on both sides of the body (Fig. 1) and rolling up into a symmetrical vortex pair. A method to predict these flow phenomena in the vicinity of circular and noncircular bodies in subsonic flow is described in References 1 and 2. The extension of the method to supersonic flow is described in Reference 3.

The purpose of this report is to describe an engineering prediction method and associated computer code developed to calculate the nonlinear aerodynamic characteristics and flow fields of noncircular noses at high angles of attack in supersonic flow. The objectives of the method are to use a three-dimensional, attached flow, supersonic panel method, or a supersonic line source and doublet method to represent the body and a two-dimensional, incompressible, separated flow model to calculate the lee side vortex shedding from the body alone at angle of attack and angle of roll. The predicted pressure distribution on the body under the influence of the free stream and the separation vortex wake will be used to calculate the aerodynamic loads on the body. Conformal mapping techniques are used to transform noncircular cross sections to a circle for calculation purposes.

The following sections of this report include a discussion of the approach to the problem and a description of the analysis and flow models required to carry out the calculation. The prediction method is evaluated through comparison of measured and predicted results on a variety of body shapes, including circular and elliptical cross sections. A user's manual for the computer code is also included. The manual consists of descriptions of input and output, and sample cases.

GENERAL APPROACH

Bodies at high angles of attack exhibit distributed vorticity fields on their lee side due to boundary-layer fluid leaving the body surface at separation lines. One approach for modeling these distributed vorticity fields has involved the use of clouds of discrete potential vortices. Underlying the basic approach is the analogy between two-dimensional unsteady flow past a body and the steady three-dimensional flow past an inclined body. In fact, the three-dimensional steady flow problem is reduced to the two-dimensional, unsteady, separated flow problem for solution. Linear theory for the attached flow model and slender body theory to represent the interactions of the vortices are combined to produce a nonlinear prediction method. The details of the application of this approach to the prediction of subsonic flow about circular and noncircular bodies are presented in References 1 and 2, and the extension to supersonic flow is described in Reference 3. Other investigators have also used this approach to successfully model the subsonic flow phenomena in the vicinity of circular cross section bodies (Refs. 4 and 5). The purpose of this report is to document the extension of the previous subsonic analysis of References 1 and 2 to supersonic flow.

The calculation procedure is carried out in the following manner. The body is represented by supersonic source panels (noncircular cross section) or supersonic line sources and doublets (circular cross section), and the strength of the individual singularities is determined to satisfy a flow tangency condition on the body in a nonseparated uniform flow at angle of attack and roll. Starting at a crossflow plane near the body nose, the pressure distribution on the body is computed using the full Bernoulli equation. The boundary layer in the crossflow plane is examined for separation

using modified versions of Stratford's separation criteria. The Stratford separation criteria are based on two-dimensional incompressible flow. At the predicted separation points, incompressible vortices with their strength determined by the vorticity transport in the boundary layer are shed into the flow field. The trajectories of these free vortices between this crossflow plane and the next plane downstream are calculated by integration of the equations of motion of each vortex, including the influence of the free stream, the body, and other vortices. The pressure and trajectory calculations are carried out by mapping the noncircular cross section shape to a circle using either analytical or numerical conformal transformations. The vortex-induced velocity contribution to the body tangency boundary condition includes image vortices in the circle plane. At the next downstream crossflow plane, new vortices are shed, adding to the vortex cloud representing the wake on the lee side of the body. This procedure is carried out in a stepwise fashion over the entire length of the body. The details of the individual methods combined into the prediction method are described in the following section.

METHODS OF ANALYSIS

The development of an engineering method to predict the pressure distributions on arbitrary missile bodies in supersonic flow at high angles of incidence requires the joining of several individual prediction methods. In this section, the individual methods are described briefly, and the section concludes with a description of the complete calculation procedure.

Conformal Mapping

The crossflow plane approach applied to arbitrary missile bodies results in a noncircular cross section shape in the presnece of a uniform crossflow velocity and free vortices in each plane normal to the body axis. The procedure used to handle the noncircular shapes is to determine a conformal transformation for mapping every point on or outside the arbitrary body to a corresponding point on or outside a circular body. The two-dimensional potential flow solution around a circular shape in the presence of a uniform flow and external vortices is well known and has been documented numerous places in the literature (Refs. 4 and 6). Thus, the procedure is to obtain the potential solution for the circular body and transform it to the noncircular body. Conformal transformations used are of two distinct types, analytical and numerical.

Analytic transformation.- For very simple shapes like an ellipse [Fig. 2(a)], the transformation to the circle can be carried out analytically as described in Reference 7. For example,

$$\sigma = \nu + \frac{a^2 - b^2}{4\nu} \tag{1}$$

where

$$\sigma = y + iz \tag{2}$$

in the real plane, and

$$\nu = \tau + i\lambda \tag{3}$$

in the circle plane. The derivative of the transformation is

$$\frac{d\sigma}{d\nu} = 1 - \left[\frac{a^2 - b^2}{4\nu^2}\right] \tag{4}$$

which is required for the velocity transformation discussed later.

Numerical transformation.- For complex noncircular shapes, the transformation cannot be carried out analytically and a numerical transformation is required. The numerical transformation chosen is described in detail in Reference 8, and a brief summary of the conformal mapping procedure follows.

The sequence of events in the numerical mapping is shown in Figure 2(b). The arbitrary cross section shape of the body in the σ-plane is required to have a vertical plane of symmetry. The transformation of interest will map the region on and outside the body in the σ-plane to the region on and outside a circle in the ν-plane. The first step is a rotation to the ζ-plane so that the cross section is symmetric about the real axis. Thus,

$$\sigma = y + iz \tag{5}$$

and

$$\begin{aligned} \zeta &= i\sigma \\ &= \xi + i\eta \end{aligned} \tag{6}$$

A mapping that transforms the outside of the body in the ζ-plane to the outside of the unit circle is

$$\zeta = \int \frac{1}{\nu^2} \prod_{r=1}^{m} (\nu - \nu_r)^{\frac{\gamma_r}{\pi}} \, d\nu \tag{7}$$

where γ_r are the exterior angles of the m segments of the body cross section. In Equation (7), π denotes a product series. For a closed body

$$\sum_{r=1}^{m} \gamma_r = 2\pi \tag{8}$$

The final transformation has the form

$$\sigma = -i\left[\nu + \sum_{\ell=1}^{L} \frac{r_o^{\ell+1} A_\ell}{\nu^\ell}\right] \tag{9}$$

where the A_ℓ coefficients are obtained through an iterative scheme described in Reference 8 and r_o is the radius of the equivalent circle in the ν-plane. The derivative of the transformation is

$$\frac{d\sigma}{d\nu} = -i\left[1 - \sum_{\ell=1}^{L} \frac{r_o^{\ell+1} \ell A_\ell}{\nu^{\ell+1}}\right] \tag{10}$$

which is required for the velocity calculations described in a later section.

The above numerical mapping procedure has been applied to a wide range of general cross section shapes with good success.

Body Model

The prediction method described in this report is applicable to both circular and noncircular bodies. Separate body models are developed for circular and noncircular shapes because arbitrary noncircular shapes require panels and numerical conformal mappings and circular bodies can be represented by more computationally efficient means. Both flow models are described in this section.

Circular bodies.- A potential flow model of an axisymmetric body in supersonic flow is described in References 9 and 10. Such a body is represented by a distribution of line

sources and sinks and line doublets on the body axis to account for volume and angle of incidence effects, respectively. The strengths of the line singularities are determined from the flow tangency condition applied at points on the body surface. A downstream marching procedure from the nose tip to the body base is used for this calculation.

The axis singularity distribution for bodies of revolution provides an accurate and efficient means to calculate the induced velocity field associated with the body at angle of incidence. The calculation requires much less computation time than a panel method, and the resulting velocity distributions are quite smooth. One restriction on the body shape is the requirement that the nose contour lie inside the Mach cone. This constitutes the major limitation to the method.

Noncircular bodies.- The configurations considered in this study are bodies alone, without fins or control surfaces. The body geometry is described by the coordinates of the cross-sectional shape at a number of axial stations, and linear interpolation between specific points is used. The body is represented by a three-dimensional lattice of supersonic source panels distributed on the surface of the body. The panels account simultaneously for volume and angle of incidence effects. The attached flow solution for a panel inclined to the flow direction is based on supersonic linear theory as described in Reference 11 and the method used is a modified version of the program code presented in Reference 12. The pitch and yaw angles are related to the included angle of attack and angle of roll by the expressions

$$\sin\alpha = \sin\alpha_c \cos\phi \tag{11}$$

$$\sin\beta = \sin\alpha_c \sin\phi \tag{12}$$

The flow tangency condition is applied at the control point located at the panel centroid of each body panel. The result is a set of linear simultaneous equations in terms of the unknown panel source strengths. Solution by an iterative approach produces the singularity strength on each panel and thus provides a means to calculate the velocity field induced by the body. The nature of the solution is such that the velocity on the body surface is correct only at the control points; therefore, linear interpolation is used to determine body surface velocity components for use in pressure calculations at points lying between control points. The body panel induced velocities are calculated one time for the entire body to provide a table of velocity components for interpolation purposes. Using a slender-body theory approximation, these velocity components are combined with other velocity components for the pressure calculation described in a later section.

There is a basic limitation in the use of the above panel method. The angle of inclination between a body source panel and the body centerline must be less than the semi-apex angle of the Mach cone associated with the free-stream Mach number. Thus, there is a limit to the body nose configurations which can be modeled by the body source panel method.

Vortex Shedding Model

The body vortex shedding model described in this section is nearly the same as the subsonic model presented in Reference 2; therefore, the following description will be brief, and only the differences between the two models will be discussed in detail.

Equations of motion.- The equations of motion of a shed nose vortex in the presence of other free vortices in the vicinity of a body in a uniform stream follow. In the circle (ν) plane, the position of a vortex, Γ_m, is

$$\nu_{m_\Gamma} = \tau_m + i\lambda_m \tag{13}$$

and the image of Γ_m is located at

$$\nu_{m_{-\Gamma}} = \frac{r_o^2}{\bar{\nu}_m} \tag{14}$$

In the real plane, the position of the vortex Γ_m is

$$\sigma_{m_\Gamma} = y_m + iz_m \tag{15}$$

The complex potential in the real plane is

$$W(\sigma) = \Phi + i\Psi \tag{16}$$

and the corresponding velocity at Γ_m is

$$v_m - iw_m = \frac{dW_m(\sigma)}{d\sigma} = \frac{d}{d\nu}\left[W_m(\sigma)\right] \left.\frac{d\nu}{d\sigma}\right|_{\substack{\sigma=\sigma_m \\ \nu=\nu_m}} \tag{17}$$

The complex potential of Γ_m is not included in Equation (17) to avoid the singularity at that point. The derivative of the transformation is obtained from Equation (4) or Equation (10).

The total velocity at Γ_m in the crossflow plane is written as

$$\frac{v_m - iw_m}{V_\infty} = G_\alpha + G_\beta + G_n + G_m + G_T + G_r \tag{18}$$

where each term in Equation (18) represents a specific velocity component in the σ-plane. The first term represents the uniform flow due to angle of attack.

$$G_\alpha = -i \sin\alpha \left[1 + \left(\frac{r_o}{\nu_m} \right)^2 \right] \left. \frac{d\nu}{d\sigma} \right|_{\sigma=\sigma_m} \tag{19}$$

The second term represents the uniform flow due to angle of yaw.

$$G_\beta = -\sin\beta \left[1 - \left(\frac{r_o}{\nu_m} \right)^2 \right] \left. \frac{d\nu}{d\sigma} \right|_{\sigma=\sigma_m} \tag{20}$$

The next term represents the influence of all vortices and their images, with the exception of Γ_m.

$$G_n = i \sum_{n=1}^{N} \frac{\Gamma_n}{2\pi r_o V_\infty} \left[\frac{1}{(\nu_m/r_o) - (r_o/\bar{\nu}_m)} - \frac{1}{(\nu_m/r_o) - (\nu_n/r_o)} \right] \Bigg|_{n \neq m} \left. \frac{d\nu}{d\sigma} \right|_{\sigma=\sigma_m} \tag{21}$$

The next term is due to the image of Γ_m.

$$G_m = i \frac{\Gamma_m}{2\pi r_o V_\infty} \left[\frac{1}{(\nu_m/r_o) - (r_o/\bar{\nu}_m)} \right] \left. \frac{d\nu}{d\sigma} \right|_{\sigma=\sigma_m} \tag{22}$$

The fifth term in Equation (18) represents the potential of Γ_m in the σ-plane and is written as

$$G_T = -i \frac{\Gamma_m}{2\pi V_\infty} \left(\frac{1}{2} \right) \frac{d}{d\nu} \left(\frac{d\nu}{d\sigma} \right) \Bigg|_{\sigma=\sigma_m} \tag{23}$$

The last term in Equation (18) represents the velocity components induced by the portion of the body panel singularities representing the body volume effects.

$$G_r = \frac{v_r - iw_r}{V_\infty} \tag{24}$$

Since the body panel singularities are three dimensional, they contribute an induced axial velocity, u_r.

The differential equations of motion for Γ_m are

$$\frac{d\bar{\sigma}_m}{dx} = \frac{v_m - iw_m}{V_\infty \cos\alpha_c + u_r} \tag{25}$$

where

$$\bar{\sigma}_m = y_m - iz_m \tag{26}$$

Therefore, the two equations which must be integrated along the body length to determine the trajectory of Γ_m are

$$\frac{dy_m}{dx} = \frac{v_m}{V_\infty \cos\alpha_c + u_r} \tag{27}$$

and

$$\frac{dz_m}{dx} = \frac{w_m}{V_\infty \cos\alpha_c + u_r} \tag{28}$$

There are a pair of equations like (27) and (28) for each vortex in the field. As new vortices are shed, the total number of equations to solve increases by two for each added vortex. These differential equations are solved numerically using a method which automatically adusts the step size to provide the specified accuracy.

Surface pressure distribution.- The surface pressure distribution on the body is required to calculate the forces on the body and the separation points. The surface pressure coefficient is determined from the Bernoulli equation in the form

$$C_p = \frac{2}{\gamma M_\infty^2}\left\{\left[1 + \frac{\gamma-1}{2} M_\infty^2 (C_{p_I})\right]^{\frac{\gamma}{\gamma-1}} - 1\right\} \tag{29}$$

where

$$C_p = \frac{p - p_\infty}{\frac{1}{2}\rho V_\infty^2} \tag{30}$$

and

$$C_{p_I} = 1 - \left(\frac{U}{V_\infty}\right)^2 - \frac{2\cos\alpha_c}{V_\infty}\frac{d\phi}{dx} \tag{31}$$

In Equation (31), U is the total velocity (including V_∞) at a point on the body. It consists of many of the components described in the previous section. The body induced velocity components from Equation (24) include the total effect of the panel solution at angle of attack and roll. As a consequence of using the full panel solution in this component, the two-dimensional doublet part of Equations (19) and (20) are not required. The vortex wake contribution is included through Equations (21) and (22).

The last term in Equation (31) represents the axial velocity missing from the two-dimensional singularities in the flow model. In this case, the shed vortices are the only singularities contributing to this term. The complex potential of a number of vortices, Γ_n, and their images in the circle plane is

$$W(\nu) = \phi + i\Psi$$

$$= \sum_{n+1}^{N} \frac{\Gamma_n}{2\pi}\left[-i\,\ell n(\nu - \nu_n) + i\,\ell n\left(\nu - \frac{r_o^2}{\bar{\nu}_n}\right)\right] \tag{32}$$

The "unsteady" term in Equation (31), evaluated on the body surface, is

$$\frac{d\phi}{dx} = \text{Real} \left. \frac{dW(\nu)}{dx} \right|_{r=r_o} \tag{33}$$

Equation (33) becomes

$$\frac{d\phi}{dx} = \sum_{n=1}^{N} \frac{\Gamma_n}{2\pi} \left\{ - \left[\frac{(\tau - \tau_n) \frac{d\lambda_n}{dx} - (\lambda - \lambda_n) \frac{d\tau_n}{dx}}{(\tau - \tau_n)^2 + (\lambda - \lambda_n)^2} \right] \right.$$

$$- \left[\frac{(\tau r_n^2 - \tau_n r_o^2) \left(2\lambda\tau_n \frac{d\tau_n}{dx} + 2\lambda\lambda_n \frac{d\lambda_n}{dx} - r_o^2 \frac{d\lambda_n}{dx} - 2r_o\lambda_n \frac{dr_o}{dx} \right)}{(\tau r_n^2 - \tau_n r_o^2)^2 + (\lambda r_n^2 - \lambda_n r_o^2)^2} \right]$$

$$\left. + \left[\frac{(\lambda r_n^2 - \lambda_n r_o^2) \left(2\tau\lambda_n \frac{d\lambda_n}{dx} + 2\tau\tau_n \frac{d\tau_n}{dx} - r_o^2 \frac{d\tau_n}{dx} - 2r_o\tau_n \frac{dr_o}{dx} \right)}{(\tau r_n^2 - \tau_n r_o^2)^2 + (\lambda r_n^2 - \lambda_n r_o^2)^2} \right] \right\} \tag{34}$$

where

$$r_n^2 = \tau_n^2 + \lambda_n^2 \tag{35}$$

Separated wake.- The separated wake on the lee side of the body is made up of a large number of discrete vortices, each vortex originating from one of two possible locations at each time step in the calculation. The major portion of the lee side vortex wake has its origin at the primary separation points on each side of the body. The remainder of the wake originates from the secondary separation points located in the reverse flow region on the lee side of the

body. Both of these points are illustrated in the sketch of a typical crossflow plane of an elliptic cross section body shown in Figure 3. The mechanics of the calculation of the individual vortices follows.

As described in References 1 and 2, the pressure distribution for the primary flow in the crossflow plane is referenced to the conditions at the minimum pressure point, and a virtual origin for the beginning of the boundary layer is assumed. The adverse pressure distribution downstream of the minimum pressure point is considered with either Stratford's laminar (Ref. 13) or turbulent (Ref. 14) separation criterion to determine whether or not separation has occurred. These criteria, based on two-dimensional, incompressible, flat plate data, are adjusted for three-dimensional crossflow effects in Reference 2. The laminar separation criterion states that the laminar boundary layer separates when

$$C_p^{1/2}\left[\xi \frac{dC_p}{d\xi}\right] \simeq 0.087 \sin\alpha_c \tag{36}$$

In a turbulent boundary layer, separation occurs when

$$C_p\left[\xi \frac{dC_p}{d\xi}\right]^{1/2} (Re_\xi \times 10^{-6})^{-0.1} \simeq 0.35 \sin\alpha_c \tag{37}$$

If the criteria indicate a separation point, the vorticity flux across the boundary layer at separation is shed into a single point vortex whose strength is

$$\frac{\Gamma}{V_\infty} = \frac{u_e^2}{2V_\infty^2} \frac{\Delta x}{\cos\alpha_c} \tag{38}$$

assuming no slip at the wall.

The initial position of the shed vortex is determined such that the surface velocity at the separation point is exactly canceled by the shed vortex and its image. When this criterion results in a vortex initial position that is too near to the body surface, certain numerical problems can cause difficulty in calculating the trajectory of this vortex. If the intial position of the vortex is nearer than five percent of the body radius from the surface, the vortex is placed five percent of the equivalent body radius from the surface. This position represents the approximate thickness of the boundary layer.

The calculation of secondary separation is carried out in the same manner as described above for primary separation. It is necessary that a reverse flow region exist on the lee side of the body and that a second minimum pressure point be found in this region. Surface flow visualization of secondary separation regions on bodies at high angles of attack in subsonic flow are shown in Reference 15. For purposes of this analysis, the reverse flow is assumed to be laminar from the lee side stagnation point to the secondary separation point, and Stratford's laminar criterion is used to locate the secondary separation point. Laminar separation in the reverse flow region is expected because of the low velocities on this portion of the body. The vortex released into the flow at the secondary separation point has the opposite sign of the primary vortex and is generally much weaker in strength.

Forces and moments.- The forces and moments on the body are computed by integration of the pressure distribution around the body. At a specified station on the body, the normal-force coefficient on a Δx length of the body is

$$c_n = \frac{\left(\frac{\Delta n}{\Delta x}\right)}{q_\infty D} = \frac{1}{D}\int_0^{2\pi} C_p r' \cos\beta' \, d\beta \tag{39}$$

where r' is the distance from the axis of the body to the body surface and β' is the local slope of the body in the crossflow plane. This is illustrated in the sketch in Figure 4. For circular bodies, $r' = r_o$ and $\beta' = \beta$. The total normal force coefficient on the body is

$$C_N = \frac{N}{q_\infty S} = \frac{D}{S}\int_0^L c_n dx \tag{40}$$

and the pitching-moment coefficient is

$$C_m = \frac{M_y}{q_\infty S \ell_{ref}} = \frac{D}{S}\int_0^L c_n \left[\frac{x_m - x}{\ell_{ref}}\right] dx \tag{41}$$

The center of pressure of the normal force is

$$\frac{x_{cp_n}}{\ell_{ref}} = \frac{x_m}{\ell_{ref}} - \frac{C_m}{C_N} \tag{42}$$

Similarly, the side-force coefficient on a Δx length of the body is

$$c_y = \frac{\left(\frac{\Delta s}{\Delta x}\right)}{q_\infty D} = -\frac{1}{D}\int_0^{2\pi} C_p r' \sin\beta' \, d\beta \tag{43}$$

The total side-force coefficient on the body is

$$C_y = \frac{F_y}{q_\infty S} = \frac{D}{S}\int_0^L c_y dx \tag{44}$$

and the yawing-moment coefficient is

$$C_n = \frac{M_z}{q_\infty S \ell_{ref}} = -\frac{D}{S} \int_0^L c_y \left[\frac{x_m - x}{\ell_{ref}}\right] dx \qquad (45)$$

The center of pressure of the side force is

$$\frac{x_{cp_y}}{\ell_{ref}} = \frac{C_n}{C_y} + \frac{x_m}{\ell_{ref}} \qquad (46)$$

A noncircular body at an arbitrary roll angle may experience a rolling moment caused by the nonsymmetry of the loading around the body. The total rolling moment on the body is calculated by summing the moments of the individual components of normal force and side force around each cross section and integrating over the body length. Using Equations (39) and (43), the rolling moment coefficient is calculated as

$$C_\ell = \frac{M_x}{q_\infty S \ell_{ref}}$$

$$= \frac{1}{S\ell_{ref}} \int_0^L \left[\int_0^{2\pi} (yC_p r' \cos\beta' - zC_p r' \sin\beta') d\beta \right] dx \qquad (47)$$

Vortex smoothing.- A problem common to discrete vortex models is the singularity in the vortex induced velocity distribution at the loction of a point vortex and the very large velocities induced near the vortex. This can lead to errors in the surface pressure distribution when there are vortices near the body surface and to errors in the vortex tracking when vortices pass in close proximity.

The vortex diffusion model described in Reference 2 has the effect of removing the singularity at the vortex, but very large induced velocities are still in evidence near the vortex, thus the noted roughness in the surface pressure distribution continues to be a problem. Several solutions to this problem have been investigated, and a discussion of these vortex flow models follows.

In Reference 16, discrete vortices are replaced by a distribution of vortices on straight line segments connecting the discrete vortex positions. In this way, the algebraic singularity is reduced to a logarithmic singularity. The strength of the uniform distribution of vorticity on each line segment is determined from the strengths of the discrete vortices at the ends of the segment. Defining G_d as the complex velocity induced at ν_m by the line segment, analogous to Equation (21), the velocity becomes

$$G_{d_j} = \frac{i\Gamma_{n'}}{2\pi V_\infty} \left(\frac{\bar{\nu}_{n+1} - \bar{\nu}_n}{|\nu_{n+1} - \nu_n|} \right) \log \left(\frac{\nu_{n+1} - \nu_m}{\nu_n - \nu_m} \right) \tag{48}$$

where ν_m is not on the line segment. The strength of the vortex segment is

$$\Gamma_{n'} = \frac{1}{2} (\Gamma_n + \Gamma_{n+1}) \tag{49}$$

except when Γ_n or Γ_{n+1} represents the last vortex in the chain. When this occurs, the remainder of the strength of the last vortex is included in the last line segment to avoid losing a portion of the shed vorticity.

This smoothing procedure was investigated for a number of calculations, and it accomplished the smoothing of the induced velocity field to a great extent. The surface pressure distributions had some residual roughness caused

by other effects, but the pressure spikes caused by locally high vortex-induced velocities were eliminated. The major disadvantage of the above smoothing technique is cost. The nature of the total calculation procedure is such that many velocity calculations are required; therefore, the additional effort to set up the smoothing procedure and calculate velocities at numerous body points causes a dramatic increase in computation time. For this reason, alternate smoothing techniques are considered.

The smoothing technique incorporated into the present version of NOZVTX is one in which a single point vortex is represented by a simple distribution of several point vortices. The smoothing calculation is carried out only for vortices which lie within 10% of the local body radius of the surface of the body, and it is used only for calculating pressures on the body surface. The vorticity is distributed according to the procedure shown in Figures 5(a) and (b). In Figure 5(a), vortex 2 is the only vortex which lies within 10% of the local body radius of the surface. The "distributed vorticity" model consists of nine smaller vortices; one located at the actual position of vortex 2, four located along the line joining vortices 1 and 2, and four along the line joining vortices 2 and 3. Each vortex has a strength equal to one-ninth of the actual vortex strength. Figure 5(b) shows distributed vorticity models for vortices which are end points of the vortex cloud; that is, for the first vortex and the most recently shed vortex. In the case of the first shed vortex, Γ_1, the distributed vorticity model consists of five point vortices, each vortex having a strength equal to one-fifth that of the actual vortex. The model for the most recent shed vortex,

Γ_3, is shown in Figure 5(b). The vorticity is distributed along two separate lines. One line is defined by the actual vortex position and its shed position at the previous axial station, indicated by 3' in Figure 5(b). The second line is defined as before, the end points being the locations of Γ_2 and Γ_3.

The smoothing technique described above was investigated for a number of geometry and flow condition combinations, and it was found to smooth pressure spikes caused by locally high vortex-induced velocities or values of $d\phi/dx$. As expected, use of the smoothing technique increases execution time, but the actual execution time is determined by the number of vortices which lie close to the body surface. This technique redistributes the vortices and tends to spread their effect over a larger area, but the model is still made up of discrete vortices, each of which has a singularity at its origin. A viscous core model for the individual vortices is required to remove the singularity in the induced velocity calculation. This model is described in the following section.

Vortex core.- The diffusion core model (Ref. 2) for the point-vortex induced velocities removes the singularity at the vortex origin and effectively reduces the velocities near the vortex. The tangential velocity induced by a single point vortex is written as

$$\frac{v_\theta}{\Gamma} = \frac{1}{2\pi r}\left[1 - \exp\left(\frac{r^2 V_\infty}{4xv}\right)\right] \tag{50}$$

where r is the distance from the vortex to the field point and x is a measure of the age of the vortex. The induced velocity from this core model is illustrated in the following sketch.

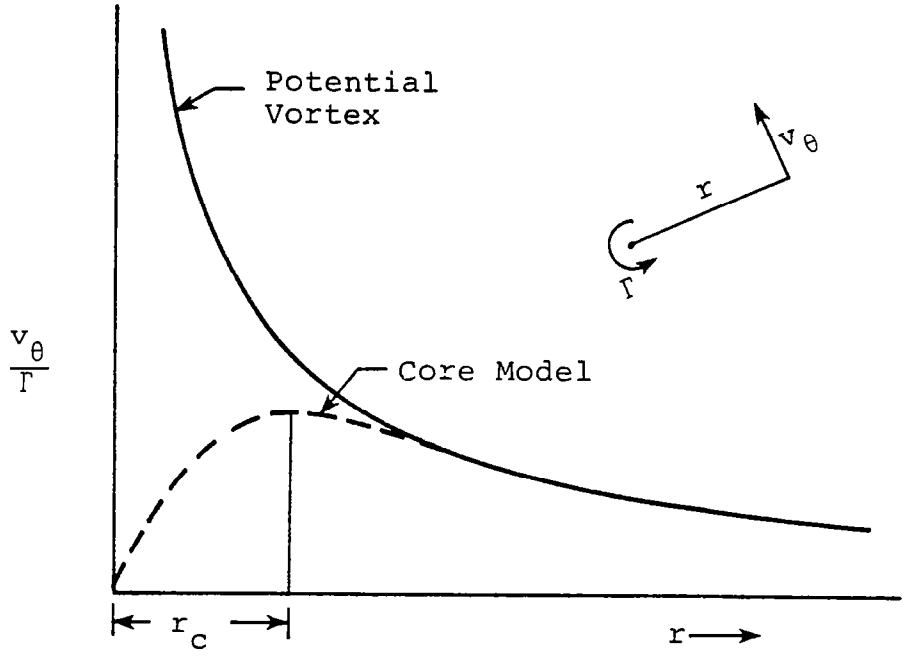

Vortex Induced Velocity

The vortex core model represented by Equation (50) has received considerable attention in the context of body vortex induced effects, and it has a number of shortcomings. Since the exponential term is a function of r, the flow medium (ν), and the age of the vortex (x), the core is constantly changing size as the vortex moves through the field. Under certain conditions, the core radius, denoted as r_c in the sketch, can become very small and the induced

velocity becomes unrealistically large. In an attempt to further modify the core model to keep the induced velocities within physically realistic limits, the following modification was made. The location of the maximum induced velocity, r_c in the sketch, is fixed at a specific radius to be selected by the user. Given a core radius, the vortex induced velocity is

$$\frac{v_\theta}{\Gamma} = \frac{1}{2\pi r}\left[1 - \exp\left[-1.256\left(\frac{r^2}{r_c^2}\right)\right]\right] \tag{51}$$

The core model described by Equation (51) is included in the version of the code described in this report, and in a later section, guidelines for the selection of an appropriate core radius are presented. Results indicate that this simple core model provides adaquate smoothing for the necessary velocity calculations.

Other investigators of discrete vortex models must use a core model of some type. Although there are many different core models, all serve the same purpose as those described above, and nearly all are directed at eliminating the singularity and reducing the maximum induced velocity. The code described in a later section is easily modified to incorporate another core model if the user desires to do so.

PROGRAM

General Description

The computer code, NOZVTX, presented in this section has application as an engineering prediction method for circular and noncircular bodies at high angles of attack in supersonic flow. The code is in effect a combination of

two separate codes. The first is the subsonic body vortex shedding method described in References 1 and 2, and the second is the supersonic body model for bodies alone described in References 10, 11, and 12. The combined code provides a means to predict the nonlinear aerodynamic characteristics and flow fields for bodies with circular and noncircular cross sections. The effect of fins is not included.

The code consists of a main program, NOZVTX, and 50 subroutines. The overall flow map of the program is shown in Figure 6 where the general relationship between the subroutines and external references can be seen. An alphabetical listing of the subroutines is shown in Table I. It was an objective of this effort to keep the two codes as distinct as possible to maintain their individual identity so that modifications to either code could be carried out without major changes in the other code. Note that the main subroutine of the body vortex shedding calculation, ELNOSE, includes the body panel code via the calls to subroutines GEOM, VELCMP, and SOLVE. The line singularity model for axisymmetric bodies is included through a call to subroutine BDYGEN. The communication of information between segments of the program is handled by name common blocks. A cross reference table for the calling relationship between the program subroutines and the external references is shown in Figure 7. A similar table for the common blocks is shown in Figure 8.

The program is written in standard FORTRAN language. Operation requires four (4) auxiliary files in addition to the usual input and output units. Core storage for execution is approximately 230,000 octal on a CDC CYBER 760 computer. Execution times on the same computer can vary from 10 to 400 or more seconds. Execution time depends on many factors such as the number of panels required for the

body, the integration interval (DX), the number of shed vortices, the use of symmetry, and even the flow conditions.

Limitations

Program NOZVTX is applicable to bodies alone at high angles of attack in supersonic flow, with some limitations. Certain of the limitations to follow are basically rules-of-thumb for the use of the program that have evolved through experience with the program and verification of the program by comparison with data. The range of applicability of the program may be extended by additional verification with appropriate data.

There is a Mach number/geometry limitation in the body model that requires the body surface to lie behind the Mach cone. This has greatest effect at high Mach numbers or on blunt noses at low Mach numbers, and a message is printed if the geometry condition is violated. It has been the experience of the authors that, when this condition arises, the nose can generally be made slightly more pointed so that it lies within the Mach cone. Often this modification is required only on the first few percent of body length, and the effect on the total nose forces and moments and shed vortex field is minimal.

An associated Mach number limitation involves the quality of the predicted surface pressure distribution at high Mach numbers. As will be shown in comparisons of experiment and theory, the predicted pressure coefficients on the windward side are much lower than those measured at body points which are near to the shock wave. This is a common problem for linear body models like the axis singularities and the panels considered in NOZVTX, and it is possible that the windward pressure can be corrected by use of nonlinear pressure prediction techniques.

Another less rigid limitation involves the Mach number/angle of attack range. It is suggested that the crossflow Mach number ($M_\infty \sin\alpha_c$) not exceed unity. A stricter limitation is that the crossflow Mach number should not exceed the critical value; that is, the local Mach number in the crossflow plane should not exceed unity at any point in the plane. The root of this limit is the vortex shedding calculation which uses an incompressible vortex model and an incompressible separation criterion. Also, when the crossflow Mach number exceeds the critical value, a complex shock near the shoulder may contribute to separation. It is important that the user be aware of these limits, particularly when the program is being used in that range. However, the author has used the program for flow conditions in which the crossflow Mach number slightly exceeded unity, and the results were quite resonable. Some of these results are presented in a later section.

Error Messages and STOPS

The program code has numerous internal error messages. These are generally explicit and they will be described below only if an explanation will provide some insight into the problem and its correction. There are several execution terminations at numbered STOP locations within the program. These are described in the table below along with some suggestions to correct the problem.

The most common message is "CONVERGENCE NOT OBTAINED IN INTEGRATION." This message, along with the axial station, XI, and the integration interval, H, is printed when the trajectory calculation does not converge within the specified tolerance, E5. One message will terminate execution at STOP 40 described in the table to follow.

The program contains several error messages pertaining to the number of panels used to describe the body. The message "ERROR - NUMBER OF ROWS OF PANELS IN BODY SECTION 1 EXCEEDS 30" is self explanatory and results in STOP 20. A similar message "ERROR - NUMBER OF ROWS OF SINGULARITY PANELS ON BODY EXCEEDS 30" results in STOP 50. The message "ERROR - NUMBER OF BODY PANELS EXCEEDS 600" results in STOP 60. The message "ERROR - BODY HAS MORE THAT 20 CIRCUMFERENTIAL PANELS" refers to the number of panels describing the body cross section circumference. This error results in STOP 200. All of the errors associated with the body panels are caused by incorrect values being input in items 32 and 41 of the input list.

If a pivot element of the matrix of panel influence coefficients is zero, the message "ERROR - THE MATRIX IS SINGULAR" is printed and the program terminates execution at STOP 300. This is a very uncommon error and is not seen for normal body panel arrangements.

As mentioned in a previous section, the slope of any panel on a noncircular body must be less than the Mach angle. If a panel has a greater slope, the message "ERROR - BODY PANEL SLOPE EXCEEDS MACH ANGLE" is printed and execution terminates at STOP 210. A modification of the body geometry to decrease the panel slopes is required to correct this situation.

The surface of an axisymmetric body must lie inside the Mach cone from the nose tip. If certain body points lie outside the Mach cone, subroutine BDYGEN will make an effort to correct the definition of the body and revise the radius distribution. If the Mach number is too high to correct the body within its specified length, the message "BODY RADIUS TOO LARGE IN RELATION TO BODY LENGTH" is printed and execution terminates at a STOP. If, in the process of

correcting the body points outside the Mach cone, the subroutine cannot locate an appropriate point, the message "MACH CONE - BODY MERIDIAN INTERSECTION NOT FOUND AFTER 100 TRIALS" is printed and execution terminates at a STOP. These difficulties are corrected by modifying the body shape or lowering the Mach number of the run.

The numerical conformal mapping procedure can generate several error messages from subroutine CONFOR. The message "***ERROR IN SUM OF EXTERIOR ANGLES***" is printed if the routine has difficulty calculating appropriate body angles within a specified tolerance. Another message "***COEFFICIENT AN(1) = ____ GREATER THAN +- .001 AFTER __ ITERATIONS OUT OF __" is printed on rare occasions when the mapping procedure is having difficulty converging on a solution. Both of the above messages are informational, and they do not result in a program STOP. However, the user is advised to check the transformed shape carefully with the actual shape before using the results. If there is a difficulty in the numerical mapping calculation, refer to the Input Preparation section for assistance.

Numbered STOP Locations

Termination Message	Description
STOP	Normal program stop or the axisymmetric body lies inside the Mach cone from the nose tip.
STOP 20	More than 30 rows of panels on body. Revise input values of NFORX and KFORX in input items 32 and 41, respectively.
STOP 40	Vortex trajectory integration has failed to converge at an axial station. This problem is usually caused by (1) two or more vortices in close proximity such that they are rotating

about each other so rapidly that the integration subroutine cannot converge on a solution, or (2) a vortex too near the body surface. These situations are often dependent on the body shape and the specific flow conditions, but the following steps should be tried to resolve the problem. Increase the integration tolerance E5, or increase the size of the combination parameter RGAM so that it is greater than the distance between the troublesome vortices. It often helps to increase the integration interval DX and restart the calculation from a previous station.

STOP 41 The vortex trajectory calculation has resulted in a vortex inside the body. This is a rare, but serious, problem; and it signifies a major problem with the solution. It usually means that the body paneling scheme is in error. If no obvious problem exists, change the paneling layout to increase the number of circumferential and axial panels.

STOP 44 Total number of shed vortices exceed 200. Combine some vortices and restart the calculation and run to completion. An alternate solution is to increase the integration interval DX so that fewer vortices are shed.

STOP 45 The number of positive or negative primary separation vortices exceeds 70. Use the same remedy as for STOP 44.

STOP 46 The number of positive or negative secondary or reverse flow separation vortices exceeds 30. Combine the secondary vortices to reduce their total number and restart the calculation;

increase DX to reduce numbers of vortices shed, or set NSEPR=0 and eliminate the secondary vortices from the calculation.

STOP 50 — More than 30 rows of panels on body. See STOP 20.

STOP 60 — More than 600 panels on body. Revise requested number of panels in input items 32 and 41.

STOP 200 — More than 20 panels on the body circumference. Revise values of NRADX and KRADX in input items 32 and 41, respectively.

STOP 202 — There is an error in the vortex tables in subroutine VTABLE. Check input values of NBLSEP, NSEPR, NVP, NVM, NVA, NVR, and RGAM in items 1 and 6.

STOP 210 — A body panel has a slope greater than the Mach angle.

STOP 300 — There is a singularity in the panel influence coefficient matrix. Check panel layout geometry for errors.

An additional comment is required here about a situation which can occur which results in a fatal execution error and termination at a TIME LIMIT with no other message. This is not a usual occurrence, but it has been observed in certain special cases. The typical case is near the end of a very long body from which a large number of vortices have been shed. The difficulty is that two differential equations of motion must be integrated for each vortex and the derivatives involve all vortices in the field. Solution by a Kutta-Merson scheme can involve many derivative calculations. The minimum time required for each axial step in the calculation is proportional to the square of the total number of

vortices. As the number of vortices increases, convergence becomes more difficult and the time for each step can increase dramatically. If this situation should occur, the best approach is to combine adjacent vortices and restart the calculation with a larger convergence criterion E5. It is sometimes useful to increase the axial interval DX.

Input Description

The purpose of this section is to describe the input to program NOZVTX. The input formats are shown in Figure 9, and the definitions of the individual variables are provided in the following paragraphs. The input to the body panel and axis singularity portion of the program is maintained nearly identical to the input requirements for program WDYBDY of Reference 10. The purpose for this was to minimize changes in WDYBDY; however, it leads to some redundancy in the preparation. The small amount of redundancy is acceptable in light of the simplification in the use of the current program. If there is a question about the input in the panel portion of the program, the user is referred to Appendix K of Reference 10 for additional information.

The remainder of this section includes a description of each of the input variables and indices required for the use of program NOZVTX. The order follows that shown in Figure 9 where the input format for each item and the location of each variable on each card is presented. Data input in I-format are right justified in the fields, data input in F-format may be placed anywhere in the field and must include a decimal point, and data input in E-format are right justified in the fields and must include the decimal point and the complete exponent designation.

Note that all length parameters in the input list are dimensional variables; therefore, special care must be taken that all lengths and areas are input in a consistent set of units.

Item 1 is a single card containing sixteen integers, each right justified in a five-column field. The variables are defined as follows.

Item	Variable	Description
1	NCIR	Cross section shape index. =0, circular cross section =1, elliptic cross section =2, arbitrary cross section
	NCF	Numerical transformation index. =0, mapping coefficients are calculated based on body shape input =1, mapping coefficients are input by user in items 18 through 22
	ISYM	Symmetry index. =0, right-left flow symmetry =1, no symmetry (required if $\phi \neq 0°$)
	NBLSEP	Body vortex separation index. =0, no separation (required if $\alpha_c = 0°$ in item 5) =1, laminar separation =2, turbulent separation
	NSEPR	Reverse flow separation index. =0, no separation =1, laminar separation in reverse flow region

NSMOTH — Vortex induced velocity smoothing index.
- =0, no smoothing
- =1, smoothing of vortex-induced velocities used in pressure calculation
- =2, smoothing of vortex-induced velocities used in pressure calculation and smoothing of $\partial\phi/\partial x$ calculation

NDFUS — Vortex core model index.
- =0, potential vortex
- =1, diffusion core model; preferred (see RCORE in item 5)

NDPHI — Unsteady pressure term index.
- =0, omit $\partial\phi/\partial x$ from C_p calculation
- =1, include $\partial\phi/\partial x$ term; preferred

INP — Nose force index.
- =0, slender body theory force on portion of nose ahead of starting point (XI)
- =1, zero force on nose ahead of XI; preferred value for restart option

NXFV — Number of x-stations at which flow field is calculated or special output generated. See item 23.

$0 \leq NXFV \leq 8$

NFV — Number of field points for flow field calculation. See item 24.

$0 \leq NFV \leq 200$

NVP — Number of $+\Gamma$ vortices on +y side of body to be input for restart calculation. See item 26.

$0 \leq NVP \leq 70$

NVR	Number of $-\Gamma$ reverse flow vortices on +y side of body to be input for restart calculation. See item 27. $0 \leq NVR \leq 30$
NVM	Number of $-\Gamma$ vortices on -y side of body to be input for restart calculation. See item 28. NVM = 0 if ISYM = 0. $0 \leq NVM \leq 70$
NVA	Number of $+\Gamma$ reverse flow vortices on -y side of body to be input for restart calculation. See item 29. NVA = 0 if ISYM = 0. $0 \leq NVA \leq 30$
NASYM	Asymmetric vortex shedding index. See item 7. =0, no forced asymmetry; preferred =1, forced asymmetry

Item 2 is a single card defining seven integer output option indices. Each index is right justified in a five column field. The indices are defined as follows.

Item	Variable	Description
2	NHEAD	Number of title cards in item 3. $NHEAD \geq 1$
	NPRNTP	Pressure distribution print index. =0, no pressure output except at special x-stations specified by item 23 =1, pressure distribution output at each x-station

NPRNTS Vortex separation print index.
=0, no output
=1, output at each x-station; preferred
=2, detailed separation calculation output; for debugging purposes only

NPRNTV Vortex cloud summary output index.
=0, no vortex cloud output
=1, vortex cloud output; preferred

NPLOTV Vortex cloud printer-plot option.
=0, no plot
=1, plot full cross section on a constant scale
=2, plot upper half cross section on a constant scale
=3, plot full cross section on a variable scale; preferred

NPLOTA Plot frequency index.
=0, no plots
=1, plot vortex cloud at x-stations specified by item 23
=2, plot vortex cloud at each x-station

NPRTVL Velocity calculation auxiliary output for debugging purposes only (Sub. VLOCTY).
=0, no output; preferred
=1, print velocity components at field points; see items 23 and 24
=2, print velocity components at body control points during pressure calculations. This option can produce massive quantities of output (not recommended).

Item 3 is a series of cards containing hollerith information indentifying the run. The cards are reproduced in the output just as they are input.

Item	Variable	Description
3	TITLE	NHEAD cards of identification. Information to be printed at top of output sheets.

Item 4 is a single card containing reference information used in forming aerodynamic coefficients. The variables are defined as follows.

Item	Variable	Description
4	REFS	Reference area. REFS > 0
	REFL	Reference length. REFL > 0
	XM	Moment center.
	SL	Body length (L).
	SD	Body maximum diameter, or equivalent non-circular body diameter (D). Used in definition of RE.

Item 5 is a single card containing the flow condition parameters. Each variable is input in a ten column field. The flow parameters are:

Item	Variable	Description
5	ALPHAC	Angle of incidence, degrees. $0° \leq \alpha_c < 90°$ If $\alpha_c = 0°$, NBLSEP = 0 in item 1.
	PHI	Angle of roll, degrees (ϕ).
	RE	Reynolds number ($V_\infty D/\nu$).

RCORE — Ratio of the local vortex core radius to the local body diameter. Default value is .025, and maximum allowable value permitted in the code is $.05*SD/r_o$.

XMACH — Mach number, M_∞.

Item 6 is a single card containing the specification of the axial extent of the run and certain parameters associated with the vortex wake. Typical values are shown with the variables.

Item	Variable	Description
6	XI	Initial x-station. XI > 0
	XF	Final x-station. XF $\geq$ XI
	DX	Increment in x for vortex shedding calculation. Typical value, DX $\approx$ D/2 when FDX = 0.0. For variable DX, set DX = 0.0 and FDX > 0.0.
	EMKF	Minimum distance of shed vortex starting position from body surface. =1.0, vortices positioned such that separation point is a stagnation point in the crossflow plane >1.0, minimum radii away from body surface for shed vortices. Typical value, EMKF = 1.05
	RGAM	Vortex combination factor. =0.0, vortices not combined; preferred >0.0, radial distance within which vortices are combined. Typical value, RGAM = 0.05 D

VRF	Vortex reduction factor to account for observed decrease in vortex strength. =0.6, for subsonic flow =1.0, for closed bodies, or supersonic flow; preferred
FDX	Factor for variable x-increments. When FDX > 0.0, DX = FDX *(local body radius). DX should be input as zero when this option is used.

Item 7 contains only one variable that is of general use in program NOZVTX, and that is the integration error tolerance, E5. The variable XTABL is for diagnostic purposes only. The next three variables concern the use of forced asymmetry for bodies at very high angles of attack. The variables are defined as follows.

Item	Variable	Description
7	E5	Error tolerance for vortex trajectory calculation. (Relative error in vortex position.) Typical range, E5 = 0.01 to 0.05.
	XTABL	x-location after which a table of corresponding points between the real body and the transformed circle is not printed. For diagnostic purposes on noncircular shapes. Typical value, XTABL = 0.0.
	XASYMI	Initial x-location at which forced asymmetry of separation points is used. Typical value, XASYMI = 0.0.
	XASYMF	Final x-location at which forced asymmetry of separation points is used. Typical value, XASYMF = 0.0.

DBETA	Amount of forced asymmetry for separation points on body, degrees. Typical value, DBETA = 0.0.

Items 8, 9, 10, and 11 provide a table of geometry characteristics that must be input for all bodies, circular or noncircular in cross section.

Item	Variable	Description
8	NXR	Number of entries in body geometry table ($1 \leq NXR \leq 50$).
9	XR	x-stations for geometry table (NXR values, 8 per card).
10	R	r_o, circular body radius at x-stations, or radius of tranformed circle (NXR values, 8 per card). For an ellipse, $r_o = (a + b)/2$.
11	DR	dr_o/dx, body slope of transformed shape at x-stations (NXR values, 8 per card).

Items 12 and 13 are included only if NCIR = 1; that is, for elliptical bodies.

Item	Variable	Description
12	AE	a, horizontal half-axis of elliptic cross section (NXR values, 8 per card).
13	BE	b, vertical half-axis of elliptic cross section (NXR values, 8 per card).

Items 14 through 22 are included only if NCIR=2; that is, for a body with arbitrary cross section that must be handled with the numerical transformation and conformal mapping procedures.

Item	Variable	Description
14	MNFC	Number of coefficients describing transformation of arbitrary body to a circle ($1 \leq MNFC \leq 25$).
	MXFC	Number of x-stations at which transformation coefficients are defined ($1 \leq MXFC \leq 10$). For a similar shape body at all cross sections, MXFC = 1.
15	XFC	x-stations at which transformation coefficients are defined. For a similar cross section body, MXFC=1, XFC(1) $\leq$ XI (MXFC values, 8 per card).

Items 16 and 17 are included when NCF = 0. This block of cards is repeated MXFC times, once for each x-station input in Item 15.

Item	Variable	Description
16	NR	Number of coordinate pairs defining the body cross section at the axial station defined by XFC(J) ($2 \leq NR \leq 30$).
17	XRC(I,J) YRC(I,J)	Coordinates of right-hand side of body. The convention for ordering the coordinates from bottom to top in a counter-clockwise fashion, as shown in Figure 10, is observed. Right/left body symmetry is required in the numerical mapping. (NR cards with one set of coordinates per card.)

Items 18 through 22 are input in lieu of Items 16 and 17 when NCF > 0. The values of these variables must be obtained from a previous run of the numerical mapping portion of the code. The only purpose for providing the option to input the mapping parameters is to eliminate the need to recompute the numerical mapping in subsequent runs and save computation time. This set of items is repeated MXFC times, once for each x-station input in Item 15.

Item	Variable	Description
18	ZZC(J) RZC(J)	Axis shift and radius of mapped cross section (one card with two values).
19	NR	Number of sets of body coordinates at a particular axial station.
20	XRC,YRC	Coordinates of right side of body defining cross section starting at $\beta = 0°$ and ending at $\beta = 180°$ (NR cards with one set of coordinates per card). See Figure 10.
21	THC	Angle of defined body points in circle plane (NR values, 8 per card).
22	AFC	Mapping coefficients (MNFC values, 6 per card).

Items 23 and 24 are included only if NXFV > 0. Item 23 specifies the axial stations at which additional output or plots are requested. Item 24 is included only if NFV > 0. Each card of this item contains the nondimensionalized y,z-coordinates of a field point at which the velocity field is calculated at each axial station specified in Item 23.

Item	Variable	Description
23	XFV	x-station at which field point velocities are calculated or at which additional output is printed (NXFV values).

Omit Item 24 if NFV = 0.

24	YFV,ZFV	y/r_o,z/r_o-coordinates of field points at which velocity field is calculated, expressed as a fraction of the local body radius (NFV cards with one set of coordinates per card). It is important that the field points lie outside the body surface.

Items 25, 26, 27, 28, and 29 are included for a restart calculation only, and the condition NVP + NVR + NVM + NVA $\neq$ 0 must be satisfied. It is not necessary to input all four types of vorticity in a restart calculation.

Item 25 is a single card containing the nose force and moment coefficients at the restart point; that is, X = XI. These values may be set equal to zero, but the resulting forces and moments from the current calculation will be in error.

Item	Variable	Description
25	CN	Normal-force coefficient.
	CY	Side-force coefficient.
	CM	Pitching-moment coefficient.
	CR	Yawing-moment coefficient.
	CSL	Rolling-moment coefficient.

Item 26 is a block of NVP cards to specify the positive separation vorticity on the right side of the body. Omit this item if NVP = 0. The variable XSHEDP associated with each vortex is used only to identify individual vortices and permit the user to follow individual vortices during the calculation.

Item	Variable	Description
26	GAMP	Γ/V_∞, positive separation vorticity on right side of body.
	YP,ZP	coordinates of discrete vortices on right side of body at starting point (XI).
	XSHEDP	x-location at which individual vortex was shed (may be 0.0).

(Item 26 consists of NVP cards.)

Item 27 is a block of NVR cards to specify the secondary or additional vorticity on the right side of the body or at any other position in the field. This array is a convenient way to put an arbitrary cloud of additional vorticity which is to be maintained separately from the other body vorticity in the field. Omit this item if NVR = 0.

Item	Variable	Description
27	GAMR	Γ/V_∞, reverse flow or additional vorticity on right side of body.
	XR,ZR	coordinates of discrete vortices on right side of body at starting point (XI).
	XSHEDR	x-location at which individual vortex was shed (may be 0.0).

(Item 27 consists of NVR cards.)

Item 28 specifies the negative separation vorticity on the left side of the body, analogous to Item 26. Omit this item if NVM = 0 or if ISYM = 0. In the case of a symmetric flow field (ISYM=0), this block of vorticity is automatically defined as the mirror image of the positive vorticity input in Item 26.

Item	Variable	Description
28	GAMM	Γ/V_∞, negative separation vorticity on left side of body.
	YM,ZM	Coordinates of discrete vortices on left side of body at starting point (XI).
	XSHEDM	x-location at which individual vortex was shed (may be 0.0).

(Item 28 consists of NVM cards.)

Item 29 specifies the secondary or additional vorticity on the left side of the body or at any other position in the field. This block of vorticity is analogous to Item 27, and it is omitted if NVA = 0 or if ISYM = 0. As with the previous item, this block of vorticity is automatically defined as the mirror image of the negative vorticity input in Item 27 if symmetry is required by ISYM = 0.

Item	Variable	Description
29	GAMA	Γ/V_∞, reverse flow or additional vorticity on left side of body.
	YA,ZA	Coordinates of discrete vortices on left side of body at starting point (XI).
	XSHEDA	x-location at which individual vortex was shed (may be 0.0).

(Item 29 consists of NVA cards.)

The above 29 items make up the body vortex shedding portion of the input deck.

Items 30 through 43 are associated with the paneling of bodies with noncircular cross sections and are taken from the input specifications for program WDYBDY (Ref. 10). Item 44 is used to describe bodies with circular cross sections. As described above, it was desired to keep the panel code input as unchanged as possible from the original WDYBDY code; however, the resulting input deck requires the specification of several variables over which the user has no control. The input deck considered herein contains only those variables which are optional to the user. Other nonoptional variables have been hard coded with their appropriate value, and these should not be changed by the user.

Omit Items 30 through 43 if NCIR = 0.

Item	Variable	Description
30	TITLE1	One card of identification information to be printed ahead of the paneling output.

Item 31 is a single card containing two indices, each index is right justified in a three column field. The purpose of IXZSYM is to define the manner in which the body paneling is carried out for different flow conditions. A symmetric body in a symmetric flow ($\phi = 0°$) can benefit from the IXZSYM = 0 option, which panels only one half of the body and then utilizes the symmetry characteristics to reduce computation time. The same symmetric body in an asymmetric flow condition ($\phi \neq 0°$) must be paneled in total, IXZSYM = 1, to pick up the nonsymmetry in the loading around the body. The body symmetry is used to reduce the input required as described later.

Item	Variable	Description
31	IXZSYM	Panel symmetry option. =0, panel symmetric half of body for symmetric flow (ϕ = 0°) =1, panel complete symmetric body using +y side geometry for a symmetric body in asymmetric flow ($\phi \neq 0°$) =-1, panel complete configuration using geometry of both sides
	ITBSYM	=0, configuration has top/bottom symmetry =1, no top/bottom symmetry (e.g., see Fig. 10)

Item 32 contains indices to specify the body geometry.

Item	Variable	Description
32	J2	Body geometry specification option. =0, no body (not recommended) =1, geometry for arbitrary shaped body =-1, circular body defined by cross-sectional area at XFUS stations (not recommended) =-2, circular body defined by radius at XFUS stations =-3, elliptic body defined by both semi-axes at XFUS stations
	J6	=0, cambered body - not available =1, body symmetrical with respect to XY-plane (uncambered body) =-1, circular or elliptic body with J2 $\neq$ 0 (preferred value)

NRADX — Number of points used to represent the body segment about the circumference. If the configuration is symmetric (IXZSYM = 0, 1), NRADX is input for the half section. If the entire configuration is input (IXZSYM = -1), NRADX is input for the full section. The half section or full section is divided into NRADX-1 equal angles, and the y- and z-coordinates of the panel corner points are defined by the intersections of these meridian angles with the body surface ($3 \leq$ NRADX ≤ 20).

It is the experience of the authors that the best panel representation of the body is obtained when NRADX is an even number; that is, there should be an odd number of panels on the half-body. It is very important for the pressure calculation that there be a panel control point on the $\beta = 90°$ meridian.

NFORX — Number of axial body stations used to define geometry ($2 \leq$ NFORX ≤ 30).

The next block of input specifies the geometry of the body for purposes of laying out the panels. This input is somewhat redundant with the input in Items 8 through 13; however, it is important that the paneling geometry be separate from the previous geometry but consistent with it. In many cases, the paneling geometry may be specified in a more coarse grid than that required by the separation portion of the program.

Item 33 is a block of cards containing the axial stations at which body geometry is input for paneling purposes. The values are input ten to a card in seven column fields with a decimal point required.

Item	Variable	Description
33	XFUS	x-stations at which body paneling geometry is input (NFORX values).

Item 34 is inlcuded only if J2 = -1 (Item 32). The circular body cross-sectional areas are specified at the XFUS stations defined in Item 33.

Item	Variable	Description
34	FUSARD	Circular body cross-sectional areas at XFUS stations (NFORX values).

Item 35 is included only if J2 = -2 (Item 32). The circular body radii are specified at the XFUS stations defined in Item 33.

Item	Variable	Description
35	FUSRAD	R, circular body radii at XFUS stations (NFORX values).

Items 36 and 37 are included only if J2 = -3 (Item 32). The elliptic body horizontal and vertical semi-axes are specified at the XFUS stations defined in Item 33.

Item	Variable	Description
36	FUSBY	Elliptic body horizontal semi-axes at XFUS stations (NFORX values).
37	FUSAZ	Elliptic body vertical semi-axes at XFUS stations (NFORX values).

Item 38 is included only if J2 = 1 (Item 32). The y,z-coordinates of points on an arbitrary cross section body are specified in Item 38, and there is one set of Item 38 for each of the axial stations defined by XFUS in Item 33. The convention for ordering the coordinates from bottom to top is observed (e.g., Fig. 10). If the full cross section is to be specified (IXZSYM = -1, Item 31) the ordering continues counter-clockwise from the top of the body back to and including the bottom point to close the cross section.

Item	Variable	Description
38	YJ,ZJ	y,z-coordinates of arbitrary body at XFUS stations (NRADX cards).

Item 38 is repeated NFORX times, once for each XFUS station.

The following portion of the input deck is described as Auxiliary Input Cards in Appendix K of Reference 10. The purpose of this input is to provide a simple means to adjust the actual panel layout keeping the geometry specified above unchanged.

Item	Variable	Description
39	TITLE2	One card of identification information for paneling geometry.

Item 40 contains an index to specify the output for the body panel portion of the program. Because of the quantity or output possible, it is recommended that |IPRINT| $\leq$ 1 be the highest level of output specified. Note that the values of the first two indices on this card are fixed.

Item	Variable	Description
40	IPRINT	Panel output option. =0, minimum output (recommended) =1, output panel corner coordinates, final source strengths, and velocities at panel control points (recommended) =2, same as IPRINT=1 and source strengths from previous iteration (not recommended) =3, print source strength for each iteration (not recommended) =4, same as IPRINT=3 and complete aerodynamic influence matrix (not recommended).

If IPRINT < 0, the panel geometry is included with the output specified by |IPRINT|. This option provides a useful means to check the paneling arrangement.

Item 41 is a single card containing two indices in three column fields. These indices provide a conventional means to change the panel layout without changing the geometry input.

Item	Variable	Description
41	KRADX	Number of meridian lines used to define panel edges on the body segment (see note for NRADX in Item 32).

KRADX =0, meridian lines are defined by NRADX in Item 32

>0, meridian lines are calculated at KRADX equally spaced points ($3 \leq$ KRADX ≤ 20)

<0, meridian lines are calculated at specified values of PHIK in Item 42 ($3 \leq |$KRADX$| \leq 20$)

For symmetric configurations (IXZSYM = 0,1), KRADX is the number of meridians on the half section. For full configurations (IXZSYM = -1), KRADX is the number of merdians on the full section including meridians at 0° and 360°.

KFORX Number of axial stations used to define leading and trailing edges of panels on the body.

=0, the panel edges are defined by NFORX and XFUS in Items 32 and 33, respectively

>0, the panel edges are defined by XFUSK in Item 43 ($2 \leq$ KFORX ≤ 30)

Item 42 is included if KRADX ≤ -3 in Item 41. This item provides a means to easily modify the panels by changing the body merdian angles which specify the panel corner points. The purpose of this option is to allow the user to pack additional panels into a region of the body which is changing rapidly.

Item	Variable	Description
42	PHIK	Body merdian angles (degrees) with PHIK = 0° at the bottom of the body and PHIK = 180° at the top (|KRADX| values).

Item 43 is included only if KFORX is nonzero. The variable XFUSK defines the axial positions of the panel edges. If this item is not included, the panels are specified by XFUS in Item 33. The purpose of this item is to simplify the changing of a panel layout without changing the entire geometry input deck.

Item	Variable	Description
43	XFUSK	Axial stations of leading and trailing edges of body panels (KFORX values).

Item 44 is included only if NCIR = 0; that is, for bodies with circular cross sections.

Item	Variable	Description
44	NXBODY	Number of line sources/sinks and line doublet singularities distributed along body centerline ($1 \leq$ NXBODY ≤ 100). Default value is NXBODY = 51.
	NCODE	Integer control index for specifying forebody shape over length of XNOSE. NCODE =0, Parabolic =1, Sears-Haack =2, Tangent ogive =3, Ellipsoidal =4, Conical
	XNOSE	Length of nose part of body, measured from nose tip.
	XLBODY	Length of body.

This concludes the input deck for a single run of program NOZVTX. The program is not set up to stack input for multiple cases because of the sometimes long and generally unpredictable run times.

Input Preparation

In this section, some additional information is provided to assist the user in the preparation of input for certain selected problems. The previous section on the input description must be used to understand the individual variables which go into NOZVTX, and this section will permit the user to select the appropriate input to get optimum results from the code.

Panel layouts.- The choice of panel arrangement to represent the noncircular body shape is perhaps the most important part of the input selection as the quality of the panel layout can determine the quality of the predicted results. Simply using the largest possible number of panels is one solution; however, this will not guarantee an optimum panel layout, nor will it guarantee the best results. In the following paragraphs, some guidelines are presented for various situations to optimize both results and computation time whenever possible.

The elliptic cross section will be considered first because the code has been checked out for a number of different elliptic bodies. In each case to follow, right/left symmetry of the panels (IXZSYM = 0 or 1 in Item 31) is assumed; therefore, only one side of the body will be shown to illustrate the panel layout.

A 2:1 elliptic cross section is shown in Figure 11 where several different panel arrangements have been selected. In Figure 11(a), nine program-determined panels (KRADX = 10

in Item 41), each specified by a 20° central angle, are shown. The only problem area is near the shoulder of the ellipse where the outer three panels miss the actual surface by a considerable amount. Increasing the number of panels to 10 (KRADX = 11) produces the arrangement shown in Figure 11(b). Even though an additional panel has been included, the region near the shoulder is not modeled better than before. In fact, this layout is missing an important physical effect because no panel has the same orientation as the shoulder ($dz/dy = \infty$), and the entire effect of the shoulder is lost.

An improved panel layout is shown in Figure 11(c) where nine panels are specified by their meridian angles (KRADX = -10). In this layout, the panels are concentrated in the region of highest curvature near the shoulder and spread out over the lessor curved region. Note that an odd number of panels is specified so that the outer panel nearest the shoulder has the proper slope. Top and bottom symmetry of the panels is shown, and this is a recommended arrangement for cross sections with top/bottom symmetry. For this particular cross section, additional panels can be specified for better resolution at the cost of increased execution time. It is important that the user check the panel layout used by the code to ensure reasonable modeling of the actual surface.

Different panel arrangements on a 3:1 elliptic cross section body are shown in Figure 12. The sharper curvature of the shoulder of this shape creates a bigger modeling problem than the 2:1 ellipse shown previously. In Figure 12(a), a 13-panel arrangement (KRADX = 14) with equal spacing is shown, and it is obvious that a large portion of the shoulder region is not modeled properly for the prediction of flow field characteristics near to the body.

For this particular shape, more panels are required for better resolution. Additional panels are added in the region $69° < \beta < 111°$ to produce the 19-panel layout (KRADX = -20) shown in Figure 12(b).

An example of reasonable panel arrangements on a lobed cross section body without top/bottom symmetry is shown in Figure 13. The shape shown in this figure is that described in References 17 and 18. The panel edges do not lie precisely on the actual body shape, a problem which is discussed in the numerical mapping section to follow. The 9-panel layout in Figure 13(a) is a resonable representation for preliminary calculations; however, certain detail is missing in the regions of greatest curvature. Additional panels are included in these regions, and the resulting layout is shown in Figure 13(b). Custom panel layouts are shown for both lobed-body examples to take advantage of the fewer panels required on the flat portion of body.

It is difficult to specify rigid guidelines for panel layout on arbitrary cross sections. The examples shown above were determined by this author after several trials, and proper panel selection becomes easier as the user gains experience with the code. The user should remember that linear interpolation of panel characteristics is used between panel control points in the current version of the code. Based on the experience of the authors, it is always useful to compare the paneling layout with the actual body shape, and generally, good engineering judgement will allow the user to select a reasonable panel layout.

Nothing has been said about axial panel layout (NFORX or KFORX) in the above discussion. Axial spacing can be critical to the predicted results, and as mentioned above, good engineering judgement will usually produce an adequate

layout. Linear interpolation is also used in the axial direction to determine panel characteristics between panel control points. This procedure can be used to great advantage for a specific class of body, the cone. Since the predicted linear results on a cone are the same at each axial cross section, fewer panels are required in the axial direction. The major requirements are the following.

1. There should be one row of panels sufficiently close to the nose tip or starting point (XI) for the calculation that a control point can fall between the starting point and the nose tip.

2. There should be a row of panels with control points located just aft of the last axial station of the calculation (XF).

3. If a conical nose is attached to the cylindrical afterbody, there should be enough axial stations specified near the junction of the nose and afterbody that adequate body characteristics are available for interpolation purposes.

An example of a panel arrangement for a cone forebody is presented in the sample cases.

Numerical mapping.- The specification of the appropriate numerical mapping parameters (Items 14 through 22) depends on the shape of the cross section. In the interest of optimum computation time, the fewest possible terms in the transformation series (MNFC in Item 14) should be used which will produce an adequate mapping. Each different shape should be checked by the user to determine the proper number of coefficients. For example, a simple cross section which is similar to a circle may require as few as 10 coefficients. The shape shown in Figure 13 required 20 coefficients for an excellent mapping. If a large number of calculations are

to be made for a noncircular shape, it is worthwhile for the user to try different numbers of coefficients in an effort to find an optimum number. Not only should the shapes be compared carefully, the unseparated flow pressure coefficients should be compared to evaluate the quality of the mapping.

The numerical mapping now included in NOZVTX has been used for a variety of cross section shapes, and very few problems have been observed. One general problem area is bodies with concave sides. The lobed body in Figure 13 has a moderate concave section on each side, and the mapping procedure had difficulty converging on a set of coefficients. When the body shape was modified slightly, as shown in Figure 13(a), to give the concave region a flat or slightly convex shape, the mapping converged easily. This small change in the shape probably has very little effect on the predicted pressure distribution. This is an example of the type of problems to which the user should be alert.

Integration interval.- Choice of the appropriate integration interval (DX in Item 6) depends to a large extent on the type of results of interest. The code permits the interval to be a constant (FDX = 0 in Item 6) or a function of the local radius (FDX > 0). If the user is interested in detailed nose loads and separation on the nose, where the radius is changing rapidly, the latter option should be used with $0.5 \leq FDX \leq 1.0$. This option can lead to a wide range of vortex strengths which, on occasion, has been determined to be the cause of certain vortex tracking difficulties. The user should be alert to this possibility. The constant interval option (DX = constant) is the best choice when the results of a major interest are the vortex clouds near the end of the body.

Vortex core.- The core size specification is referenced to the local body diameter (RCORE in Item 5). The default value is 0.025, and this value is adequate for most cases. The larger the core radius specified, the more the vortex effects are reduced. To eliminate the possibility of negating the vortex effect entirely, a maximum vortex core of .05 times the maximum body diameter is built into the code. Except in unusual situations, the default value is recommended, and this is the value used in the comparisons with data shown in a later section.

Sample Cases

In this section, 11 sample input decks are described to illustrate the input preparation and use of the program for a wide range of configurations and flow conditions. Insofar as possible, each major option in the program is illustrated in the set of sample cases. The major features of each sample case are identified in Table II to assist the user in finding an appropriate example to suit a specific need.

Sample Cases 1 through 11 shown in Table II are designed to exercise the most common options of program NOZVTX, and Sample Case 1 is included specifically to provide a short computer run for testing purposes. The input decks for the sample cases are shown in Figures 14(a) through (k). The sample cases are based on typical bodies used in the data comparisons to follow in a later section, and the reference in which the configuration is defined is noted on each sample case.

Sample Case 1 is a test case based on the 3:1 elliptic missile body in Reference 19; however, only a portion of the nose is considered to keep the execution time and output at a minimum. The purpose of this run is to provide the

user with a short run to check out the code. The output from this case is described in the next section. Sample Case 2 in Figure 14(b) is a restart of the previous run, and it illustrates the continuation of a calculation. Sample Case 3 in Figure 14(c) is the input deck for a complete run of this 3:1 elliptic missile. The first three sample cases do not necessarily use the optimum panel arrangement in an effort to minimize execution time. For production runs, the authors recommend a panel layout similar to that shown in Figure 12(b).

Sample Case 4, Figure 14(d), illustrates the missile body in a rolled condition (ϕ = 45°). The lack of flow symmetry and consequently the lack of right/left panel symmetry dictate the use of a smaller number of panels because the entire cross section must be paneled. This run is typical of any noncircular body in a rolled flow condition.

Sample Cases 5 and 6, Figures 14(e) and (f), illustrate input decks for circular cross section bodies (Refs. 20 and 21). Since axis singularities are used in place of panels, the input is shorter and easier to prepare. The primary objective of Sample Case 6, an axisymmetric body at α_c = 0°, is the prediction of the surface pressure distribution with no separation effects included.

Sample Cases 7 and 8, Figures 14(g) and (h), are input decks for a 2:1 elliptic cross section forebody from Reference 18. The first case is for a standard panel layout determined by the code. The panels for the second case are tailored to the cross section shape by specification of the central angles of the panel edges.

Sample Case 9 is a 3:1 elliptic cross section conical forebody (Ref. 17). The input specifies a variable axial

integration interval, and the axial panel distribution is determined by the conical shape. Because of the character of conical flow, a very small number of axial panels is required as discussed in a previous section on input preparation.

Sample Case 10, Figure 14(j), is a lobed cross section forebody from Reference 18. This is an arbitrary noncircular body and numerical mapping is required for solution as indicated in the input. Since the cross section is changing at each x-station, the cross section shape must be input at a number of stations thus accounting for the large quantity of input. The number of axial stations must be sufficient to provide acceptable accuracy in the body shape using linear interpolation between input stations.

Sample Case 11, Figure 14(k), is set up for the 2:1 elliptic cross section missile body in Reference 22. The panel layout for this body is the same as that shown in Figure 11(c).

Output

A typical set of output from program NOZVTX is described in this section. In general, the output quantities are labeled and each page is headed with appropriate descriptive information. The actual output obtained is determined by the output options selected by the user. For purposes of this description, representative pages from Sample Case 1, described in a previous section, are presented in Figure 15.

The total output from Sample Case 1 is contained on 30 pages, including pages which are continuations of another page. The first page shown in Figure 15(a) is headed by the title cards input as Item 3. The remainder of this

page, the following two pages shown in Figures 15(b) and (c), and the top of the fourth page shown in Figure 15(d) contain all the input data with appropriate labels. Body source panel geometry is shown on pages 5 through 13, Figures 15(e) through (m). Page 5, shown in Figure 15(e) and the following two pages shown in Figures 15(f) and (g) indicate the panel corner coordinates. Pages 8, 9, and 10, shown in Figures 15(h), (i), and (j), contain a table of the body panel centroid coordinates. This is followed by a table of body panel areas and inclination angles. The inclination angles DELTA and THETA orient the panels in the body coordinate system. Detailed descriptions of these angles are given in Reference 10. This table continues onto page 12 and the top of page 13, shown in Figures 15(ℓ) and (m). The next item on page 13, GB(N), is the list of source strengths for the body at angle of attack. This is followed by a table of velocity components at the control point of each panel. Each component is labeled, and the table continues onto pages 14 and 15 shown in Figures 15(n) and (o). The last item on page 15, under the heading MODIFIED SOURCE STRENGTH, is the source strength on each panel of the body with no cross-flow influence. This panel strength represents the volume solution of the body for purposes of tracking vortices. This list of source strengths continues onto page 16 shown in Figure 15(p).

The next two pages, shown in Figures 15(q) and (r), contain the predicted pressure distribution around the body at the first axial station. A summary of the geometric characteristics and the Mach number is printed at the top of page 17, followed by the pressure distribution. The columns are labeled, but a brief explanation of the printed items follow. The first three columns, Y, Z, and BETA, locate the specific points on the body cross section. U/VO is the local axial velocity referenced to the free-stream

velocity. V/VO and W/VO are the local lateral and vertical velocities, respectively. These velocities include all perturbation effects including vortex induced velocity components. The column VT/VO is the total velocity in the crossflow plane given as the vector sum of the V/VO and W/VO velocities. A positive VT/VO represents flow in a counterclockwise direction when viewed from the rear. CP(M) is the compressible pressure coefficient as calculated from Equation (29). DPHI/DT is the unsteady part of the incompressible pressure relation as represented by the last term in Equation (31). CPZ is the steady part of Equation (31), and CP(I) is given by Equation (31) in its entirety. VCP/VO is the local two-dimensional crossflow plane velocity whose positive sense is the same as that for VT/VO.

The local force and moment coefficients are printed at the middle of page 18. CN(X) and CY(X) are local force coefficients calculated by Equations (39) and (43), respectively. The remainder of the forces and moments represent total quantities on the nose between the origin and the local axial station. The normal force and pitching moment coefficients, CN and CM, are calculated with Equations (40) and (41), and the axial center of pressure of the normal force, XCPN, is given by Equation (42). XCPN is not normalized by the reference length on page 7. The corresponding side force and yawing-moment coefficients and center of pressure of the side force are given by Equations (44), (45), and (46), respectively. The rolling-moment coefficient, CSL, is positive in a counterclockwise sense when viewed from the rear of the body. The small value shown in this output is due to numerical round-off error during the calculation. The same is true for all lateral coefficients which appear as very small, nonzero,

values when a symmetric body and symmetric flow conditions dictate that they are identically zero.

Page 19 of the output from Sample Case 1, Figure 15(s), summarizes the important points in the pressure distribution and the separation calculation. The last two lines of output contain specific information on the vortices shed at this station. The vortex numbers, NV, assigned here are the cumulative numbers of vortices in the flow field. The vortex strength, GAM/V, is obtained from Equation (38) where the boundary layer edge velocity u_e/V_∞ is shown as VT/V in this line of output. M(K) is the actual distance of the vortex from the body surface. The position of the vortex in the body plane is given by Y, Z, and BETA. The position of the vortex in the circle plane is given by the coordinates YC, ZC. The radial position of the vortex in the transformed circle plane is RG/R. The latter quantity is useful in providing a quick estimate of the relative positions of new vortices being shed into the wake.

Page 20, shown in Figure 15(t), summarizes the vortex field after the trajectories have been calculated over one axial interval. The x-station at the top of this page is exactly DX downstream of the previous x-station. Information to locate each individual vortex in both the body plane and the circle plane is provided. One additional piece of information for each vortex is XSHED, the x-station at which the individual vortex originated. This is printed to allow the user to keep track of any individual vortex throughout the trajectory calculation. Each vortex maintains its individual identity and the right and left side vortices are grouped together on this page. Centroids of the individual groups of vorticity also show on page 20. The only exception to the above discussion of individual vortices occurs when vortices are allowed to combine through use of the parameter

RGAM in Item 6 of the input list. When vortices are combined, the particular vortices are identified in a special line of output.

This completes one cycle of output. The next page of output is the pressure distribution at the new axial station, and the format is the same as page 17 shown in Figure 15(q). At each axial station, the output repeats through the cycle shown in Figures 15(q), (r), (s), and (t). At specified axial stations, certain additional output is available. A simple plot of the body cross section and the vortex field at x = 4.2 is shown in Figure 15(u). This particular output is on page 23 of the actual output from Sample Case 1. Each type of vortex is shown with a different symbol in this figure. Postive body vorticity shed from the right side of the body is shown as an X, and negative vorticity from the left side is represented by an O. If it is requested, the calculated velocity field appears as shown in Figure 15(u). This output appears on page 24 of the actual output. The coordinates and velocities shown on this page are in the body plane. The normalizing diameter, D, in the last two columns is the equivalent diameter of the noncircular body.

The last page of output is shown in Figure 15(w). The top portion of the output is the summary page for the separation calculation at the last x-station, X = XF. This part of the output is similar to that shown in Figure 15(s). The lower part of the page is printed only at the completion of the calculation, and it contains a summary of the forces and moments and the vortex strengths and centroids at the end of the body.

RESULTS

For purposes of evaluating the accuracy and range of applicability of the engineering prediction method and associated program code NOZVTX described above, comparisons of measured and predicted aerodynamic characteristics of various configurations have been made. The objective of the method is to predict the characteristics for noncircular cross section bodies, but selected data for bodies of revolution will also be considered to illustrate certain features of the prediction method. Typical results from the prediction method are presented in the following sections.

Circular Bodies

The prediction method was applied to an ogive-cylinder model (Ref. 21) in supersonic flow to evaluate the ability of the prediction method to calculate pressure distributions. The configuration has a circular cross section and a three caliber ogive nose followed by 3.67-caliber cylindrical afterbody. Circumferential pressure distributions at a large number of axial stations are available for a range of angles of attack and supersonic Mach numbers. The free-stream Reynolds number, based on diameter, is 0.5×10^6 for the results to follow.

The model is represented by 51 line sources on the body body axis for the calculation at $\alpha_c = 0°$. The measured and predicted pressure distributions at three Mach numbers are compared in Figure 16 where the multiple data symbols at each axial station represent the range of scatter in the data. The purpose of this comparison is to verify the body model and the pressure calculation technique under conditions in which there are neither crossflow nor separation effects.

In Figure 16(a), the agreement is very good at $M_\infty = 1.6$ except in the region very near the nose. As seen in Figures 16(b) and (c), the agreement between measured and predicted pressures on the nose gets progressively poorer as the Mach number increases. It is possible that nonlinear effects caused by the close proximity of the shock wave are responsible for this disagreement. For purposes of this investigation, a small error in the pressure very near the nose will have very little effect on the vortex shedding from the remainder of the body. As a further check on the body model, a panel distribution of 13 rings of 14 equally spaced circumferential panels was used for the same calculation. The pressure results are virtually identical to those obtained from the line singularity model.

The prediction method was next applied to the same model at $\alpha_c = 20°$ angle of attack and $M_\infty = 1.6$. At this angle of incidence, the separation vortex wake on the lee side of the body is well developed. Measured and predicted pressure distributions at two axial stations on the nose and one station on the cylinder are compared in Figure 17. The agreement between experiment and theory at $x/D \approx 0.8$ is very good except on the windward side of the body upstream of the minimum pressure point. Similar results are illustrated in the lower portion of Figure 17(a) for a station near the end of the nose ($x/D = 2.8$). The predicted minimum pressure point is upstream of the measured value, but the general trend of the predicted pressure distribution is correct. The slightly irregular behavior of the predicted curve near $\beta = 130°$ is caused by local interference of the lee side separation vortices.

Measured and predicted pressures on the cylindrical portion of the body ($x/D = 5.1$) are shown in Figure 17(b). A large vortex wake, also shown in the figure, has developed

on the lee side, and it has a dominant effect on the pressure distribution. The solid curve, representing the predicted pressure distribution in the presence of the vortex wake, is in good agreement with the measured results near the minimum pressure point and on the lee side. The predicted pressures are lower than those measured on the windward side of the body. There is also some disagreement between experiment and theory near $\beta = 130°$ where it appears that some of the vortex induced effects are missing from the predictions. Contrast the solid curve with the dashed curve representing a predicted pressure distribution with no separation effects included.

The prediction method was next applied to an ogive-cylinder model for which detailed lee side flow field measurements are available (Ref. 20). This model is an ogive-cylinder with a two-caliber nose and a thirteen-caliber cylindrical afterbody. The tests were conducted at Mach numbers of 2 and 3 at a free-stream Reynolds number, based on diameter, of approximately 2×10^6. The data consist of lee side velocity components and separation vortex strengths and positions. Neither pressure nor force and moment data are available from these tests.

The model is represented by 51 line source and doublet singularities on the body axis. The predicted vortex cloud pattern at $x/D = 10$ is shown in Figure 18 for $M_\infty = 2$ and $\alpha_c = 15°$. The vortex shedding is symmetric on both sides of the body. Also shown in this figure are the separation points located at approximately 86 degrees measured from the windward stagnation point. The measured and predicted vortex strength and centroid of vorticity are shown to be in reasonable agreement in this figure. The predicted vortex wake is approximately 9 percent stronger than the measured value, and the centroid of the predicted vortex cloud is

slightly lower and more outboard than the measured results. Again, as a further check on the body model, the body was represented by 15 rings of 14 equally-spaced circumferential panels. The predicted results were nearly identical in each case; however, the execution time for the line singularity model was only 20 percent of that required for the panel solution.

Measured and predicted body vortex strengths on the same ogive cylinder at Mach numbers 2 and 3 and angles of attack 10, 15, and 20 degrees are compared in Figure 19. At $M_\infty = 2$, the predicted results are slightly higher than those measured. At $M_\infty = 3$, the predicted results are lower than those measured on the forward portion of the body and in good agreement on the rear portion. The slopes of the predicted curves are in good agreement with the experimental results, an indication that the predicted shedding rate and strengths of the shed vortices are correct. The difference in magnitude between the measured and predicted vortex strength in Figure 19 is attributable in part to the location of the onset of separation. If separation is predicted to start further aft on the body than the actual start of separation, the predicted vortex strength will be less than measured. The maximum error in vortex strength exhibited in Figure 19 represents an error in the predicted axial position of onset of separation of less than one body diameter except at the highest angles of attack.

Measured and predicted downwash velocity fields in the plane of symmetry of the model at $M_\infty = 2$ and $\alpha_c = 15°$ are shown in Figure 20 for three axial stations. The results are generally in good agreement, and the predicted velocity distribution exhibits the correct trend in every case. The vortex field used to calculate the induced velocities at $x/D = 10$ is the distribution shown in Figure 18.

Additional comparisons of measured and predicted downwash velocities on the lee side of the body at x/D = 10 are shown in Figure 21. In Figure 21(a), the velocities are calculated along a line at z/D = .75 which passes through the predicted centroid of vorticity. The agreement is only fair in the vicinity of the centroid (y/D ≈ 0.4), an indication that the present discrete vortex cloud model is not completely reliable inside the cloud. In Figure 21(b), the measured and predicted velocities are compared along a line at z/D = 1.05 which passes above both the measured and predicted centroid of vorticity. These results indicate the correct trend in the predicted velcoity distribution; however, since the strength of the wake vorticity is nearly correct, it appears that a cloud model that is higher off the body is required to bring the predicted velocities into better agreement with measurements. The need for a higher cloud is verified in Figure 18 where it is shown that the actual centroid of vorticity is approximately .15D above the predicted centroid. As shown in Figure 19, the strength of the vortex cloud is in good agreement with experiment.

Similar comparisons of measured and predicted downwash velocity fields on the lee side of the ogive cylinder at $M_\infty = 3$, $\alpha_c = 15°$ are shown in Figures 22 and 23. The results on the plane of symmetry on the model lee side are shown in Figure 22 where it is obvious that the comparisons are not as good as those shown in Figure 20 for $M_\infty = 2$. The general trends are correct, but the magnitude of the velocity components is in error. This is likely due to a combination of circumstances. For example, in Figure 19, the predicted vortex strength corresponding to $M_\infty = 3$, $\alpha_c = 15°$ is less than that measured at x/D = 7 and in good agreement with measurements at x/D = 13. As seen in Figure 22, the vortex induced velocity is less than that measured at x/D = 7 and nearly correct at x/D = 13. The fact that the predicted

velocity profiles are not in agreement may be due, in part, to the problem discussed previously, the error in the predicted centroid of vorticity. The velocity profiles indicate that the predicted centroid of the separation vorticity may be too low, a possible problem at higher Mach numbers.

Analogous to the $M_\infty = 2$ results in Figure 21, comparisons of measured and predicted velocity profiles on the lee side of the body at $x/D = 10$ are shown in Figure 23 for $M_\infty = 3$. The results look very good in Figure 23(a) at $z/D = .75$ where the region of comparison is in the vortex cloud and near the vertical centroid of vorticity. In Figure 23(b), the agreement between the velocity profiles is poor with the predicted velocities being much less than those measured.

Elliptic Bodies

The prediction method has been applied to a number of different elliptic cross section bodies. A variety of results are presented for several configurations under a range of flow conditions, the major objective being to examine a large number of configurations to identify the strengths and weaknesses of the code.

The 3:1 elliptic cross section missile of primary interest in these comparisons is the sharp-nose body described in References 19, 23, and 24. The tests were conducted at $M_\infty = 2.5$ and a free-stream Reynolds number of 2×10^6 per foot. The sharp-nose body considered in the comparisons to follow was modeled with 18 circumferential panels around the cross section and 29 axial rings of panels. Sample Cases 3 and 4 described in Table II and Figures 14(c) and (d), respectively, produce the results to follow.

Flow visualization via vapor-screen photographs (Ref. 23) and pressure data (Ref. 24) are available for comparison with the theoretical results. For better visualization of the vortex development along the body, the photographs were digitized. These results are presented in the upper left corner of Figure 24 for the missile at $M_\infty = 2.5$, $\alpha_c = 20°$, and $\phi = 0°$ and 45°. Cross sections through the body at three axial stations are shown. The extent of the vortices from the vapor screen photographs are shown by the solid curve, and the predicted discrete vortex wake is shown by the individual vortices connected by a dashed line. The unrolled flow condition ($\phi = 0°$) shown in Figure 24(a) illustrates very good agreement between the predicted vortex cloud and the vapor screen results. The strength of the predicted vortex cloud is shown at each axial station, and because of symmetry, the left and right vortices are of equal magnitude and opposite sign.

The rolled flow condition ($\phi = 45°$) is shown in Figure 24(b). To be consistent with the output from the code, the body is shown unrolled with the flow angle rolled 45 degrees. The general character of the predicted vortices is in fair agreement with the experimental results; however, there are certain areas of disagreement. The theoretical vortex on the right side has rolled up much tighter than the vapor screen indicates, and the left theoretical vortex has not moved out away from the body as far as the actual vortex, nor has it rolled up as tightly as the actual vortex.

Comparison of measured and predicted pressure distributions at $x/L = 0.60$ on the body are shown in Figure 25 for the unrolled and rolled condition. The unrolled results shown in Figure 25(a) illustrate some of the same problem areas discussed for circular bodies. The predicted

stagnation pressure on the windward side is in good agreement with experiment, but the predicted pressure around the shoulder region of the cross section is much lower than the measurements. The pressure on the lee side is also underpredicted, possibly due to vortex interference effects. As shown in Figure 24(a), there is a strong concentrated vortex field developed on the lee side at this axial station ($x/L = 0.60$). The irregularities in the predicted pressures near the shoulder region are caused by local vortex interference effects. As noted in the discussion for the circular bodies, the discrepancy in the pressure comparisons on the windward side of the body near the shoulders may be caused by nonlinear effects induced by the close proximity of the shock wave.

The measured and predicted pressures on the 3:1 elliptic body in a rolled flow condition are compared in Figure 25(b). The qualitative agreement is very good, but a problem on the windward side of the body is in evidence. The vortex induced effects cause the irregularities in the predicted pressures, and it appears that the induced effects are too large on the positive lee side ($\theta \approx 320°$). In Figure 24(b) it is obvious that the close proximity of the predicted wake will have a large effect on the pressure distributions, and it is likely that the predicted wake is causing the lack of agreement in this region.

NOZVTX was also applied to a conical forebody with a 3:1 elliptic cross section shape (Ref. 17). The major axis, in planform, is defined by a 20-degree half angle, and the total length of the forebody is 14 inches. The test was conducted at a free-stream Reynolds number of 2×10^6 per foot. The panel model representation consists of 17 circumferential panels on the half body (34 panels on the total cross section) and four axial rings of panels. The limited number of axial

panels is permissible because of the similar characteristics on a conical configuration in supersonic flow described in the previous section on input preparation. The detailed panel layout is described in Sample Case 9.

Comparisons of measured and predicted pressure distributions on the conical forebody are shown in Figure 26 for two axial stations. Except for small differences on the lee side of the body, the measured pressure distributions are nearly identical at the two axial stations. In Figure 26(a), the theoretical pressure distribution is not in good agreement with experiment on the windward side of the body, particularly near the shoulders. On the lee side, two prediced curves are shown; the dashed curve represents no separation vortex effects, the solid curve has vortex effects included. There is considerable difference in these results, all of the difference attributable to the vortex induced effects. The vortex effects improve the predicted pressures in the region around $\beta = 120°$ on the body, but they detract from the agreement near the lee side stagnation point, $150° < \beta < 180°$. This may be an indication that the actual lee side vorticity is rolled up tightly around $\beta = 120°$, whereas the predicted vortex cloud is distributed over the entire lee side of the body as illustrated in Figure 27.

The prediction method has been applied to the elliptic cross section body described in Reference 22 and illustrated in Figure 28. The major axis of the cross section is specified by an ogive distribution on the nose, and the cross section is a 2:1 ellipse over the entire body length. The equivalent base diameter of this body is 1.125 inches. Circumferential pressure measurements at numerous axial stations are available at $M_\infty = 1.5$ and a range of angles of incidence and angles of roll. The tests were conducted at a free-stream Reynolds number, based on the equivalent diameter, of approximately 0.3×10^6.

This 2:1 elliptic cross section body is modeled with 18 circumferential panels around the complete cross section and 15 axial rings of panels. No smoothing is used in any of the calculations to follow. The general layout of the geometry is illustrated in Sample Case 11 in Figure 14(k).

Measured and predicted pressure distributions on the elliptic cross section body at $M_\infty = 1.5$, $\alpha_c = 15°$, and several roll angles are compared in Figure 29 at two axial stations on the nose. The agreement between experiment and theory for $\phi = 0°$ is better away from the tip of the nose as shown in Figure 29(a). This is consistent with the circular body results described previously. The sparse nature of the measurements make it difficult to fully evaluate the prediction method other than to observe that the basic trends of the pressure distribution are predicted. At $x/D \simeq 2.1$, the separation vorticity has grown in strength and scope, and the major region of vortex wake influence covers the region between $\beta = 90°$ and 130°.

The predicted pressure distributions on the same body at roll angles of 22.5° and 45° are shown in Figures 29(b) and 29(c), respectively. The predicted results are generally in good agreement with experiment, and the correct trends of the data are modeled by the theory in each case. The local irregularities in the predicted curves are due to the influence of the separation vortices.

NOZVTX was next applied to a 2:1 elliptic cross section cone (forebody 4 in Ref. 17) in an unrolled flow condition. The pressure results for $M_\infty = 1.7$ and $\alpha_c = 20.35°$ are shown in Figure 30 where it is obvious that agreement is poor over much of the surface. The lack of agreement on the windward side and near the body shoulder is typical of previous results on elliptical cross section bodies. On the lee side, there is a large effect of the predicted vortex field which

is spread out over much of the lee side. The effects of the vortices on the measured pressures appear to be more limited in scope. These results are the same as those shown on the 3:1 elliptic cone forebody in Figure 26(a).

The final 2:1 elliptic cross section body considered in these comparisons is forebody 2 from Reference 18, and the predicted results are from Sample Case 8 in Figure 14(f). The comparison of measured and predicted pressure distributions in Figure 31 are in good agreement over the entire body surface, even on the windward side. The pressure distribution on the body is such that separation does not occur over most of the length of the forebody. Separation begins at approximately $x/L = 0.8$, but in contrast to the elliptic cross section bodies with their major axis horizontal, the vortices are very weak and located near the lee side stagnation point.

Arbitrary Bodies

The arbitrary noncircular body option in NOZVTX has been checked out for a number of different cross section shapes to verify the numerical transformation. Some of the shapes considered are a square cross section with rounded corners, a diamond cross section with rounded corners, and a lobed or pear shape cross section. The latter cross section is the only shape for which pressure data are available, therefore, results on this configuration are described as follows.

The configuration selected for these comparisons is the lobed cross section body, forebody 3 from Reference 18, shown in Figure 13. The panel arrangement shown in Figure 13(b) is used for the predicted results included herein, and the specific calculations were made using Sample Case 10. Comparison of measured and predicted pressure distributions

at two axial stations are shown in Figure 32. At $x/L = .14$ in Figure 32(a), the agreement is very good on the windward side of the body, only fair in the region of minimum pressure, and poor near the lee side stagnation point. This particular location near the nose of the body has minimal vortex interference effects. At the mid-point of the forebody length, $x/L = 0.5$, shown in Figure 32(b), the agreement is only fair over the entire circumference even though the trend of the data is predicted well. One unusual result in Figure 32(b) is the overpredicted pressure on the windward side of the body, a situtation which has not occurred on any other configuration. The roughness in the predicted pressure distribution on the lee side of the body is caused by local vortex interference effects. The vortices are distributed along the body surface, and they have not started to roll up. A sketch of actual predicted vortex positions is shown in Figure 33.

CONCLUSIONS

An engineering method and the program code NOZVTX to predict the vortex shedding from circular and noncircular bodies in supersonic flow at angles of attack and roll are described. The coupling of a supersonic panel method, an axisymmetric source and doublet model and a two-dimensional crossflow vortex shedding method has proved to be a successful means to predict the general flow characteristics about slender, circular and noncircular bodies at large angles of incidence and moderate Mach numbers. Comparisons of measured and predicted pressure distributions and associated flow fields on a variety of bodies indicate that the principal features of the flow phenomena are modeled. The predicted vorticity distributions in the wake of a body of

revolution in supersonic flow are in reasonable agreement with experiment. This also results in reasonable agreement between measured and predicted velocity components in the flow field of the body. The ability to model the correct flow field near the body leads to the capability to calculate wake induced interference effects on fins and other control surfaces as well as surface pressure distributions. The vortex shedding analysis described herein can be incorporated into an overall computation method for missiles and aircraft.

RECOMMENDATIONS

In the course of development of the program code NOZVTX, several specific areas for needed improvements to the method were discovered. These improvements were beyond the scope of the present study, but they are noted here as specific recommendations for future work.

The first, and possibly the most important, recommendation involves a thorough testing of program NOZVTX. Limited numbers of comparisons with experimental results on a variety of bodies are included herein, but many other comparisons are needed. The program should be tested over a wide range of angles of attack and roll and Mach numbers to better define the operational limits of the method. The program should also be applied to a wide range of noncircular body shapes for which data are available.

A critical weakness in the prediction method appears to be the difficulty in calculating accurate pressure distributions on the windward side of certain bodies. For example, from the comparisons with experiment described in a previous section, the method has problems with conical

forebodies at all Mach numbers and most shapes at high Mach numbers. These difficulties may be caused by nonlinear effects induced by the shock wave when it is relatively near to the windward body surface. Further investigation into this problem is recommended.

Comparisons of measured and predicted velocity components on the lee side of an axisymmetric body at high angle of attack indicate the method has a potential capability to handle this problem. However, some additional work on the details of the vortex cloud are required. This may involve a different procedure to blend the discrete vortices when velocities in the midst of the cloud are to be calculated. With regard to the cloud itself, qualitative results on a 3:1 missile body are in excellent agreement with experiment; but based on one set of experimental results, predicted vortex clouds on an axisymmetric body are typically lower than those measured. Additional investigation into the mechanics of the vortex tracking procedure may explain this disagreement.

The final set of recommendations involve improvements to various parts of the program. The Stratford separation criteria have proved to work very well even though they are based on incompressible flow; however, similar criteria or corrections to the existing criteria should be developed for compressible flow. In this same area, it has been observed in surface flow visualization studies that the separation line on a body exhibits characteristics of laminar, turbulent, and transitional flow. At the present time, the crossflow plane separation may be either laminar or turbulent but not transitional or a combination of laminar and turbulent. It may be possible to use surface flow visualization information to correlate the three separation regions on the body and build this feature into the prediction method.

REFERENCES

1. Spangler, S. B. and Mendenhall, M. R.: Further Studies of Aerodynamic Loads at Spin Entry. Report ONR CR212-225-3, U.S. Navy, June 30, 1977.

2. Mendenhall, M. R., Spangler, S. B., and Perkins, S. C., Jr.: Vortex Shedding from Circular and Noncircular Bodies at High Angles of Attack. AIAA Paper 79-0026, Jan. 1979.

3. Mendenhall, M. R.: Predicted Vortex Shedding from Noncircular Bodies in Supersonic Flow. J. Spacecraft & Rockets, Vol. 18, No. 5, Sept.-Oct. 1981, pp. 385-392.

4. Marshall, F. J. and Deffenbaugh, F. D.: Separated Flow Over Bodies of Revolution Using an Unsteady Discrete-Vorticity Cross Wake. NASA CR-2414, June 1974.

5. Deffenbaugh, F. D. and Koerner, W. G.: Asymmetric Wake Development and Associated Side Force on Missiles at High Angles of Attack. AIAA Paper 76-364, July 1976.

6. Mendenhall, M. R. and Nielsen, J. N.: Effect of Symmetrical Vortex Shedding on the Longitudinal Aerodynamic Characteristics of Wing-Body-Tail Combinations. NASA CR-2473, Jan. 1975.

7. Nielsen, J. N.: Missile Aerodynamics. McGraw-Hill Book Co., Inc., 1960.

8. Skulsky, R. S.: A Conformal Mapping Method to Predict Low-Speed Aerodynamic Characteristics of Arbitrary Slender Re-Entry Shapes. J. of Spacecaft, Vol. 3, No. 2, Feb. 1966.

9. Dillenius, M. F. E., Goodwin, F. K., and Nielsen, J. N.: Prediction of Supersonic Store Separation Characteristics. Vol. I - Theoretical Methods and Comparisons with Experiment. AFFDL-TR-76-41, Vol. I, May 1976.

10. Dillenius, M. F. E. and Nielsen, J. N.: Computer Programs for Calculating Pressure Distributions Including Vortex Effects on Supersonic Monoplane or Cruciform Wing-Body-Tail Combinations With Round or Elliptical Bodies. NASA CR-3122, Apr. 1979.

11. Woodward, F. A.: An Improved Method for the Aerodynamic Analysis of Wing-Body-Tail Configurations in Subsonic and Supersonic Flow. Part I - Theory and Application. NASA CR-2228, Part I, May 1973.

12. Woodward, F. A.: An Improved Method for the Aerodynamic Analysis of Wing-Body Tail Configurations in Subsonic and Supersonic Flow. Part II - Computer Program Description. NASA CR-2228, Part II, May 1973.

13. Cebeci, T., Mosinskis, G. J., and Smith, A. M. O.: Calculation of Viscous Drag and Turbulent Boundary-Layer Separation on Two-Dimensional and Axisymmetric Bodies in Incompressible Flow. McDonnell Douglas Rept. MDC JO 973-01 (Contract N00014-70-C-0099), Nov. 1970.

14. Stratford, B. S.: The Prediction of Separation of the Turbulent Boundary Layer. J. of Fluid Mech., Vol. 5, 1959, pp. 1-16.

15. Keener, E.: Oil-Flow Separation Patterns on an Ogive Forebody. NASA TM-81314, Oct. 1981.

16. Barger, R. L.: A Distributed Vortex Method for Computing the Vortex Field of a Missile. NASA TP-1183, June 1978.

17. Townsend, J. C., Collins, I. K., Howell, D. T., and Hayes, C.: Surface Pressure Data on a Series of Conical Forebodies at Mach Numbers From 1.70 to 4.50 and Combined Angles of Attack and Sideslip. NASA TM-78808, Mar. 1979.

18. Townsend, J. C., Howell, D. T., Collins, I. K., and Hayes, C.: Surface Pressure Data on a Series of Analytic Forebodies at Mach Numbers from 1.70 to 4.50 and Combined Angles of Attack and Sideslip. NASA TM-80062, June 1979.

19. Graves, E. B.: Aerodynamic Characteristics of a Monoplanar Missile Concept With Bodies of Circular and Elliptical Cross Sections. NASA TM-74079, Dec. 1977.

20. Oberkampf, W. L. and Bartell, T. J.: Supersonic Flow Measurements in the Body Vortex Wake of an Ogive Nose Cylinder. AFATL-TR-78-127, Nov. 1978,

21. Landrum E. J.: Wind-Tunnel Pressure Data at Mach Numbers from 1.6 to 4.63 for a Series of Bodies of Revolution at Angles of Attack From -4° to 60°. NASA TM X-3558, Oct. 1977.

22. Goodwin, F. K. and Dyer, C. L.: Data Report for an Extensive Store Separation Test Program Conducted at Supersonic Speeds. AFFDL-TR-79-3130, U.S. Air Force, Dec. 1979.

23. Allen, J. M. and Pittman, J. L.: Analysis of Surface Pressure Distributions on Two Elliptic Missile Configurations. AIAA Paper 83-1841, July 13-15, 1983.

24. Allen, J. M., Hernandez, G., and Lamb, M.: Body-Surface Pressure Data on Two Monoplane-Wing Missile Configurations With Elliptical Cross Sections at Mach 2.50. NASA TM-85645, 1983.

TABLE I - NOZVTX SUBROUTINE LIST

Subroutines	Subroutines
NOZVTX*	
AMAP	ITRATE
ASUM	NEWRAD
BDYGEN	PANEL
BMAP	PARTIN
BODPAN	PLOTA2
BODVEL	PLOTA5
BODYR	PLOTA6
CMAP	PLOTA7
COMBIN	PLOTA8
CONFIG	PLOTV
CONFOR	SEPRAT
DFEQKM	SHAPE
DIAGIN	SMOOTH
DOUBLT	SOLVE
DPHIDT	SORPAN
DTABLE	SOURCE
DZDNU	SRFVEL
ELNOSE	SUM
F	VCENTR
FLDVEL	VELCAL
FORCEP	VELCMP
FPVEL	VLOCTY
GEOM	VOLUME
INPT	VTABLE
INVERT	Z

*Main program.

TABLE II - SAMPLE CASES FOR PROGRAM NOZVTX

Sample Case	Ref.	Fig.	Body Cross Section	M_∞	α_c	ϕ	General Comments	Execution Time (CDC-CYBER 760)
1	19	14(a)	3:1 Ellipse	2.5	20°	0°	An elliptic missile body case with flow symmetry, panel symmetry; surface pressure calculation, vortex field plots at each axial station, and velocity field calculation at selected axial stations (TEST CASE).	8.6 sec.
2	19	14(b)	3:1 Ellipse	2.5	20°	0°	Restart of Sample Case 1	N/A
3	19	14(c)	3:1 Ellipse	2.5	20°	0°	Full run for missile body in Sample Case 1	--
4	19	14(d)	3:1 Ellipse	2.5	20°	45°	Same elliptic missile body from Sample Case 1; no flow symmetry, surface pressure calculation and vortex field plots at each axial station.	N/A
5	20	14(e)	Circle	2.0	15°	0°	An ogive cylinder body case with line sources and doublets, flow symmetry; surface pressure calculation and vortex field plots at each axial station, flow field calculation at selected axial stations.	15.5 sec.

Table II - Continued

Sample Case	Ref.	Fig.	Body Cross Section	M_∞	α_c	ϕ	General Comments	Execution Time (CDC-CYBER 760)
6	21	14(f)	Circle	1.6	0°	0°	An ogive cylinder body case with line sources and doublets and variable DX; surface pressure calculation and no separation.	6.0 sec.
7	18	14(g)	2:1 Ellipse	1.7	20.36°	0°	An elliptic cross section forebody with panel symmetry; surface pressure calculation and vortex field plots at each axial station.	28.1 sec.
8	18	14(h)	2:1 Ellipse	1.7	20.36°	0°	Same as Sample Case 6 with body panels tailored to the shape by specification of the central angles of the panel edges.	28.1 sec.
9	17	14(i)	3:1 Ellipse	1.7	20.35°	0°	An elliptic cross section conical forebody with panel symmetry, flow symmetry, and variable integration interval; surface pressure calculation with vortex smoothing.	61.8 sec.

Table II - Concluded

Sample Case	Ref.	Fig.	Body Cross Section	M_∞	α_c	ϕ	General Comments	Execution Time (CDC-CYBER 760)
10	18	14(j)	Lobed	1.7	20.36°	0°	A lobed cross section forebody case with left/right panel symmetry, flow symmetry, variable DX, and numerical mapping; surface pressure calculation with vortex smoothing.	47.0 sec.
11	22	14(k)	2:1 Ellipse	1.5	15°	0°	An elliptic cross section missile body with panel symmetry, flow symmetry; surface pressure calculation, periodic vortex field plots.	N/A

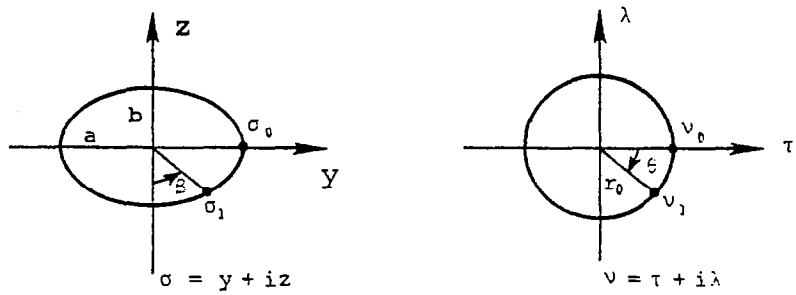

(a) Analytical transformation procedure

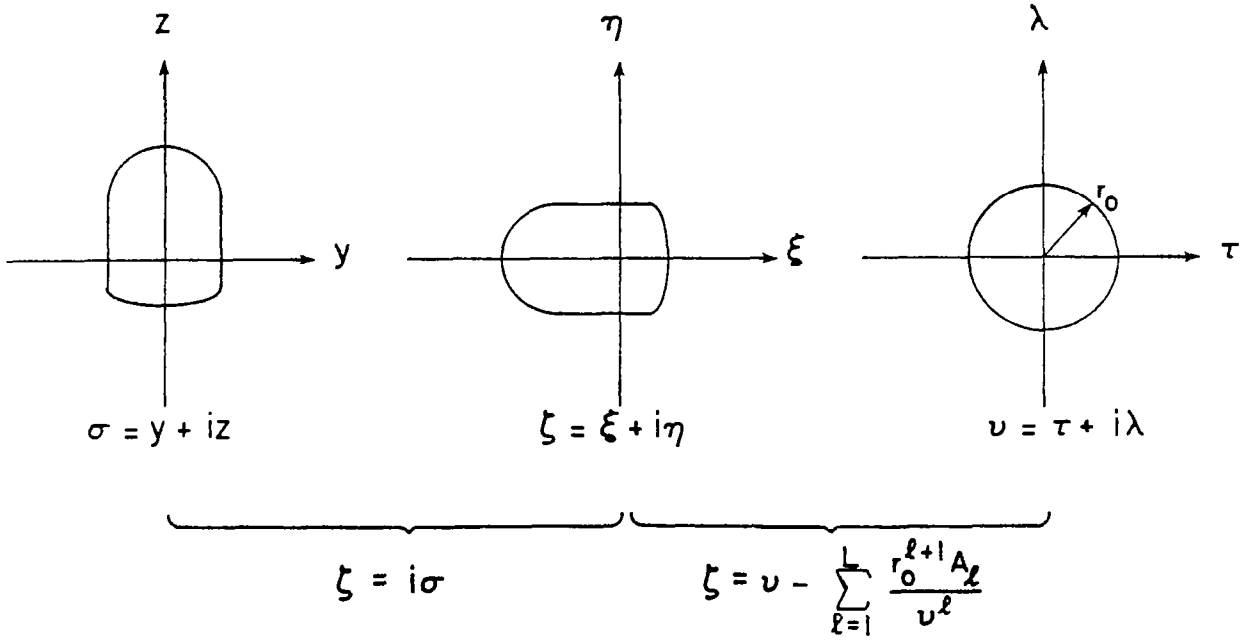

(b) Numerical transformation procedure

Figure 2.- Conformal mapping nomenclature.

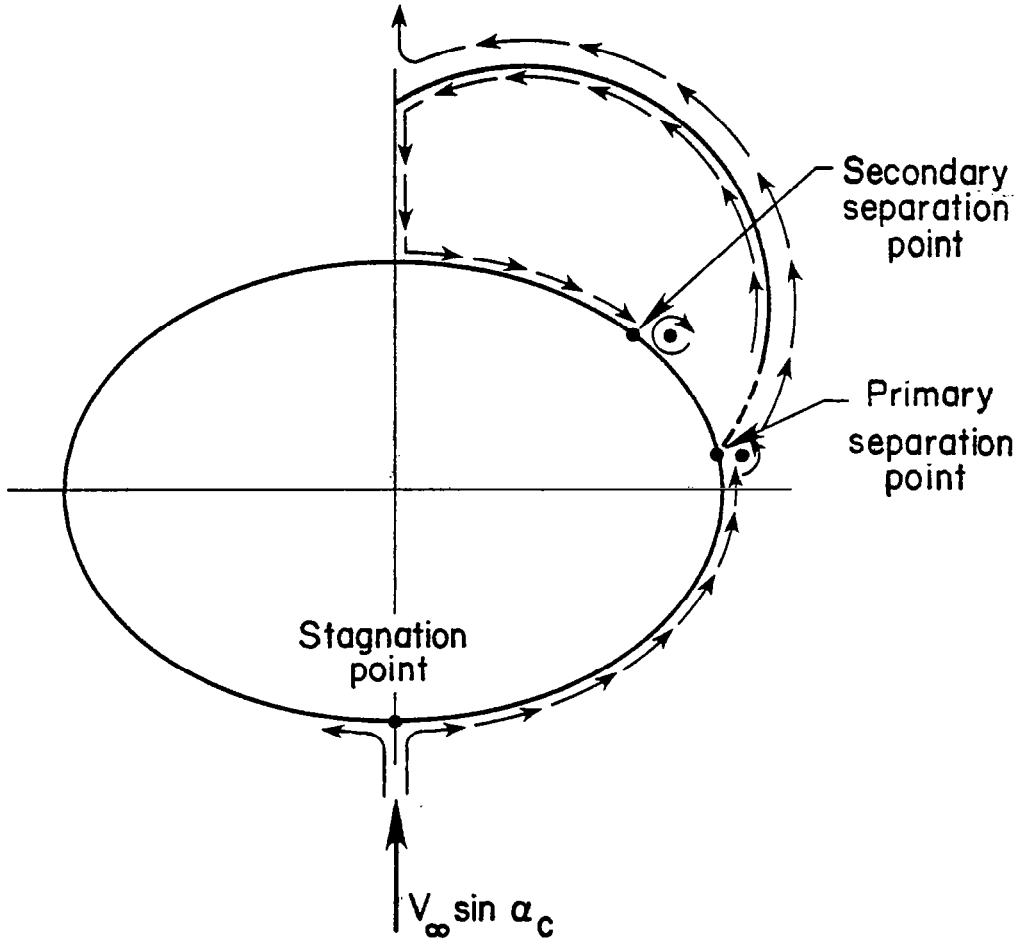

Figure 3. - Sketch of crossflow plane separation points.

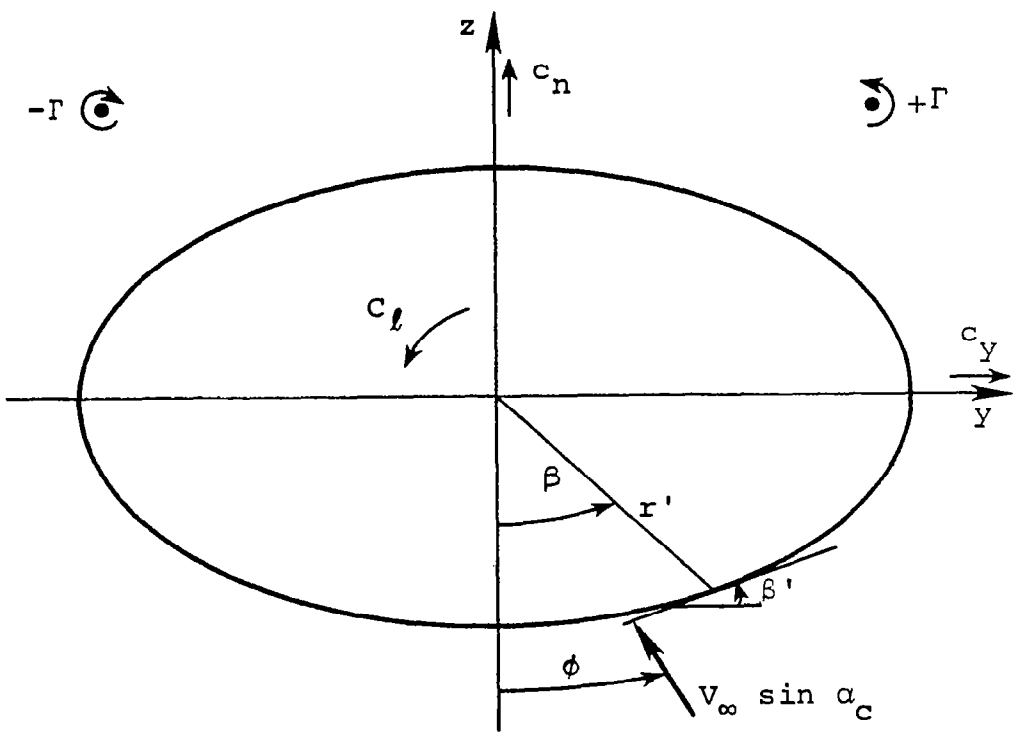

Figure 4. - Body crossflow plane nomenclature.

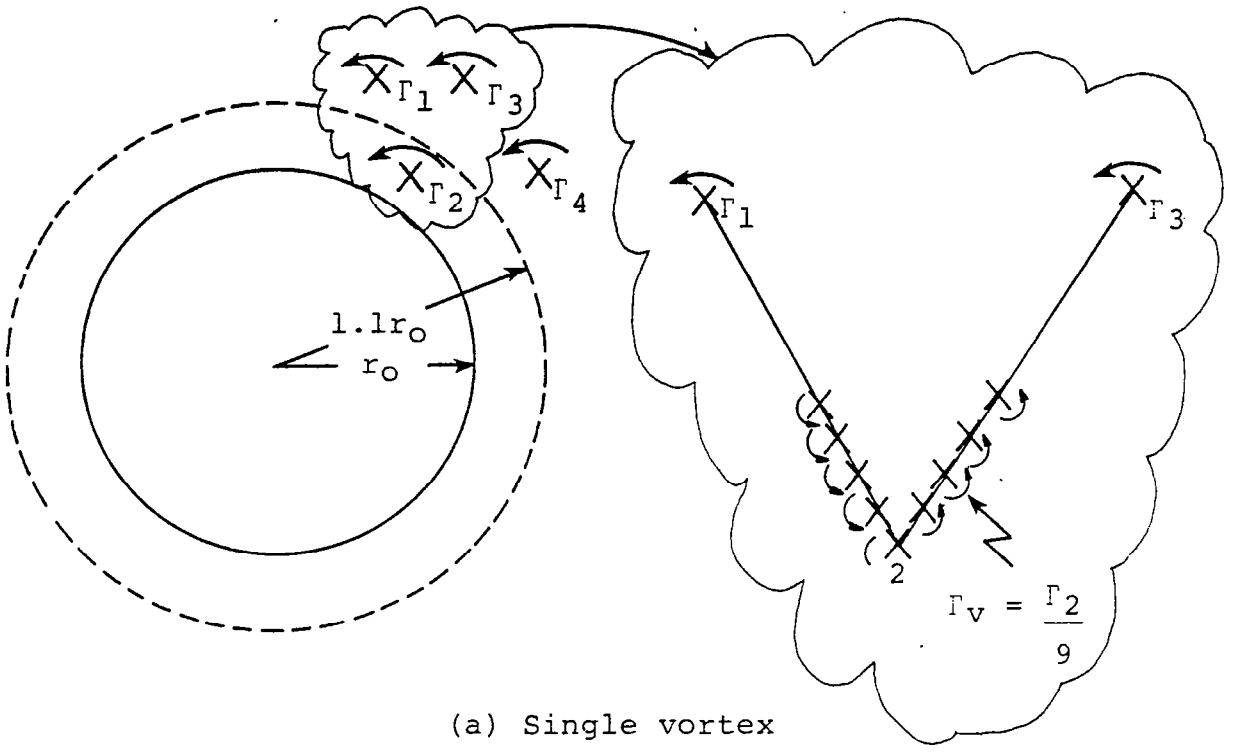

(a) Single vortex

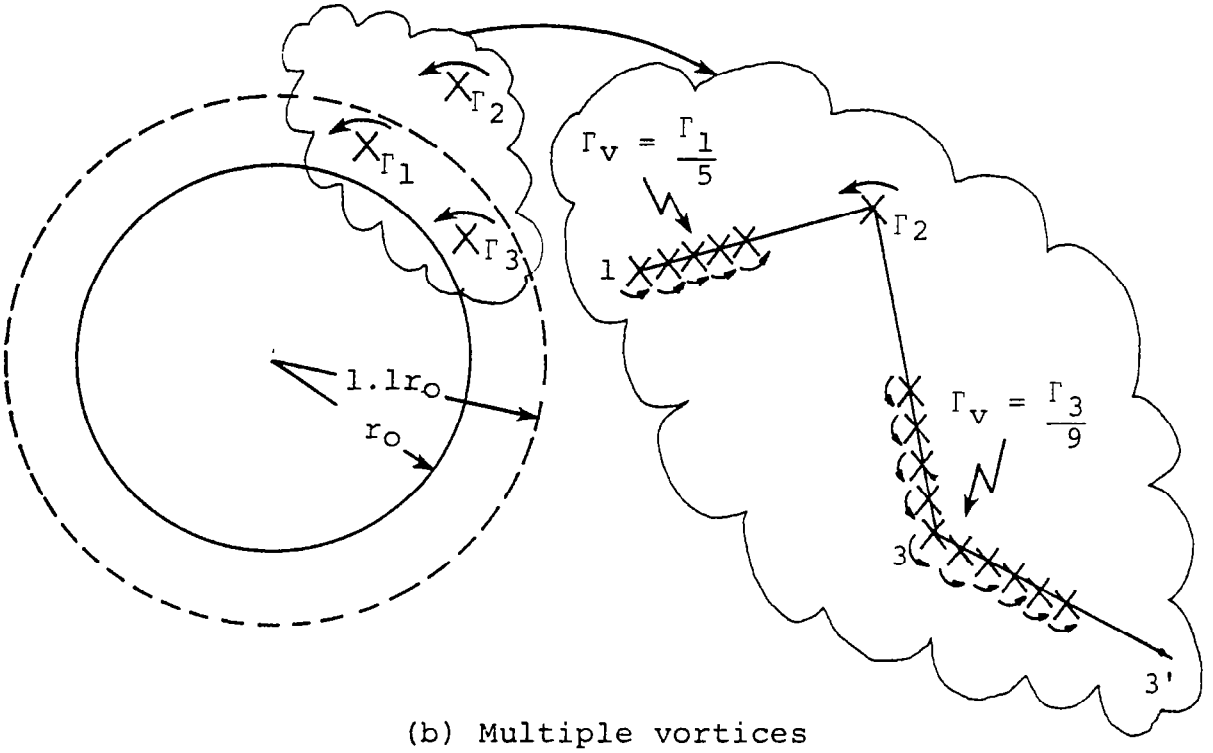

(b) Multiple vortices

Figure 5.- Vortex smoothing procedure.

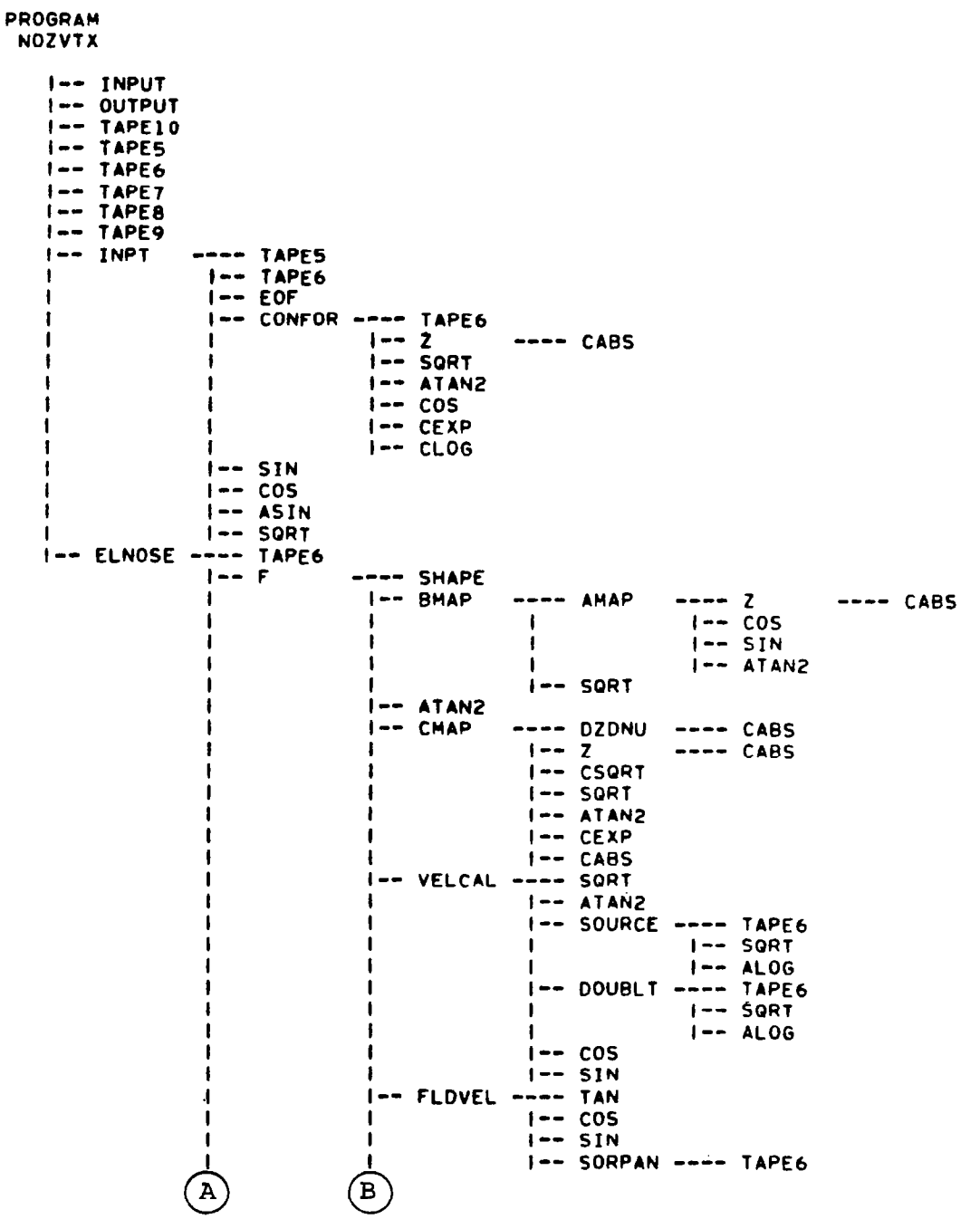

(a) Page 1

Figure 6.- Flow map of program NOZVTX.

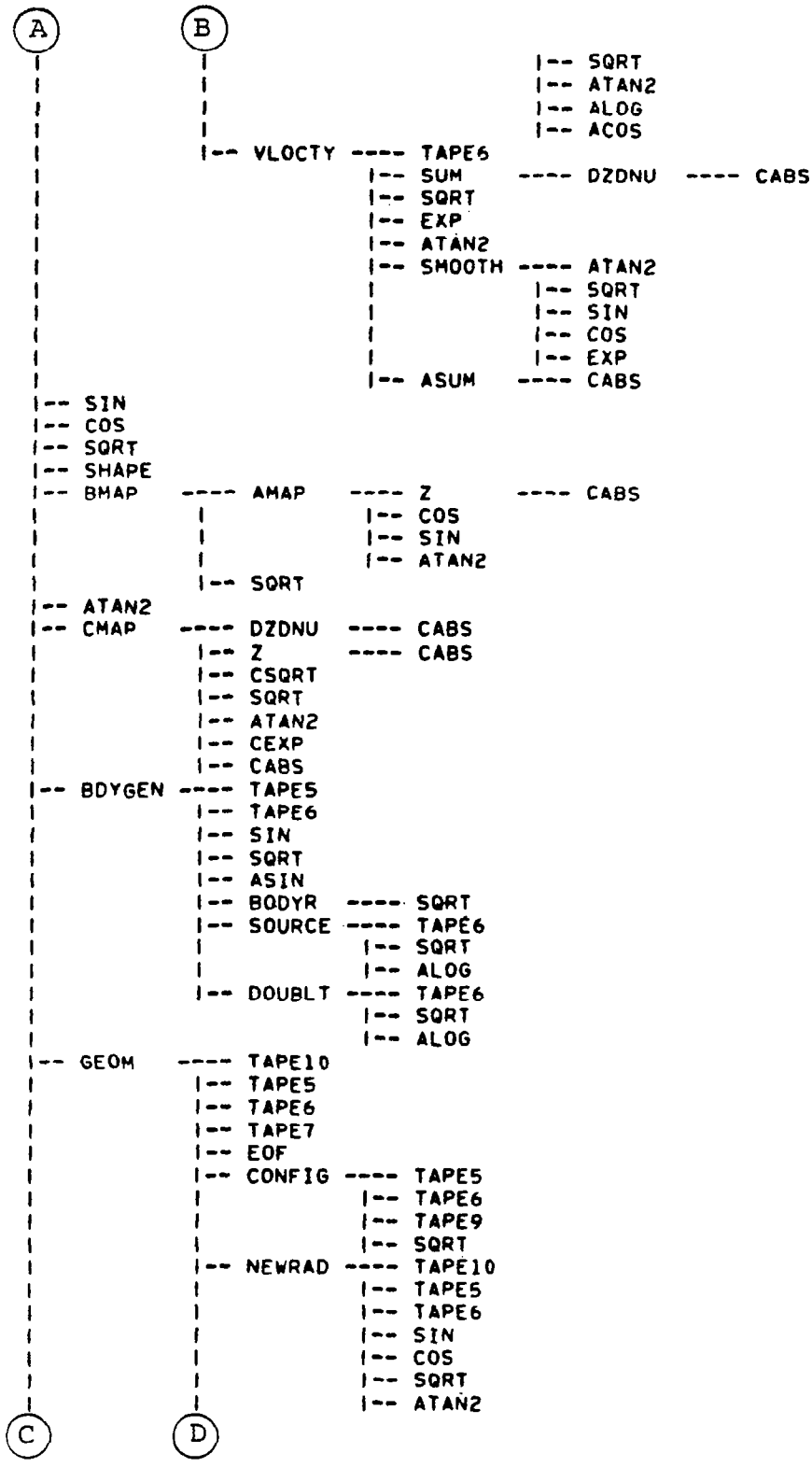

(b) Page 2

Figure 6.- Continued.

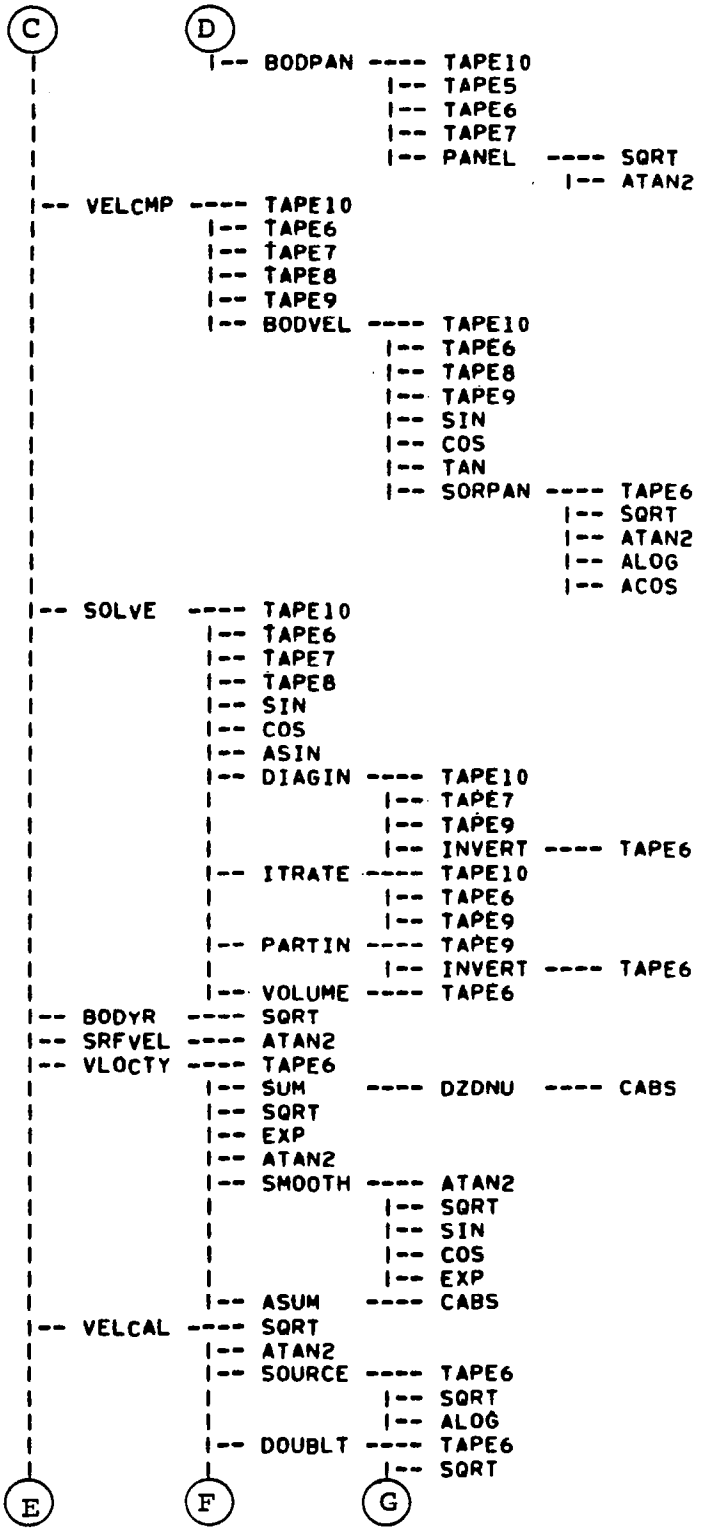

(c) Page 3

Figure 6.- Continued.

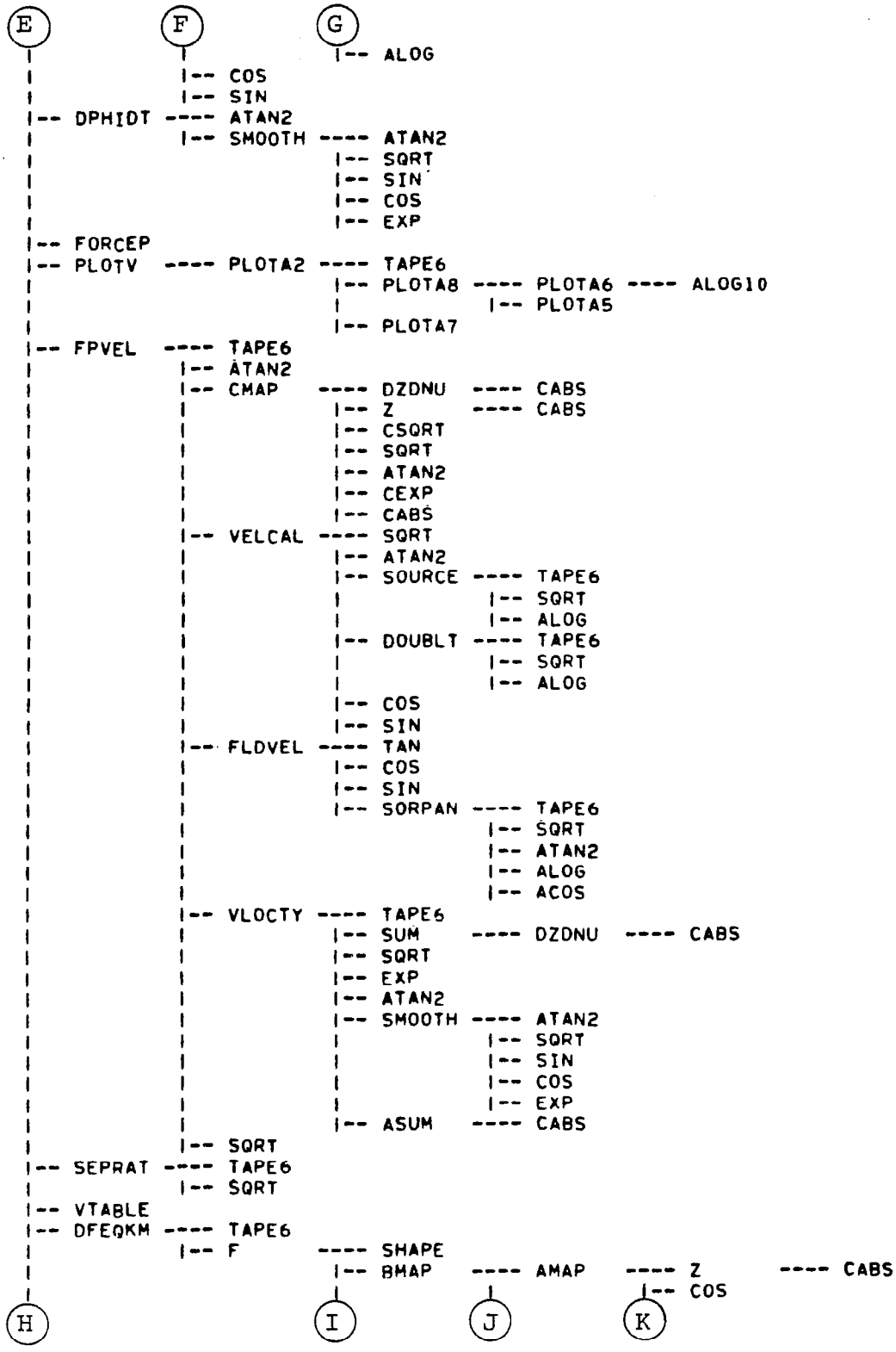

(d) Page 4

Figure 6.- Continued.

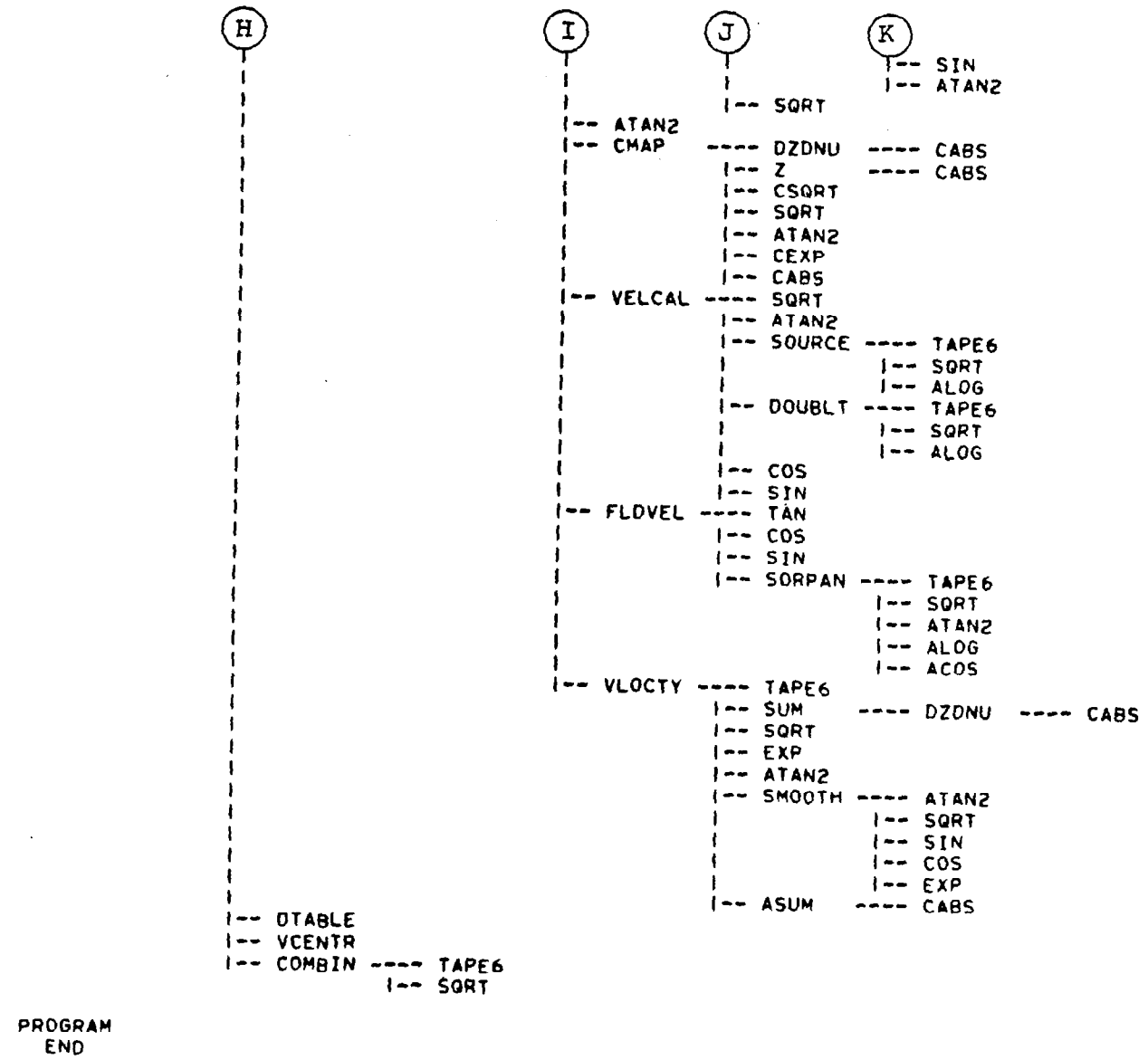

(e) Page 5

Figure 6.- Concluded.

SUBROUTINE NAME / EXTERNAL REFERENCES	AMAP	ASUM	BDYGEN	BMAP	BODPAN	BODOVER	BODVEL	BODYR	CABS	CEXP	CLOG	CMAP	COMBIN	CONFIG	CONFOR	COS	CSQRT	DFEQKM	DIAGIN	DOUBLT	DPHIDT	DTABLE	DZDNU	ELNOSE	EOF	EXP
ACOS																										
ALOG10																										
ALOG																										
AMAP				X																						
ASIN			X																							
ASUM																										
ATAN2	X					X				X	X															
BDYGEN																										
BMAP																										
BODPAN																										
BODVEL																										
BODYR			X																							
CABS		X				X																				
CEXP						X																				
CLOG						X																				
CMAP																										
COMBIN																										
CONFIG																										
CONFOR																										
COS	X					X				X	X															
CSQRT																										
DFEQKM																										
DIAGIN																										
DOUBLT																										
DPHIDT																										
DTABLE																										
DZDNU																										
ELNOSE																										
EOF																										
EXP																										

(a) Page 1

Figure 7.- Subroutine Cross Reference Table for Program NOZVTX.

SUBROUTINE NAME / EXTERNAL REFERENCES	AMAP	ASUM	BDYGEN	BMAP	BODPAN	BODVEL	BODYER	CMAP	COMBIN	CONFIG	CONFOR	DFEQKM	DIAGIN	DOUBLT	DPHIDT	DTABLE	DZDNU	ELNOSE	FLDVEL	FORCEP
FLDVEL																				
FORCEP																		X		
FPVEL																		X		
F												X						X		
GEOM																		X		
INPT																				
INPUT																				
INVERT													X							
ITRATE																				
NEWRAD																				
OUTPUT																				
PANEL					X															
PARTIN																				
PLOTA2																				
PLOTA5																				
PLOTA6																				
PLOTA7																				
PLOTA8																				
PLOTV																		X		
SEPRAT																		X		
SHAPE																		X		
SIN	X		X			X												X	X	
SMOOTH															X					
SOLVE																		X		
SORPAN						X													X	
SOURCE			X																	
SQRT			X	X			X	X	X	X	X			X				X		
SRFVEL																		X		
SUM																				
TAN						X													X	

SUBROUTINE NAME / EXTERNAL REFERENCES	FPVEL	F	GEOM	INPT	INVERT	ITRATE	NEWRAD	NOZVTX	PÂNEL	PÂRTÎN	PLOTÂ2	PLOTÂ5	PLOTÂ6	PLOTÂ7	PLOTÂ8	PLOTV	SEPRAT	SHAPE	SMOOTH	SOLVE
FLDVEL	X	X																		
FORCEP																				
FPVEL																				
F																				
GEOM																				
INPT								X												
INPUT								X												
INVERT										X										
ITRATE																				X
NEWRAD			X																	
OUTPUT								X												
PANEL																				
PARTIN																				X
PLOTA2																X				
PLOTA5															X					
PLOTA6															X					
PLOTA7											X									
PLOTA8											X									
PLOTV																				
SEPRAT																				
SHAPE		X																		
SIN				X			X												X	X
SMOOTH																				
SOLVE																				
SORPAN																				
SOURCE																				
SQRT	X			X			X		X								X		X	
SRFVEL																				
SUM																				
TAN																				

(b) Page 2

Figure 7.- Continued.

SUBROUTINE NAME / EXTERNAL REFERENCES	AMAP	ASUM	BDYGEN	BMAP	BODPAN	BODVEL	BODYER	COMAP	COMBIN	CONFIG	COFORM	DFEQK	DIAGNL	DOUBLT	DPHIDT	DTABLE	DZDNUS	ELNOSE	FLDVEL	FORCEP	FPVEL	GEOM	INPUT	INVERT	INTERAT	NEWRED	NOZVTX	PANEL	PÅRTIN	PLOTÅ2	PLOTÅ5	PLOTÅ6	PLOTÅ7	PLOTÅ8	PLOTV	SEPART	SHAPET	SMOOTH	SOLVE
TAPE10				X		X							X									X			X	X	X											X
TAPE5			X		X					X												X	X			X	X											
TAPE6			X		X	X			X	X	X	X		X				X			X	X	X	X	X	X	X		X						X		X	
TAPE7					X								X									X				X											X	
TAPER						X																				X											X	
TAPE9						X				X			X												X		X		X									
VCENTR																		X																				
VELCAL																		X			X	X																
VELCMP																		X																				
VLOCTY																		X			X	X																
VOLUME																																						X
VTABLE																		X																				
Z	X						X				X																											

(c) Page 3

Figure 7.- Continued.

SUBROUTINE NAME / EXTERNAL REFERENCES	SORPACE	SSORUFV	SSRUMEL	VCENTR	VVECLAM	VVELLCP	VLOCMTY	VOLUME	VTABLE	Z
ACOS	X									
ALOG10										
ALOG	X	X								
AMAP										
ASIN										
ASUM							X			
ATAN2	X		X		X		X			
BDYGEN										
BMAP										
BODPAN										
BODVEL						X				
BODYR										
CABS										X
CEXP										
CLOG										
CMAP										
COMBIN										
CONFIG										
CONFOR										
COS						X				
CSQRT										
DFEQKM										
DIAGIN										
DOUBLT						X				
DPHIDT										
DTABLE										
DZDNU				X						
ELNOSE										
EOF										
EXP							X			

(d) Page 4

Figure 7.- Continued.

SUBROUTINE NAME / EXTERNAL REFERENCES	SORPAN	SOURCE	SRFVEL	SUM	VECTOR	VELCAM	VELCMP	VELOCY	VOLUME	VTABLE	Z
FLOVEL											
FORCEP											
FPVEL											
F											
GEOM											
INPT											
INPUT											
INVERT											
ITRATE											
NEWRAD											
OUTPUT											
PANEL											
PARTIN											
PLOTA2											
PLOTA5											
PLOTA6											
PLOTA7											
PLOTA8											
PLOTV											
SEPRAT											
SHAPE											
SIN						X					
SMOOTH								X			
SOLVE											
SORPAN											
SOURCE						X					
SQRT	X	X				X		X			
SRFVEL											
SUM								X			
TAN											

(e) Page 5

Figure 7.- Continued.

SUBROUTINE NAME / EXTERNAL REFERENCES	SPARNE	SOURCE	SRFVEL	SUMVEL	VCENTR	VELCAL	VELCMP	VLOCTY	VOLUME	VTABLE	Z
TAPE10					X						
TAPE5											
TAPE6	X	X			X	X	X				
TAPE7					X						
TAPE8					X						
TAPE9					X						
VCENTR											
VELCAL											
VELCMP											
VLOCTY											
VOLUME											
VTABLE											
Z											

(f) Page 6

Figure 7.- Concluded.

SUBROUTINE NAME / COMMON BLOCKS	AMAP	ASUM	BDYGEN	BMAP	BODPAN	BODVEL	BODYER	COMAP	COMBIN	CONFIG	CONFORM	DFEQK	DIAGMN	DOBLNT	DPHIDT	DTABLE	DZDNUSE	ELNOSEL	FLDVEL	FORCEP	FPVEL	GEOM	INPT	INVERT	INTRARTED	NEWZVTX	NOZVTX	PANETIN	PLOT0TÀ2	PLOT0TÀ5	PLOT0TÀ6	PLOT0TÀ7	PLOT0TÀ8	PLOTV	SEPRAT	SHAPE	SMOOTH	SOLVE
BLREV																	X						X												X			
BLSEP																	X						X												X			
BODCOM						X												X																				
BODYGN			X																				X															
BPLTA1																													X			X	X					
BPLTA2																													X									
BSCALE																													X				X		X			
BTHET				X		X																																
BVEL																																						
CBODY																	X						X															
CFLAG														X			X						X															
CFLT																	X						X															
CLDS																	X									X												
CNTROD																	X																					
CONF							X				X												X													X		
CONST	X			X			X				X			X			X		X	X			X		X											X		
COP																	X						X															
CTRANS			X																																		
CVRTX																	X									X												
DYDX								X						X		X	X						X															
DZDX								X						X		X	X						X															
EXTRA																	X																			X		
FLOW														X			X			X			X													X		
HEAD																						X															
ITERAT																						X			X												
JOPTNS				X		X			X								X	X				X			X											X		X
LIMITS														X			X																			X		
LOADP																	X		X				X															
MAPB	X		X					X									X		X	X																	
MAPC	X		X					X									X		X	X																	

(a) Page 1

Figure 8.- Common Block Cross Reference Table for Program NOZVTX.

SUBROUTINE NAME / COMMON BLOCKS	AMAP	ASUM	BDYGEN	BMAP	BODPAN	BOODVEL	BOOYR	CMAP	COMBIN	CONFIG	CONFORM	DEQKMN	DFIELD	DGAIN	DIAGBLT	DUPLIDT	DTABLE	DZDNUS	ELNOSE	FLDVELP	FLORCEE	FPVEL	GEOM	INPUT	INVERT	INTRWARTED	NEWZVEX	NOATVL	PARAMETN	PLOTAA1	PLOTAA2	PLOTAA5	PLOTAA6	PLOTAA7	PLOTAA8	PLOTVT	SEPARAT	SHAPE	SMOOTH	SOLVE
MAPNTH				X																				X															
MAPN	X	X		X				X			X							X					X													X			
MAPP	X							X			X							X					X													X			
MAPX																			X				X																
MAP1	X	X		X				X			X					X		X	X		X	X	X													X	X	X	
MAP2				X															X		X			X											X	X			
MATCOM																																							X
NEWCOM				X		X														X			X			X													X
ONE			X																																				
PARAM			X	X		X				X				X					X				X						X										X
PHI																X			X																			X	
POINT				X		X							X							X										X	X			X				X
PRESS																			X		X															X			
PRINT			X																																				
REF																			X		X			X												X	X		X	
RZZZ																								X													X			
SEG																							X																	
SHPE																			X					X													X			
SMOOTH																X			X																					
SPSANG			X																																				
STACK			X																																				
SYMTRY																			X			X		X												X			
TRANS																								X																
TWO			X				X								X																									
VELCOM				X		X								X						X				X															X
VEL																X			X			X		X													X			
VFPTS																			X			X		X																
VORTEX									X							X		X	X	X			X	X												X		X		
VSTART																			X																			X		
VTXTBL									X									X	X					X												X		X		

(b) Page 2

Figure 8.- Continued.

SUBROUTINE NAME / COMMON BLOCKS	AMAP	ASUM	BOYGEN	BMAP	BODPAN	BODVEL	BODYR	CMAP	COMBIN	CONFIG	CONFOR	DEQMN	DIAGNT	DOBUT	DOPHID	DTADBLE	DZDNU	ELNOSE	FLDVEL	FLORCEP	FPVEL	FEOM	GENOM	INPT	INVERT	INTRATED	NWRXT	NOVEL	PANET	PARTIN	PLOTAA2	PLOTAA5	PLOTAA6	PLOTAA7	PLOTAA8	PLOTVT	PLOTRAT	SEPAE	SHAPETH	SMOOTH	SOLVE
WBTR1			X															X																							
WBTR			X																																						
ZFLOW																		X						X													X				
/ /	X				X	X				X	X									X		X				X X		X X												X	

(c) Page 3

Figure 8.- Continued.

SUBROUTINE NAME / COMMON BLOCKS	SPACE	SOURCE	SRFVEL	SUM	VCENTR	VELCAL	VVELCMP	VLOCTY	VOLUME	VTABLE	Z
BLREV											
BLSEP											
BODCOM	X										
BODYGN											
BPLTA1											
BPLTA2											
BSCALE											
BTHET											
BVEL						X					
CBODY											
CFLAG								X			
CFLT											
CLDS											
CNTROD					X						
CONF											
CONST								X			
COP											
CTRANS											
CVRTX					X						
DYDX											
DZDX											
EXTRA											
FLOW								X			
HEAD											
ITERAT											
JOPTNS							X		X		
LIMITS								X			
LOADP											
MAPB											
MAPC											

(d) Page 4

Figure 8.- Continued.

SUBROUTINE NAME / COMMON BLOCKS	SPACE	SOURCE	SRFVEL	SUM	VCENTR	VELCOM	VELCOM	VELCOM	VOLUME	VTABLE	Z
MAPNTH											
MAPN											X
MAPP											X
MAPX											
MAP1				X				X			X
MAP2											
MATCOM							X				
NEWCOM			X				X		X		
ONE						X					
PARAM			X				X		X		
PHI								X			
POINT			X				X				
PRESS											
PRINT											
REF								X			
RZZZ											
SEG							X				
SHPE											
SMOOTH								X			
SPSANG											
STACK						X					
SYMTRY											
TRANS							X				
TWO		X				X					
VELCOM							X				
VEL								X			
VFPTS											
VORTEX					X			X		X	
VSTART											
VTXTBL					X			X		X	

(e) Page 5

Figure 8.- Continued.

SUBROUTINE NAME / COMMON BLOCKS	SSORPAN	SSURFCE	SSURFVL	SVCENTR	VVELCAL	VVELCMP	VVELOCTY	VVOLUME	VTABLE	Z
WBTR1										
WBTR										
ZFLOW										
/ /			X			X		X		

(f) Page 6

Figure 8.- Concluded.

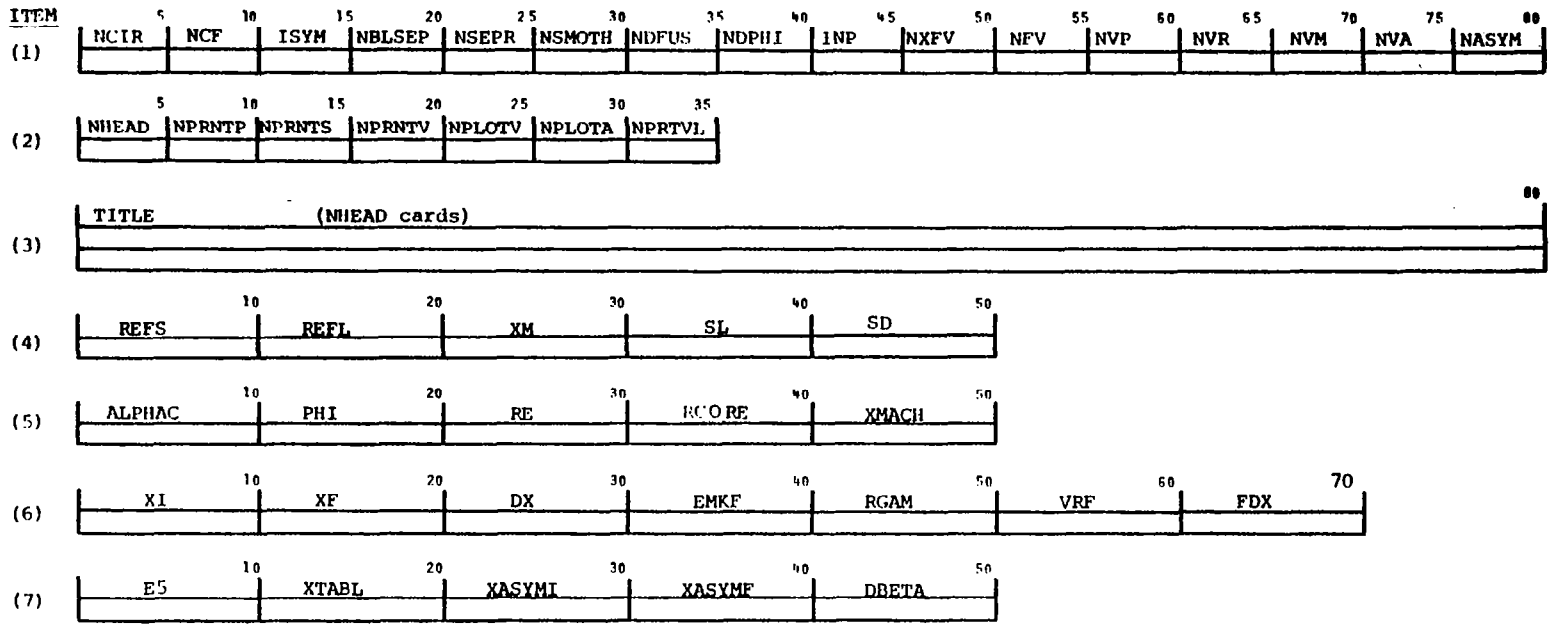

(a) Page 1

Figure 9.- Input forms for Program NOZVTX.

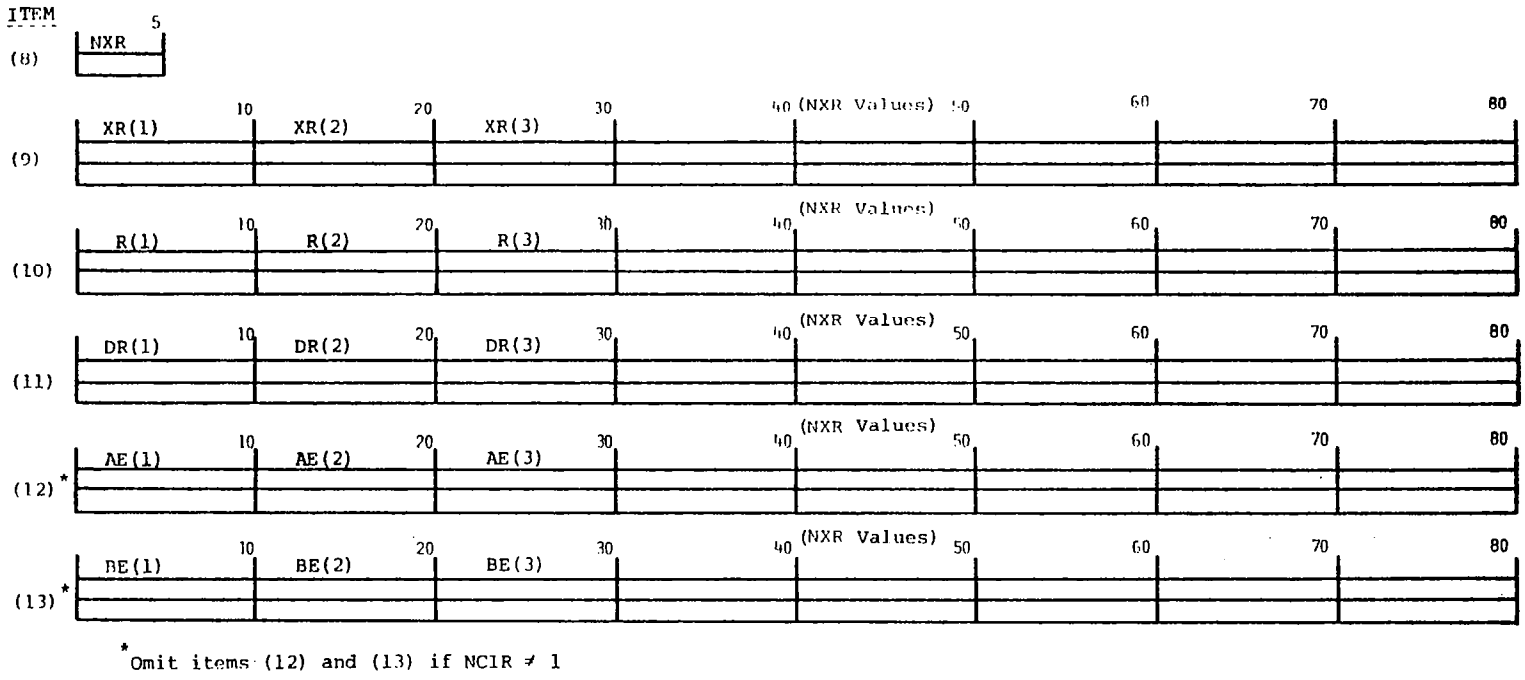

*Omit items (12) and (13) if NC1R ≠ 1

(b) Page 2

Figure 9.- Continued.

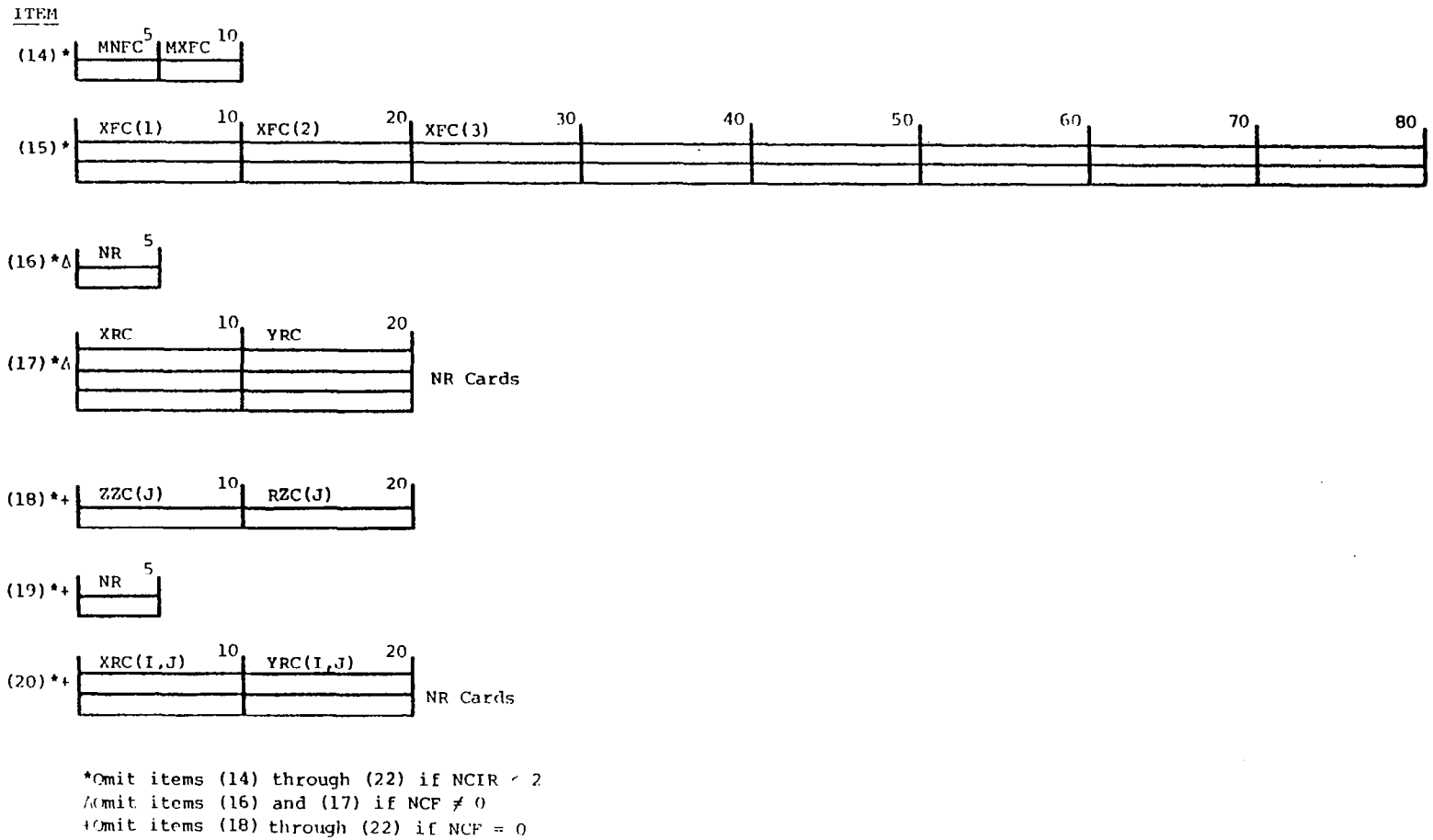

(c) Page 3

Figure 9.- Continued.

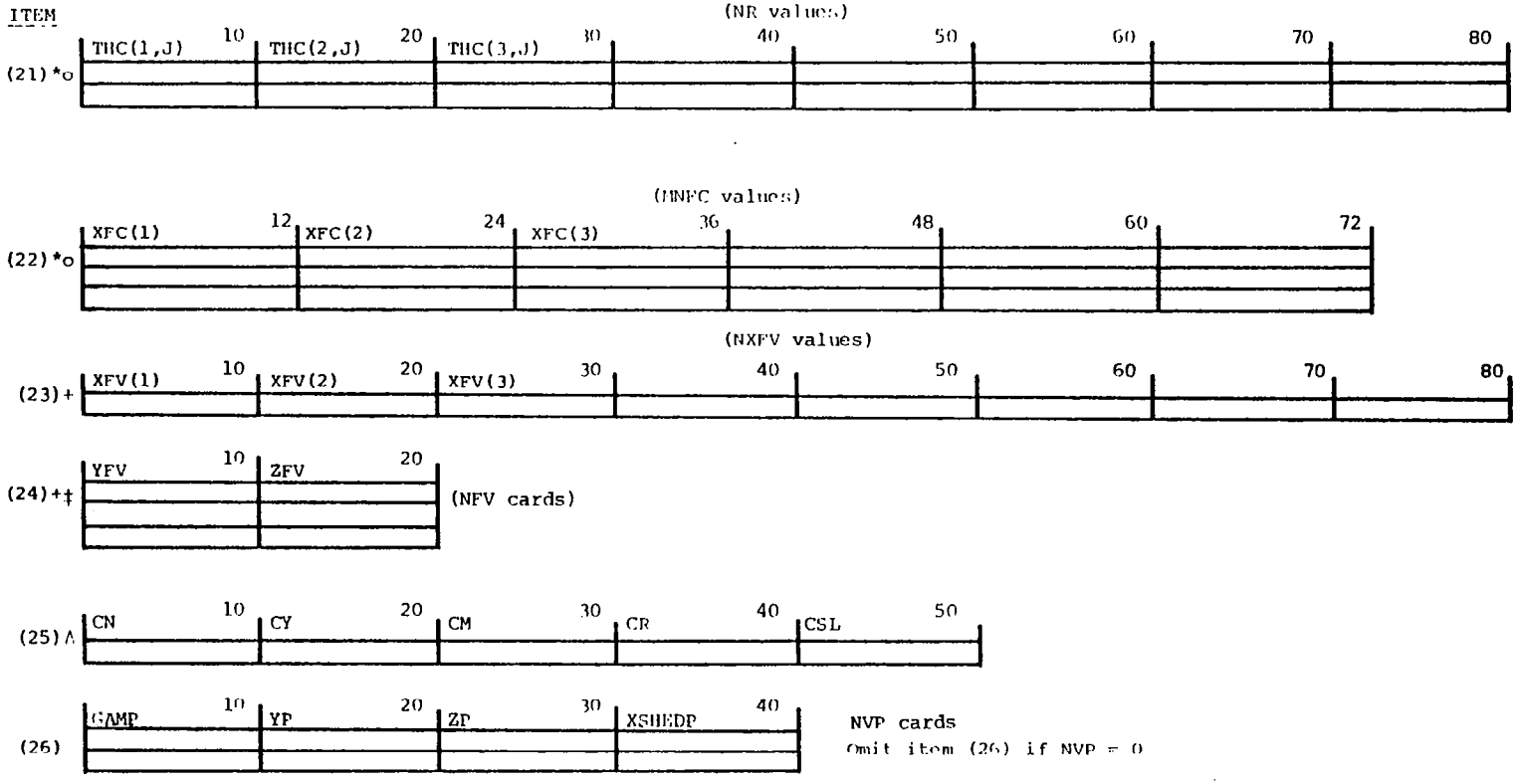

ΔOmit items (25) through (29) if NVP + NVR + NVM + NVA = 0
+Omit items (23), (24) if NXFV = 0
‡Omit item (24) if NFV = 0
*Omit items (21), (22) if NCIR < 2
oOmit items (21), (22) if NCF = 0

(d) Page 4

Figure 9.- Continued.

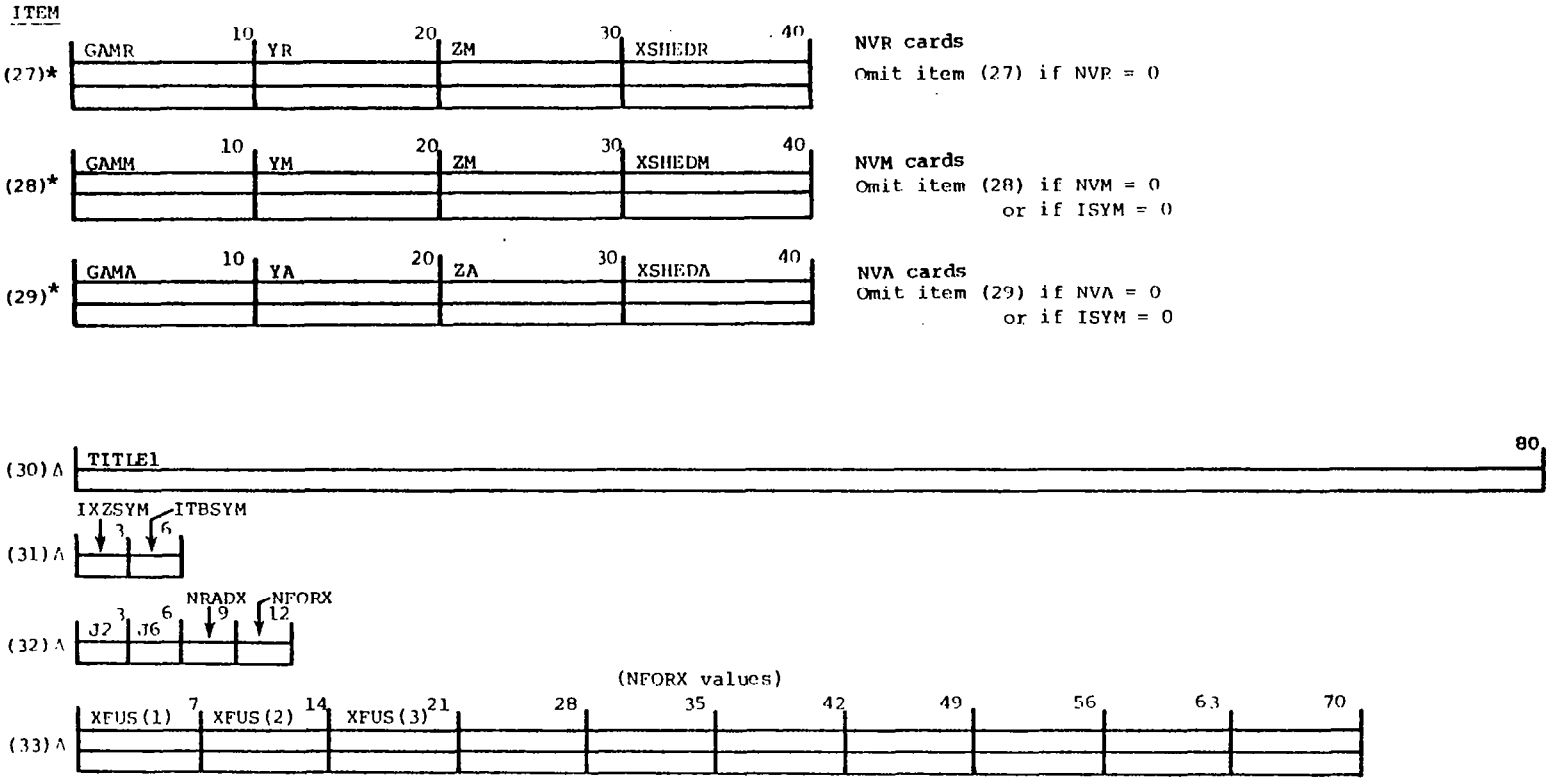

ΔOmit items (30)-(43) if NCIR = 0
*Omit items (27),(28),(29) if
NVP + NVR + NVM + NVA = 0

(e) Page 5

Figure 9.- Continued.

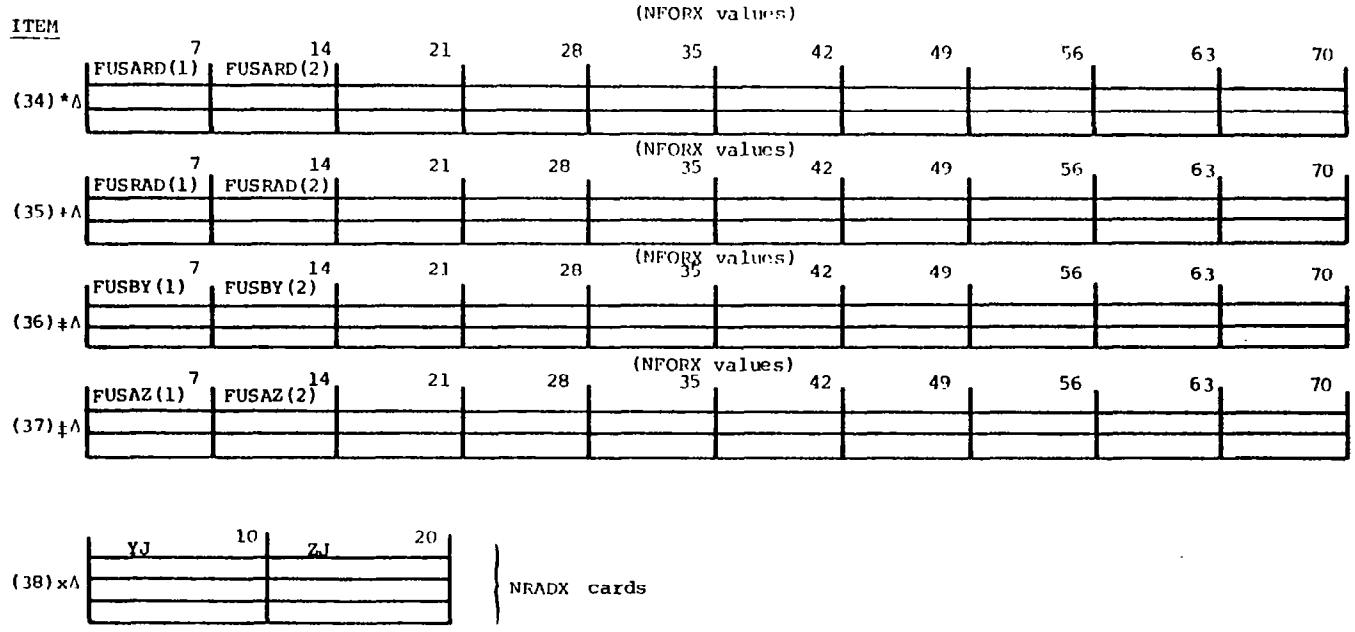

*Omit item (34) if J2 ≠ -1

+Omit item (35) if J2 ≠ -2

‡Omit items (36), (37) if J2 ≠ -3

x { Omit item (38) if J2 ≠ 1
  { Repeat item (38) NFORX times

ΛOmit items (34)-(43) if NCIR = 0

(f) Page 6

Figure 9.- Continued.

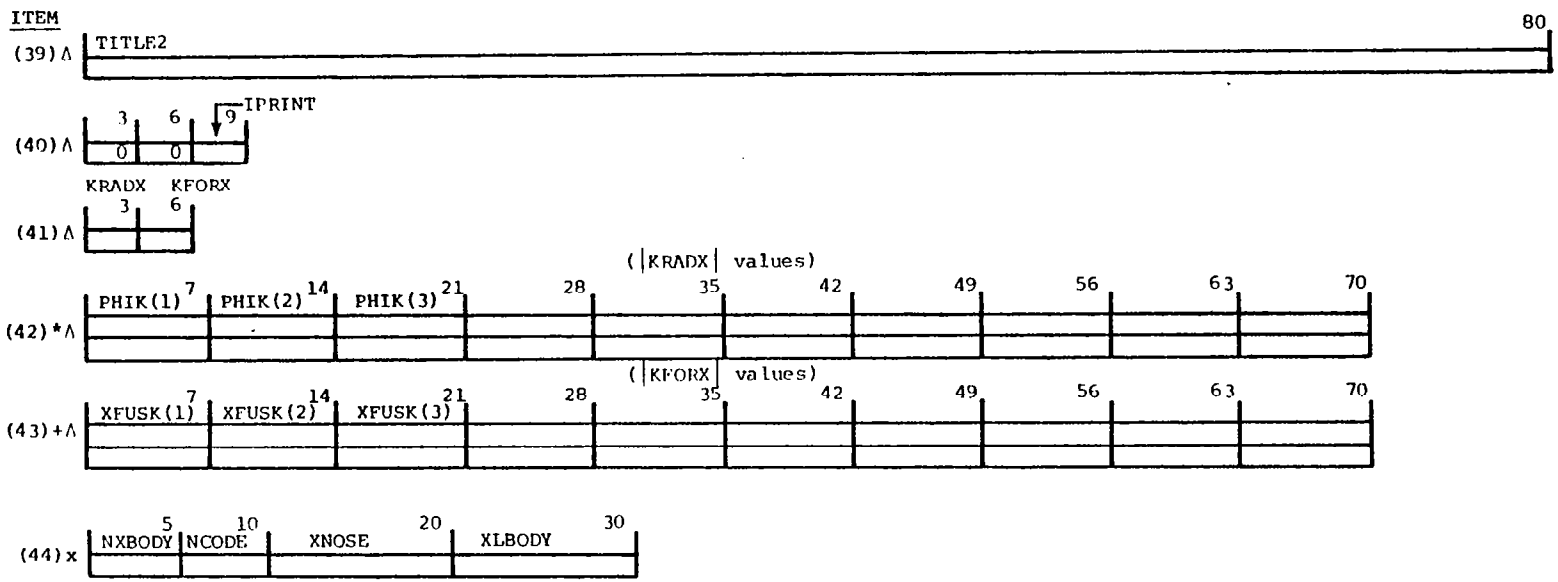

*Omit item (42) if KRADX ≥ 0

+Omit item (43) if KFORX = 0

ΛOmit items (39)-(43) if NCIR = 0

xOmit item (44) if NCIR ≠ 0

(g) Page 7

Figure 9.- Concluded.

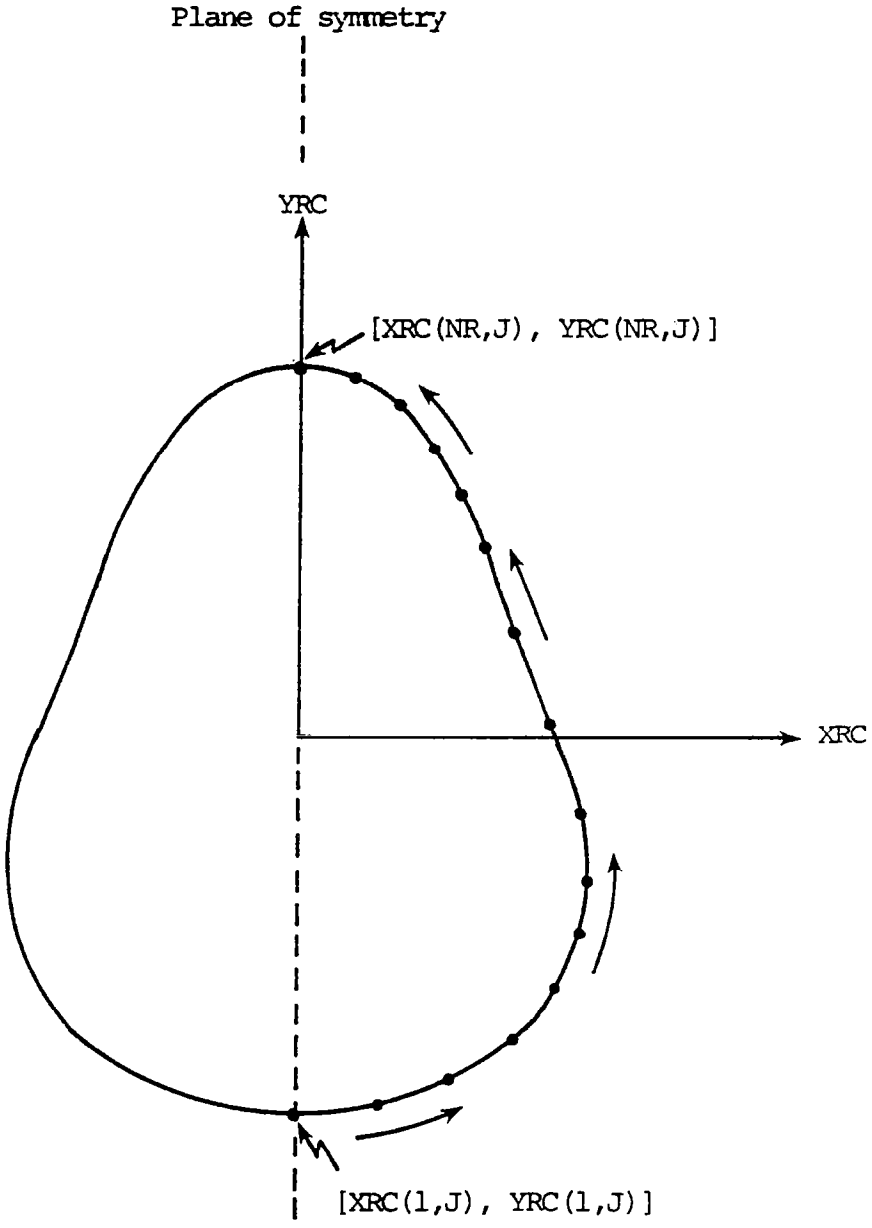

Figure 10.- Convention for ordering coordinates for a noncircular cross section at X = XFC(J).

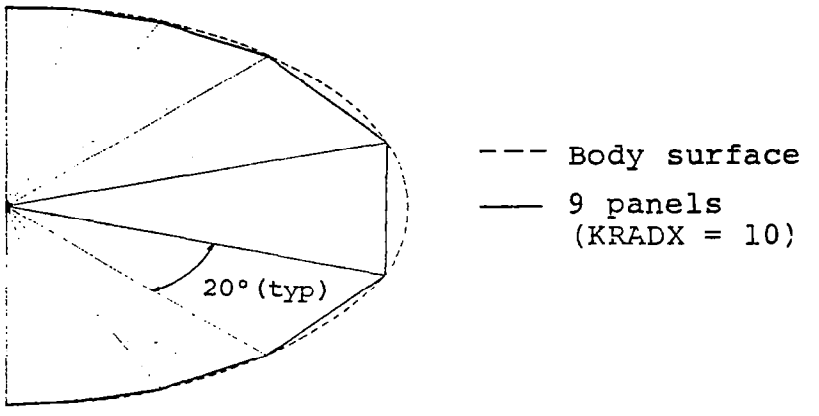

(a) 9 panels, equal spacing

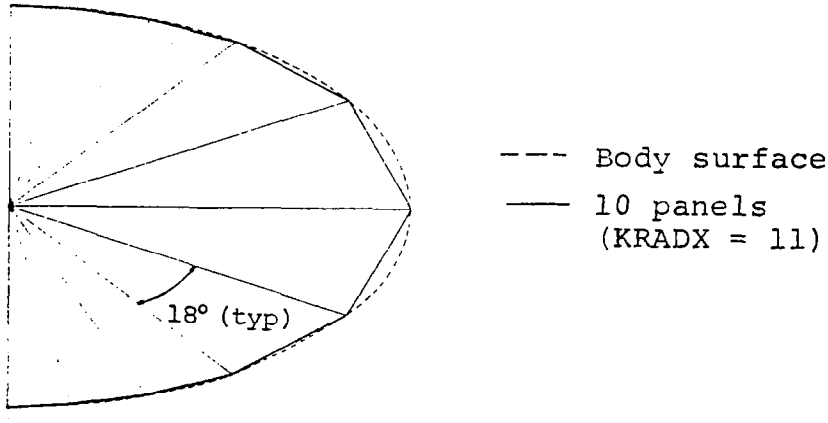

(b) 10 panels, equal spacing

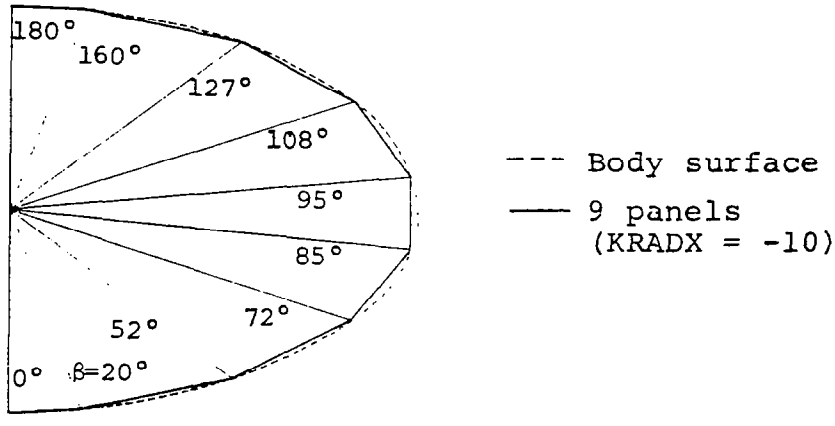

(c) 9 panels, custom spacing

Figure 11.- Panel layout on a 2:1 elliptic cross section.

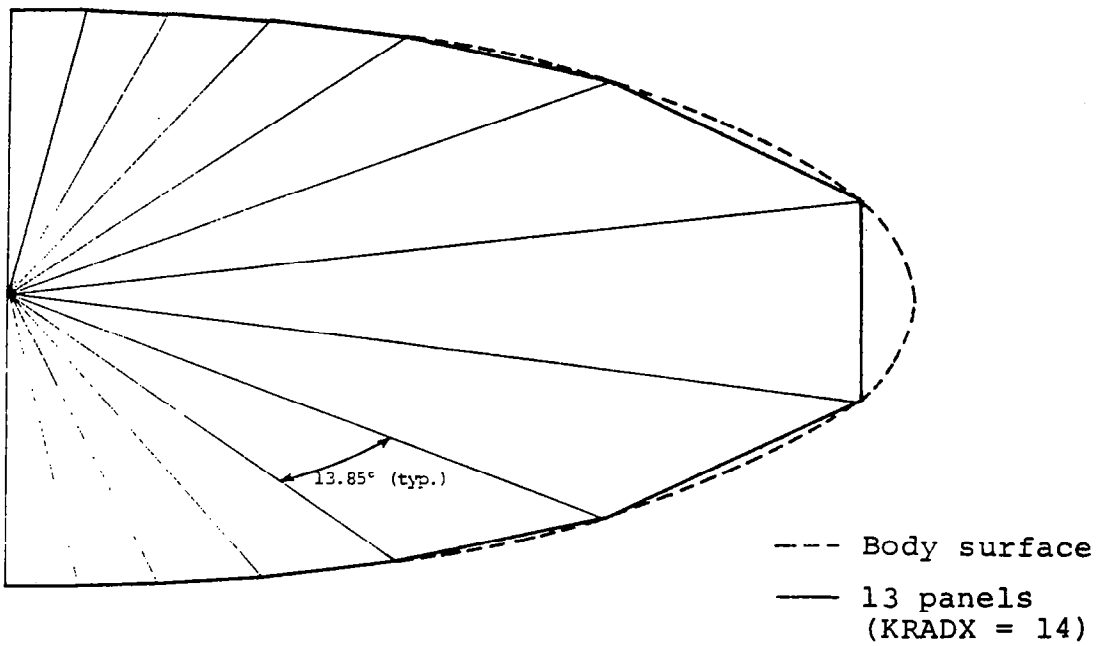

(a) 13 panels, equal spacing

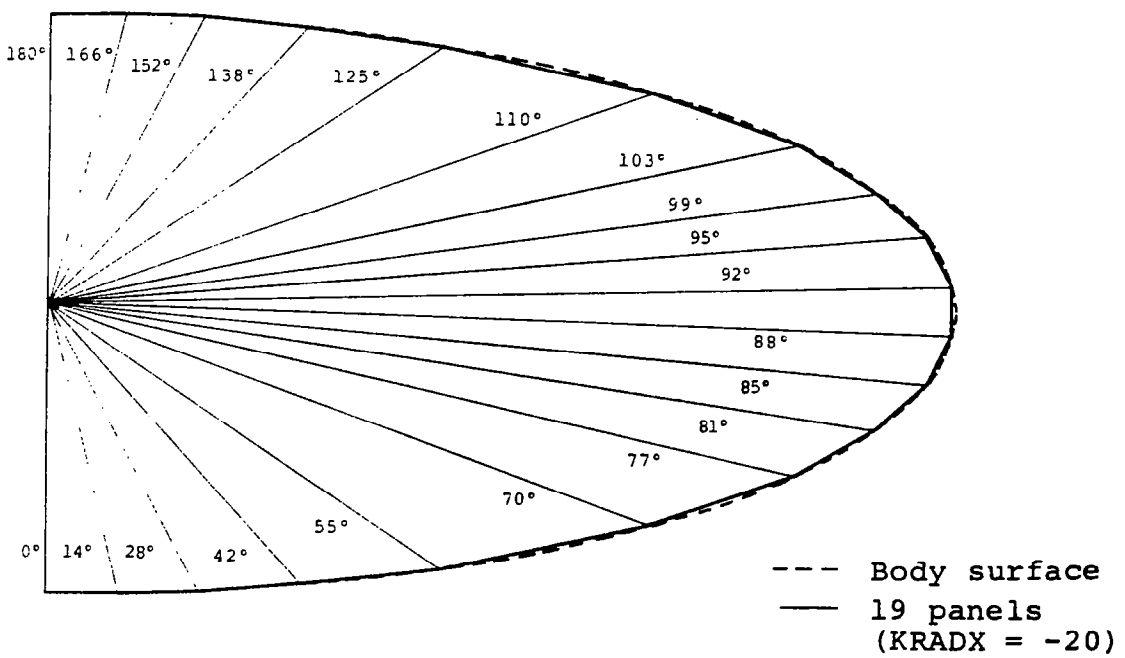

(b) 19 panels, custom spacing

Figure 12.- Panels layout on a 3:1 elliptic cross section.

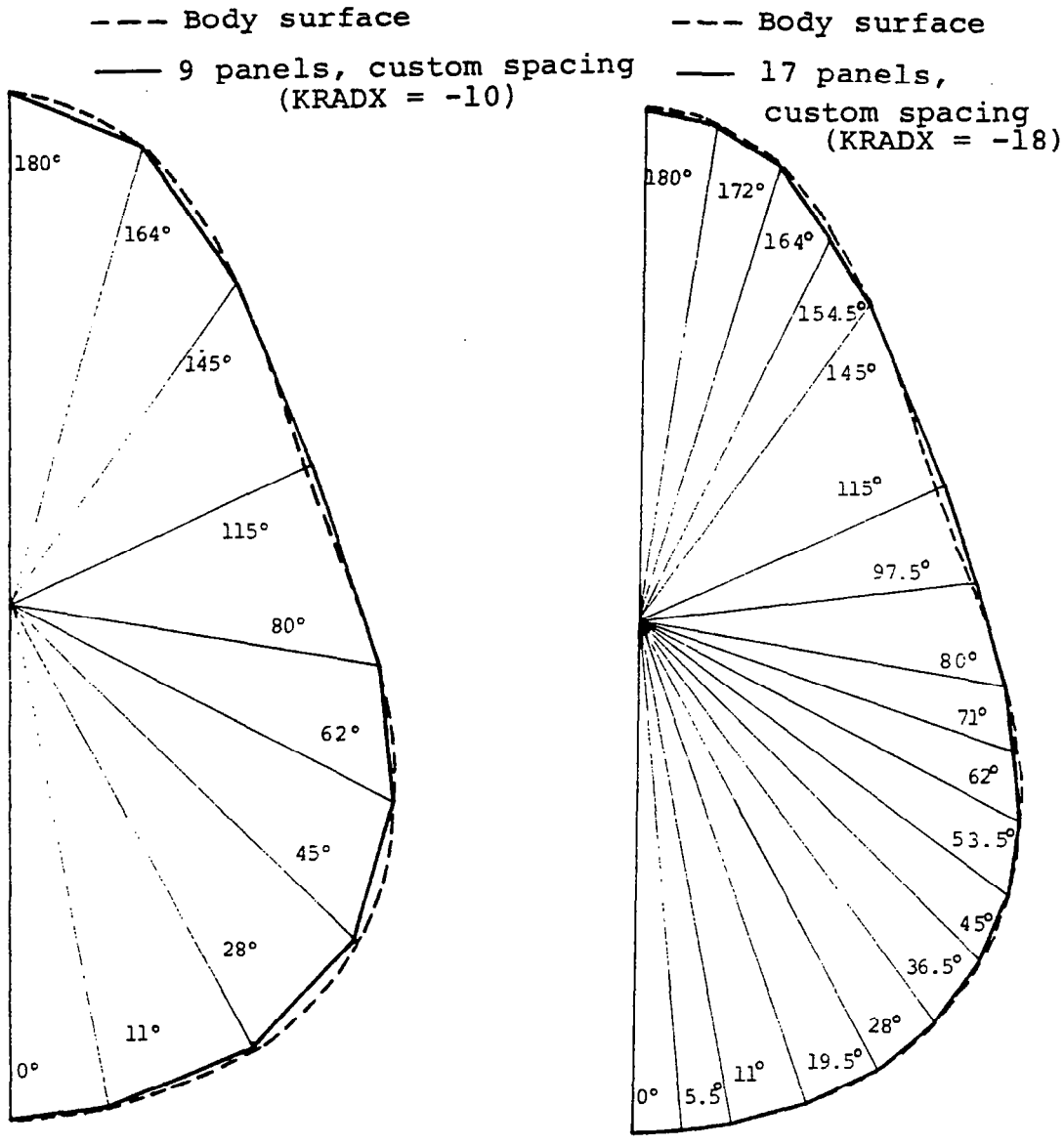

(a) 9 panels, custom spacing (b) 17 panels, custom spacing

Figure 13.- Panel layout on a lobed cross section.

```
Item
(1)       1    0    0    1    0    0    1    1    0    1   10    0    0    0    0    0
(2)       4    1    1    1    3    2    0
(3)      NIELSEN ENGINEERING & RESEARCH, INC.                PROGRAM NOZVTX
         SAMPLE CASE 1
         3:1 ELLIPTICAL CROSS-SECTION BODY                REF: NASA TM-74079 BY GRAVES
         MACH NO = 2.5, ALPHAC = 20 DEGREES, PHI = 0 DEGREES
(4)    12.56588     4.0        16.8        28.0        4.0
(5)     20.0         0.0      666463.       0.0        2.5
(6)     2.8         5.6        1.4         1.05        0.0         1.0         0.0
(7)     .01          0.0        0.0         0.0         0.0
(8)      30
(9)     0.0          .420       .700       2.100       3.500       4.900       5.600       6.300
        7.700       8.400       9.100      10.500      11.900      12.600      13.300      14.700
       15.400      16.800      17.500      18.200      19.040      19.700      20.300      21.000
       22.400      23.100      24.500      25.900      26.600      28.000
(10)    0.0         .118       .196        .587        .850       1.078       1.182       1.281
        1.465       1.550      1.631       1.781       1.916       1.977       2.034       2.136
        2.179       2.252      2.279       2.299       2.309       2.304       2.288       2.265
        2.202       2.165      2.086       2.006       1.970       1.923
(11)    .280        .280       .280        .234        .175        .158        .145        .135
        .128        .119       .110        .102        .093        .085        .076        .069
        .055        .047       .034        .020        .004       -.017       -.030       -.041
       -.047       -.055      -.057       -.055       -.039       -.034
(12)    0.00        .176       .294        .881       1.275       1.617       1.774       1.922
       2.198       2.326      2.447       2.672       2.874       2.965       3.051       3.203
        3.269       3.378      3.418       3.448       3.464       3.456       3.432       3.397
        3.303       3.248      3.128       3.009       2.955       2.885
(13)    0.00        .059       .098        .294        .425        .539        .591        .641
       .733         .775       .816        .891        .958        .988       1.017       1.068
        1.090       1.126      1.140       1.149       1.155       1.152       1.144       1.132
        1.101       1.083      1.043       1.003        .985        .962
(23)     4.20
(24)    .25         .75
        .25         1.0
        .50         .75
        .50         1.0
        .75         .50
        .75         1.0
        1.0         .50
        1.0         1.0
       1.25         .50
       1.25         1.0
(30)     3:1 ELLIPTICAL CROSS-SECTION BODY  -  WDYBDY GEOMETRY INPUT
(31)    0  0
(32)   -3 -1 10 30
(33)   0.0     .420    .700   2.10   3.50   4.90   5.60   6.30   7.70   8.40
       9.10   10.50   11.90  12.60  13.30  14.70  15.40  16.80  17.50  18.20
      19.040  19.70   20.30  21.00  22.40  23.10  24.50  25.90  26.60  28.00
(36)   0.0     .176    .294   .881   1.275  1.617  1.774  1.922  2.198  2.326
      2.447   2.672   2.874  2.965  3.051  3.203  3.269  3.378  3.418  3.448
       3.464  3.456   3.432  3.397  3.303  3.248  3.128  3.009  2.955  2.885
(37)   0.0     .059    .098   .294    .425   .539   .591   .641   .733   .775
       .816   .891    .958   .988   1.017  1.068  1.090  1.126  1.140  1.149
       1.155  1.152   1.144  1.132  1.101  1.083  1.043  1.003   .985   .962
(39)     3:1 ELLIPTICAL CROSS-SECTION BODY  -  ADDITIONAL PANELING INPUT
(40)    0  0 -1
(41)    0  8
(43)   0.0     .420    .700   2.10   3.50   4.90   5.60   6.30
```

(a) Sample Case 1

Figure 14.- Sample input decks for program NOZVTX.

```
  1    0    0    1    0    0    1    1    0    0    0    3    0    3    0    0
  4    1    1    1    3    2    0
  NIELSEN ENGINEERING & RESEARCH, INC.                PROGRAM NOZVTX
  SAMPLE CASE 2
  3:1 ELLIPTICAL CROSS-SECTION BODY                REF: NASA TM-74079 BY GRAVES
  MACH NO = 2.5, ALPHAC = 20 DEGREES, PHI = 0 DEGREES
12.56588      4.0        16.8        28.0        4.0
 20.0         0.0       664463.      0.0         2.5
  5.6        28.0        1.4         1.05        0.0         1.0         0.0
  .01         0.0        0.0         0.0         0.0
  30
 0.0          .420        .700       2.100       3.500       4.900       5.600       6.300
 7.700       8.400       9.100      10.500      11.900      12.600      13.300      14.700
 15.400      16.800      17.500      18.200      19.040      19.700      20.300      21.000
 22.400      23.100      24.500      25.900      26.600      26.000
 0.0          .118        .196        .587        .850       1.078       1.182       1.281
 1.465       1.550       1.631       1.781       1.916       1.977       2.034       2.136
 2.179       2.252       2.279       2.299       2.309       2.304       2.288       2.265
 2.202       2.165       2.086       2.006       1.970       1.923
 .280        .280        .280        .234        .175        .158        .145        .135
 .128        .119        .110        .102        .093        .085        .076        .069
 .055        .047        .034        .020        .004       -.017       -.030       -.041
-.047       -.055       -.057       -.055       -.039       -.034
 0.00        .176        .294        .881       1.275       1.617       1.774       1.922
2.198       2.326       2.447       2.672       2.874       2.965       3.051       3.203
 3.269       3.378       3.418       3.448       3.464       3.456       3.432       3.397
 3.303       3.248       3.128       3.009       2.955       2.885
 0.00        .059        .098        .294        .425        .539        .591        .641
.733         .775        .816        .891        .958        .988       1.017       1.068
 1.090       1.126       1.140       1.149       1.155       1.152       1.144       1.132
 1.101       1.043       1.043       1.003        .985        .962
 .38251     1.20011     0.0         0.0         0.0
 .45032     1.02464     .99661      2.80
 .42231     1.59082     .77324      4.20
 .40346     1.9411      .0970       5.60
  3:1 ELLIPTICAL CROSS-SECTION BODY  -  BODYBY GEOMETRY INPUT
 0  0
-3 -1 10 30
 0.0     .420    .700   2.10   3.50   4.90   5.60   6.30   7.70   8.40
 9.10  10.50   11.90  12.60  13.30  14.70  15.40  16.80  17.50  18.20
19.040 19.70  20.30  21.00  22.40  23.10  24.50  25.90  26.60  28.00
 0.0     .176    .294   .881  1.275  1.617  1.774  1.922  2.198  2.326
2.447   2.672  2.874  2.965  3.051  3.203  3.269  3.378  3.418  3.448
 3.464  3.456  3.432  3.397  3.303  3.248  3.128  3.009  2.955  2.885
 0.0     .059    .098   .294   .425   .539   .591   .641   .733   .775
 .816   .891   .958   .988  1.017  1.068  1.090  1.126  1.140  1.149
1.155  1.152  1.144  1.132  1.101  1.043  1.043  1.003   .985   .962
  3:1 ELLIPTICAL CROSS-SECTION BODY  -  ADDITIONAL PANELING INPUT
 0  0 -1
 0  0
```

(b) Sample Case 2

Figure 14.- Continued.

```
   1    0    0    1    0    0    1    1    0    0    0    0    0    0    0    0
   4    1    1    1    3    2    0
  NIELSEN ENGINEERING & RESEARCH, INC.                PROGRAM NOZVTX
  SAMPLE CASE 3
  3:1 ELLIPTICAL CROSS-SECTION BODY                REF: NASA TM-74079 BY GRAVES
  MACH NO = 2.5, ALPHAC = 20 DEGREES, PHI = 0 DEGREES
12.56588     4.0         16.8        28.0         4.0
 20.0         0.0       666463.       0.0        2.5
 2.8         28.0        1.4         1.05        0.0         1.0         0.0
 .01          0.0         0.0         0.0         0.0
  30
 0.0          .420        .700       2.100       3.500       4.900       5.600       6.300
 7.700       8.400       9.100      10.500      11.900      12.600      13.300      14.700
 15.400      16.800      17.500      18.200      19.040      19.700      20.300      21.000
 22.400      23.100      24.500      25.900      26.600      28.000
 0.0          .118        .196        .587        .850       1.078       1.182       1.281
 1.465       1.550       1.631       1.781       1.916       1.977       2.034       2.136
 2.179       2.252       2.279       2.299       2.309       2.304       2.288       2.265
 2.202       2.165       2.086       2.006       1.970       1.923
 .280        .280        .280        .234        .175        .156        .145        .135
 .128        .119        .110        .102        .093        .085        .076        .069
 .055        .047        .034        .020        .004       -.017       -.030       -.041
-.047       -.055       -.057       -.055       -.039       -.034
 0.00        .176        .294        .881       1.275       1.617       1.774       1.922
2.198       2.326       2.447       2.672       2.874       2.965       3.051       3.203
 3.249       3.378       3.418       3.448       3.464       3.456       3.432       3.397
 3.303       3.248       3.128       3.009       2.955       2.885
 0.00        .059        .098        .294        .425        .539        .591        .641
.733         .775        .816        .891        .958        .988       1.017       1.068
 1.090       1.126       1.140       1.149       1.155       1.152       1.144       1.132
 1.101       1.083       1.043       1.003        .985        .962
  3:1 ELLIPTICAL CROSS-SECTION BODY  -  wDYEDY GEOMETRY INPUT
 0  0
-3 -1 10 30
 0.0    .420   .700   2.10   3.50   4.90   5.60   6.30   7.70   8.40
 9.10  10.50  11.90  12.60  13.30  14.70  15.40  16.80  17.50  18.20
19.040 19.70  20.30  21.00  22.40  23.10  24.50  25.90  26.60  28.00
 0.0    .176   .294   .881  1.275  1.617  1.774  1.922  2.198  2.326
2.447  2.672  2.874  2.965  3.051  3.203  3.269  3.378  3.418  3.448
 3.464  3.456  3.432  3.397  3.303  3.248  3.128  3.009  2.955  2.885
 0.0    .059   .098   .294   .425   .539   .591   .641   .733   .775
 .816   .891   .958   .988  1.017  1.068  1.090  1.126  1.140  1.149
1.155  1.152  1.144  1.132  1.101  1.083  1.043  1.003   .985   .962
  3:1 ELLIPTICAL CROSS-SECTION BODY  -  ADDITIONAL PANELING INPUT
 0  0 -1
 0  0
```

(c) Sample Case 3

Figure 14.- Continued.

```
    1     0     1     1     0     0     1     1     0     0     0     0     0     0     0     0
    4     1     1     1     3     2     0
   NIELSEN ENGINEERING & RESEARCH, INC.                PROGRAM NOZVTX
   SAMPLE CASE 4
   3:1 ELLIPTICAL CROSS-SECTION BODY                REF: NASA TM-74079 BY GRAVES
   MACH NO.= 2.5, ALPHAC = 20 DEGREES, PHI = 45 DEGREES
 12.56588      4.0          16.8          28.0          4.0
  20.0         45.0       666463.         0.0          2.5
  2.8          28.0         1.4           1.05         0.0          1.0          0.0
  .01           0.0         0.0           0.0          0.0
   30
  0.0          .420         .700         2.100         3.500        4.900        5.600        6.300
  7.700        8.400        9.100        10.500        11.900       12.600       13.300       14.700
  15.400       16.800       17.500        18.200        19.040       19.700       20.300       21.000
  22.400       23.100       24.500        25.900        26.600       28.000
  0.0          .118         .196          .587          .850        1.078        1.182        1.281
  1.465        1.550        1.631         1.781         1.916        1.977        2.034        2.136
  2.179        2.252        2.279         2.299         2.309        2.304        2.288        2.265
  2.202        2.165        2.096         2.006         1.970        1.923
  .280         .280         .280          .234          .175         .158         .145         .135
  .128         .119         .110          .102          .093         .085         .076         .069
  .055         .047         .034          .020          .004        -.017        -.030        -.041
 -.047        -.055        -.057         -.055         -.039        -.034
  0.00         .176         .294          .881         1.275        1.617        1.774        1.922
 2.198        2.326        2.447         2.672         2.874        2.965        3.051        3.203
  3.269        3.378        3.418         3.448         3.464        3.456        3.432        3.397
  3.303        3.248        3.128         3.009         2.955        2.885
  0.00         .059         .098          .294          .425         .539         .591         .641
 .733          .775         .816          .891          .958         .988        1.017        1.068
  1.090        1.126        1.140         1.149         1.155        1.152        1.144        1.132
  1.101        1.083        1.043         1.003          .985         .962
   3:1 ELLIPTICAL CROSS-SECTION BODY  -  #DYBDY GEOMETRY INPUT
  1   0
 -3  -1  10  30
 0.0     .420    .700    2.10    3.50    4.90    5.60    6.30    7.70    8.40
 9.10   10.50   11.90   12.60   13.30   14.70   15.40   16.80   17.50   18.20
19.040  19.70   20.30   21.00   22.40   23.10   24.50   25.90   26.60   28.00
 0.0     .176    .294    .881   1.275   1.617   1.774   1.922   2.198   2.326
2.447   2.672   2.874   2.965   3.051   3.203   3.269   3.378   3.418   3.448
 3.464   3.456   3.432   3.397   3.303   3.248   3.128   3.009   2.955   2.885
 0.0     .059    .098    .294    .425    .539    .591    .641    .733    .775
 .816    .891    .958    .988   1.017   1.068   1.090   1.126   1.140   1.149
1.155   1.152   1.144   1.132   1.101   1.083   1.043   1.003    .985    .962
   3:1 ELLIPTICAL CROSS-SECTION BODY  -  ADDITIONAL PANELING INPUT
  0   0  -1
  0   0
```

(d) Sample Case 4

Figure 14.- Continued.

```
  0    0    0    1    0    0    1    1    0    3  169    .0    0    0    0    0    0
  4    1    1    1    3    2    0
 NIELSEN ENGINEERING & RESEARCH, INC.                    PROGRAM NOZVTX
 SAMPLE CASE 5
 CIRCULAR OGIVE CYLINDER                  REF: AFATL TR-78-127 BY OBERKAMPF
 MACH NO.= 2.0, ALPHAC = 15 DEGREES, PHI = 0 DEGREES
7.06858     3.0         6.0         39.         3.0
 15.0       0.0      1750000.       0.0         2.0
 3.0        39.         1.5        1.05        0.0         1.0         0.0
 .01        0.0         0.0        0.0         0.0
 26
 0.0        .25         .50        .75        1.00        1.25        1.50        1.75
 2.00       2.25        2.50       2.75       3.00        3.25        3.50        3.75
 4.00       4.25        4.50       4.75       5.00        5.25        5.50        5.75
 6.00       36.0
 0.0       .12981      .25272     .36895     .47870      .58216      .67948      .77082
.85630     .93606     1.01020    1.07883    1.14203     1.19990     1.25250     1.29990
1.34216    1.37933    1.41146    1.43858    1.46072     1.47792     1.49019     1.49755
 1.500      1.500
.53333     .50528      .47815     .45185     .42630      .40145      .37722      .35355
.33041     .30773      .28548     .26361     .24209      .22089      .19996      .17928
.15883     .13857      .11847     .09851     .07867      .05893      .03925      .01961
 0.0        0.0
 21.0       30.         39.
 0.0        1.2
 0.0        1.50
 0.0        1.80
 0.0        2.10
 0.0        2.40
 0.0        2.70
 0.0         3.00
 .30        1.2
 .3         1.50
 .3         1.80
 .3         2.10
 .3         2.40
 .3         2.70
 .3          3.00
 .45        1.05
 .45        1.10
 .45        1.2
 .45        1.30
 .45        1.40
 .45        1.50
 .45        1.60
 .45        1.70
 .45        1.80
 .45        1.90
 .45        2.00
 .45        2.10
 .45        2.20
 .45        2.30
 .45        2.40
 .45        2.70
 .45         3.00
 .60        1.05
 .60        1.10
 .60        1.2
  .60       1.30
  .60       1.40
 .6         1.50
 .6         1.60
```

(e) Sample Case 5

Figure 14.- Continued.

```
.6          1.70
.6          1.80
.6          1.90
.6          2.00
.6          2.10
.6          2.20
.6          2.30
 .6         2.40
 .6         2.70
.6           3.00
.75        1.2
.75         1.30
.75        1.4
.75        1.50
.75         1.6
.75         1.7
.75         1.80
.75         1.9
.75        2.0
.75         2.10
.75         2.20
.75         2.3
.75         2.40
.75         2.70
.75          3.00
.9         .75
.9          .8
.9          .9
.9          1.0
.9          1.1
.90        1.2
.9          1.3
.9          1.4
.9         1.50
.9          1.6
.9          1.7
.9          1.8
.9          1.9
.9          2.0
.9          2.10
.9          2.2
.9          2.3
.9          2.40
 .9         2.70
.9           3.00
1.05        .6
1.05        .7
1.05        .8
1.05        .9
1.05        1.0
1.05        1.1
1.05       1.2
1.05        1.3
1.05        1.4
1.05       1.50
1.05        1.6
1.05        1.7
1.05        1.80
1.05        1.9
1.05        2.0
1.05        2.10
1.05       2.2
1.05        2.3
1.05        2.40
1.05        2.70
1.05         3.00
```

(e) Sample Case 5, Continued.

Figure 14.- Continued.

```
1.20      0.0
1.20       .10
1.20       .2
1.20        .3
1.20      .4
1.20      .5
1.20       .6
1.20      .7
1.20      .8
1.20        .9
1.20       1.0
1.20      1.1
1.20      1.2
1.20       1.3
1.20       1.4
1.2       1.50
1.2        1.6
1.2       1.7
1.2        1.8
1.2        1.9
1.2          2.0
1.2        2.10
1.2        2.2
1.2        2.3
1.2        2.40
1.2        2.70
1.2         3.00
1.35       0.0
1.35       .1
1.35       .2
1.35       .3
1.35       .4
1.35      .5
1.35       .6
1.35        .7
1.35       .8
1.35       .9
1.35       1.0
1.35       1.1
1.35      1.2
1.35      1.3
1.35      1.4
1.35      1.50
1.35      1.6
1.35       1.7
1.35       1.80
1.35      1.9
1.35       2.0
1.35       2.10
1.35       2.2
1.35      2.3
1.35       2.40
1.35       2.70
1.35        3.00
1.50       0.0
1.50       .3
1.50       .6
1.50       .9
1.50      1.2
1.50      1.50
1.50       1.80
1.50       2.10
1.50       2.40
1.50       2.70
1.50        3.00
 51    2    6.0        39.
```

(e) Sample Case 5, Concluded.

Figure 14.- Continued.

```
  0     0     0     0     0     0     1     1     0     0     0     0     0     0     0     0
  4     1     0     0     0     0     0
 NIELSEN ENGINEERING & RESEARCH, INC.                    PROGRAM NOZVTX
 SAMPLE CASE 6
 CIRCULAR OGIVE CYLINDER                    REF: NASA TM X-3558 BY LANDRUM
 MACH NO.= 1.6, ALPHAC = 0 DEGREES, PHI = 0 DEGREES
7.07        20.0        9.0         20.0        3.0
0.0         0.0         500000.     0.0         1.6
.50         19.5        0.0         1.05        0.0         1.0         1.0
.01         0.0         0.0         0.0         0.0
 11
0.          1.          2.          3.          4.          5.          6.          7.
8.          9.          20.
0.          .32         .60         .84         1.04        1.22        1.34        1.42
1.48        1.50        1.50
.343        .301        .261        .221        .183        .146        .109        .072
.036        0.0         0.0
 51     2   9.0         20.
```

(f) Sample Case 6

Figure 14.- Continued.

```
  1    0    0    1    0    0    1    1    0    0    0    0    0    0    0    0
  4    1    1    1    3    2    0
 NIELSEN ENGINEERING & RESEARCH, INC.                PROGRAM NOZVTX
 SAMPLE CASE 7
 2:1 ELLIPTICAL CROSS SECTION FOREBODY     REF: NASA TM-80062 BY TOWNSEND
 MACH NO.= 1.7, ALPHAC = 20.36 DEGREES, PHI = 0 DEGREES
13.17679   14.0       7.0       14.0      3.60342
 20.36     0.0      900855.     0.0       1.7
 .50       14.0      .50       1.05      0.0       1.0       0.0
 .05       0.0       0.0       0.0       0.0
 39
 0.0       .25       .50       .75       1.00      1.25      1.50      1.75
 2.00      2.25      2.50      2.75      3.00      3.25      3.50      3.75
 4.00      4.25      4.50      4.75      5.00      5.50      6.00      6.50
 7.00      7.50      8.00      8.50      9.00      9.50      10.0      10.50
 11.0      11.50     12.0      12.50     13.0      13.50     14.0
0.00000   0.06764   0.13405   0.19925   0.26323   0.32599   0.38753   0.44785
0.50696   0.56484   0.62151   0.67696   0.73119   0.78420   0.83599   0.88657
0.93592   0.98406   1.03098   1.07668   1.12116   1.20646   1.28689   1.36245
1.43313   1.49894   1.55987   1.61593   1.66711   1.71342   1.75486   1.79142
1.82310   1.84991   1.87185   1.88891   1.90109   1.90841   1.911
0.27300   0.26810   0.26322   0.25836   0.25348   0.24860   0.24372   0.23886
0.23398   0.22910   0.22424   0.21936   0.21448   0.20960   0.20474   0.19986
0.19498   0.19012   0.18524   0.18036   0.17426   0.16573   0.15599   0.14624
0.13649   0.12674   0.11699   0.10724   0.09749   0.08775   0.07800   0.06824
0.05849   0.04875   0.03900   0.02924   0.01950   0.00991   0.00000
0.00000   0.04509   0.08937   0.13283   0.17549   0.21733   0.25835   0.29857
0.33797   0.37656   0.41434   0.45131   0.48746   0.52280   0.55733   0.59105
0.62395   0.65604   0.68732   0.71779   0.74744   0.80431   0.85793   0.90830
0.95542   0.99929   1.03991   1.07729   1.11141   1.14228   1.16990   1.19428
1.21540   1.23327   1.24790   1.25927   1.26740   1.27227   1.27400
0.00000   0.09018   0.17874   0.26567   0.35097   0.43465   0.51671   0.59714
0.67594   0.75319   0.82868   0.90261   0.97492   1.04560   1.11466   1.18209
1.24790   1.31208   1.37464   1.43557   1.49488   1.60862   1.71586   1.81660
1.91084   1.99859   2.07983   2.15457   2.22282   2.28456   2.33981   2.38855
2.43080   2.46655   2.49580   2.51854   2.53479   2.54454   2.54800
 2:1 ELLIPTICAL CROSS-SECTION FOREBODY  -  BODYBODY GEOMETRY INPUT
 0  0
-3 -1 18 29
 0.0      .50     1.0     1.5      2.0     2.5      3.0     3.5     4.0      4.5
 5.0      5.5     6.0     6.5      7.0     7.5      8.0     8.5     9.0      9.5
 10.0     10.5    11.     11.5     12.     12.5     13.     13.5    14.
 0.0    .08937 .17549 .25835 .33797 .41434 .48746 .55733 .62395 .68732
.74744 .80431 .85793 .90830 .95542 .999291.039911.077291.111411.14228
1.169901.194281.215401.233271.247901.259271.267401.272271.274
 0.0   .17874  .35097 .51671 .67594 .82868 .974211.114661.247901.37464
1.494881.608621.715861.816601.910841.998592.079832.154572.222822.28456
2.339812.388552.430802.466552.495802.518542.534792.544542.548
 2:1 ELLIPTICAL CROSS-SECTION FOREBODY  -  ADDITIONAL PANELING INPUT
 0  0 -1
 0 11
 0.0  1.0      2.0      3.0    4.0      5.0     6.0     8.0    10.0   12.
 14.
```

(g) Sample Case 7

Figure 14.- Continued.

```
  1    0    0    1    0    0    1    1    0    0    0    0    0    0    0    0
  4    1    1    1    3    2    0
 NIELSEN ENGINEERING & RESEARCH, INC.                PROGRAM NOZVTX
 SAMPLE CASE A
 2:1 ELLIPTICAL CROSS SECTION FOREBODY     REF: NASA TM-80062 BY TOWNSEND
 MACH NO.= 1.7, ALPHAC = 20.36 DEGREES, PHI = 0 DEGREES
13.17679   14.0        7.0        14.0       3.60342
 20.36      0.0      900855.       0.0        1.7
 .50       14.0       .50        1.05        0.0         1.0         0.0
 .05        0.0        0.0        0.0        0.0
 39
 0.0        .25        .50        .75        1.00        1.25        1.50        1.75
 2.00       2.25       2.50       2.75       3.00        3.25        3.50        3.75
 4.00      4.25       4.50       4.75        5.00        5.50        6.00       6.50
 7.00       7.50       8.00       8.50       9.00        9.50        10.0       10.50
 11.0       11.50      12.0       12.50       13.0       13.50       14.0
0.00000   0.06764   0.13405   0.19925   0.26323   0.32599   0.38753   0.44785
0.50696   0.56484   0.62151   0.67696   0.73119   0.78420   0.83599   0.88657
0.93592   0.98406   1.03098   1.07668   1.12116   1.16446   1.20689   1.36245
1.43313   1.49894   1.55987   1.61593   1.66711   1.71342   1.75486   1.79142
1.82310   1.84991   1.87185   1.88891   1.90109   1.90841   1.911
0.27300   0.26810   0.26322   0.25836   0.25348   0.24860   0.24372   0.23886
0.23398   0.22910   0.22424   0.21936   0.21448   0.20960   0.20474   0.19986
0.19498   0.19012   0.18524   0.18036   0.17426   0.16573   0.15599   0.14624
0.13649   0.12674   0.11699   0.10724   0.09749   0.08775   0.07800   0.06824
0.05849   0.04875   0.03900   0.02924   0.01950   0.00991   0.00000
0.00000   0.04509   0.08937   0.13283   0.17549   0.21733   0.25835   0.29857
0.33797   0.37656   0.41434   0.45131   0.48746   0.52280   0.55733   0.59105
0.62395   0.65604   0.68732   0.71779   0.74744   0.80431   0.85793   0.90830
0.95542   0.99929   1.03991   1.07729   1.11141   1.14228   1.16990   1.19428
1.21540   1.23327   1.24790   1.25927   1.26740   1.27227   1.27400
0.00000   0.09018   0.17874   0.26567   0.35097   0.43465   0.51671   0.59714
0.67594   0.75319   0.82868   0.90261   0.97492   1.04560   1.11466   1.18209
1.24790   1.31208   1.37464   1.43557   1.49488   1.60862   1.71586   1.81660
1.91084   1.99859   2.07983   2.15457   2.22282   2.28456   2.33981   2.38855
2.43080   2.46655   2.49580   2.51854   2.53479   2.54454   2.54800
 2:1 ELLIPTICAL CROSS-SECTION FOREBODY  -  WDYBDY GEOMETRY INPUT
 0  0
-3 -1 18 29
 0.0       .50     1.0     1.5      2.0     2.5      3.0     3.5     4.0      4.5
 5.0       5.5     6.0     6.5      7.0     7.5      8.0     8.5     9.0      9.5
 10.0     10.5     11.     11.5     12.     12.5     13.     13.5    14.
 0.0    .08937 .17549 .25835 .33797 .41434 .48746 .55733 .62395 .68732
.74744 .80431 .85793 .90830 .95542 .999291.039911.077291.111411.14228
1.169901.194281.215401.233271.247901.259271.267401.272271.274
 0.0   .17874  .35097 .51671 .67594 .82868 .974211.114661.247901.37464
1.494881.608621.715861.816601.910841.998592.079832.154572.222822.28456
2.339812.388552.430802.466552.495802.518542.534792.544542.548
 2:1 ELLIPTICAL CROSS-SECTION FOREBODY  -  ADDITIONAL PANELING INPUT
 0  0 -1
-18 11
 0.0  5.      10.     18.     26.     30.5    45.     58.75  72.5    107.5
 121.25 135.  144.5  154.    162.    170.    175.    180.
 0.0  1.0      2.0      3.0    4.0      5.0     6.0     8.0    10.0   12.
 14.
```

(h) Sample Case 8

Figure 14.- Continued.

```
   1    0    0    1    0    2    1    1    0    0    0    0    0    0    0    0
   4    1    1    1    3    2    0
  SAMPLE CASE 9
  3:1 ELLIPTICAL CROSS SECTION CONE        REF: NASA TM-78808 BY TOWNSEND
  MACH NO.= 1.7. ALPHAC = 20.35 DEGREES. PHI = 0 DEGREES
27.1896     6.794      7.0       14.0      6.794
 20.35       0.0     1130000.     .25      1.70
  .50        7.0       0.0       1.05      0.0       1.0        .50
 .01         0.0       0.0       0.0       0.0
   2
 0.0        14.0
 0.0       3.397
 .2427      .2427
 0.0       5.0955
 0.0       1.6985
 3:1 CONICAL ELLIPSE  -  WDYBDY GEOMETRY INPUT
 0  0
-3 -1 18  2
0.     14.0
 0.0  5.0955
0.0   1.6985
 3:1 CONICAL ELLIPSE  -   ADDITIONAL PANELING INPUT
 0  0 -1
-18  5
 0.0   13.85  27.69  41.54  55.38  69.50  77.00  81.50  87.00  93.00
93.50  103.  110.5  124.62  138.46 152.31 166.15 180.
0.0   .50     6.25  12.0    14.0
```

(i) Sample Case 9

Figure 14.- Continued.

```
   2    0    0    1    0    2    1    1    0    0    0    0    0    0    0    0
   4    1    1    1    3    2    0
  NIELSEN ENGINEERING & RESEARCH, INC.                PROGRAM NOZVTX
  SAMPLE CASE 10
  LOBED CROSS SECTION FOREBODY          REF: NASA TM-80062 BY TOWNSEND
  MACH NO.= 1.7, ALPHAC = 20.36 DEGREES, PHI = 0 DEGREES
15.05941    14.0        7.0        14.0       4.37884
 20.36       0.0       728764.     .075        1.7
 .50         7.0        0.0        1.05        0.0         1.0         1.0
 .05         0.0        0.0        0.0         0.0
  29
 0.0         .50        1.0        1.5         2.0         2.5         3.0         3.5
  4.0        4.5        5.0        5.5         6.0         6.5         7.0         7.5
 8.0         8.5         9.0        9.5        10.         10.5        11.0        11.5
 12.0        12.5       13.0       13.5        14.0
 0.0        .15359      .30160     .44403      .58087      .71212      .83779      .95787
1.07237    1.18128     1.28461    1.38235     1.47451     1.56108     1.64207     1.71747
1.78728    1.85151     1.91016    1.96322     2.01069     2.05258     2.08889     2.11961
2.14474    2.16429     2.17825    2.18663     2.18942
.31         .30160     .29044     .27927      .26809      .25692      .24575      .23458
.22341      .21224     .20107     .18990      .17873      .16756      .15639      .14521
.13404      .12288     .11171     .10053      .08936      .07820      .06703      .05585
.04468      .03351     .02234     .01117      0.0
  20     1
 .50
  28
   .00000    -.17874
   .01558    -.17809
   .03105    -.17612
   .04629    -.17275
   .06110    -.16786
   .07524    -.16134
   .08840    -.15312
   .10026    -.14319
   .11049    -.13168
   .11882    -.11882
   .12508    -.10496
   .12926    -.09051
   .13147    -.07590
   .13194    -.06152
   .13097    -.04767
   .12891    -.03454
   .12607    -.02223
   .11400     .01900
   .10000     .05800
   .08365     .09970
   .07847     .11206
   .07212     .12492
   .06431     .13791
   .05476     .15044
   .04333     .16171
   .03011     .17077
   .01546     .17668
   .00000     .17874
LOBED CROSS SECTION BODY  -   WDYBDY GEOMETRY INPUT
 0  1
 1  1 20 29
 0.     .5     1.0     1.5     2.0     2.5    3.0     3.5     4.0     4.5
5.0    5.5     6.0     6.5     7.0     7.5    8.0     8.5     9.0     9.5
10.    10.5    11.0    11.5    12.     12.5   13.     13.5    14.
 0.0        0.0
 0.0        0.0
```

(j) Sample Case 10

Figure 14.- Continued.

```
   0.0          0.0
   0.0          0.0
   0.0          0.0
   0.0          0.0
   0.0          0.0
   0.0          0.0
   0.0          0.0
   0.0          0.0
   0.0          0.0
   0.0          0.0
   0.0          0.0
   0.0          0.0
   0.0          0.0
   0.0          0.0
   0.0          0.0
   0.0          0.0
   0.0          0.0
   0.0          0.0
   0.0          0.0
    .00000       -.17874
    .01558       -.17809
    .03105       -.17612
    .04629       -.17275
    .06110       -.16786
    .08840       -.15312
    .11049       -.13168
    .12508       -.10496
    .13147       -.07590
    .13097       -.04767
    .12607       -.02223
  .11400        .019
  .10000        .058
    .08365        .09970
    .07212        .12492
    .05476        .15044
    .04333        .16171
    .03011        .17077
    .01546        .17668
    .00000        .17874
    .00000       -.35097
    .03059       -.34970
    .06098       -.34584
    .09089       -.33922
    .11997       -.32962
    .17359       -.30067
    .21696       -.25857
    .24561       -.20609
    .25816       -.14905
    .25719       -.09361
    .24756       -.04365
 .2239         .0373
.1964          .1139
    .16427        .19577
    .14162        .24530
    .10752        .29541
    .08509        .31755
    .05913        .33534
    .03035        .34693
   0.00000        .35097
    .00000       -.51671
    .04504       -.51484
    .08978       -.50915
    .13381       -.49940
    .17662       -.48527
    .25557       -.44265
    .31942       -.38067
    .36160       -.30342
```

(j) Sample Case 10, Continued.

Figure 14.- Continued.

```
    .38006    -.21943
    .37863    -.13781
    .36447    -.06427
.32956     .05493
.28909     .16747
    .24184     .28821
    .20850     .36114
    .15830     .43492
    .12527     .46750
    .08705     .49369
    .04469     .51076
  0.00000      .51671
    .00000    -.67594
    .05892    -.67350
    .11744    -.66606
    .17505    -.65331
    .23106    -.63482
    .33432    -.57907
    .41786    -.49798
    .47304    -.39692
    .49719    -.28705
    .49532    -.18028
    .47678    -.08407
.43113     .07185
.37818     .21935
    .31637     .37703
    .27276     .47243
    .20708     .56895
    .16387     .61158
    .11388     .64583
    .05846     .66817
  0.00000      .67594
    .00000    -.82868
    .07224    -.82569
    .14398    -.81656
    .21461    -.80093
    .28327    -.77827
    .40987    -.70991
    .51228    -.61051
    .57992    -.48661
    .60953    -.35191
    .60724    -.22102
    .58452    -.10307
.52856     .08809
.46364     .26891
    .38785     .46222
    .33439     .57919
    .25387     .69751
    .20090     .74977
    .13961     .79177
    .07167     .81915
  0.00000      .82868
    .00000    -.97492
    .08499    -.97139
    .16939    -.96066
    .25248    -.94227
    .33325    -.91561
    .48220    -.83519
    .60268    -.71825
    .68226    -.57249
    .71710    -.41402
    .71440    -.26002
    .68767    -.12125
.62182     .10364
.54545     .31636
    .45630     .54379
```

(j) Sample Case 10, Continued.

Figure 14.- Continued.

```
      .39340     .68139
      .29867     .82060
      .23635     .88208
      .16425     .93149
      .08431     .96371
     0.00000     .97492
      .00000   -1.11466
      .09717   -1.11063
      .19367   -1.09835
      .28867   -1.07733
      .38102   -1.04685
      .55131    -.95491
      .68906    -.82120
      .78005    -.65454
      .81988    -.47336
      .81680    -.29729
      .78624    -.13863
  .71095     .11849
  .62364     .36171
      .52170     .62174
      .44979     .77906
      .34148     .93822
      .27023    1.00851
      .18779    1.06500
      .09640    1.10184
     0.00000    1.11466
      .00000   -1.24790
      .10878   -1.24339
      .21682   -1.22964
      .32317   -1.20610
      .42657   -1.17198
      .61722   -1.06905
      .77143    -.91936
      .87330    -.73278
      .91789    -.52994
      .91444    -.33243
      .88022    -.15521
  .79593     .13265
  .69818     .40495
      .58406     .69605
      .50355     .87218
      .39230    1.05036
      .30253    1.12906
      .21024    1.19231
      .10792    1.23355
     0.00000    1.24790
      .00000   -1.37464
      .11983   -1.36967
      .23884   -1.35453
      .35600   -1.32860
      .46989   -1.29101
      .67990   -1.17762
      .84978   -1.01273
      .96199    -.80721
    1.01111    -.58376
    1.00731    -.36663
      .96961    -.17097
  .87676     .14613
  .76909     .44607
      .64338     .76675
      .55470     .96076
      .42113    1.15704
      .33326    1.24373
      .23159    1.31340
      .11888    1.35883
     0.00000    1.37464
```

(j) Sample Case 10, Continued.

Figure 14.- Continued.

```
      .00000  -1.49488
      .13031  -1.48947
      .25973  -1.47301
      .38714  -1.44481
      .51099  -1.40393
      .73937  -1.28063
      .92411  -1.10131
     1.04614   -.87781
     1.09955   -.63483
     1.09542   -.39870
     1.05443   -.18592
 .95345     .15891
 .83636     .48509
      .69965     .83382
      .60322    1.04480
      .45796    1.25825
      .36241    1.35252
      .25184    1.42828
      .12928    1.47768
     0.00000    1.49488
      .00000  -1.60862
      .14023  -1.60280
      .27949  -1.58509
      .41659  -1.55474
      .54987  -1.51076
      .79563  -1.37807
      .99442  -1.18511
     1.12573   -.94460
     1.18321   -.68313
     1.17877   -.42904
     1.13466   -.20007
 1.02600    .17100
 .90000     .52200
      .75289     .89726
      .64911    1.12430
      .49281    1.35398
      .38998    1.45543
      .27101    1.53696
      .13912    1.59012
     0.00000    1.60862
      .00000  -1.71586
      .14958  -1.70965
      .29813  -1.69076
      .44437  -1.65839
      .58653  -1.61147
      .84867  -1.46994
     1.06072  -1.26411
     1.20078  -1.00758
     1.26210   -.72867
     1.25735   -.45764
     1.21030   -.21341
 1.09400    .18240
 .96000     .55680
      .80308     .95708
      .69239    1.19925
      .52566    1.44425
      .41598    1.55246
      .28907    1.63942
      .14839    1.69612
     0.00000    1.71586
      .00000  -1.81660
      .15836  -1.81003
      .31563  -1.79003
      .47045  -1.75576
      .62096  -1.70609
      .89850  -1.55624
```

(j) Sample Case 10, Continued.

Figure 14.- Continued.

```
   1.12299  -1.33833
   1.27128  -1.06673
   1.33620    -.77145
   1.33117    -.48451
   1.28136    -.22594
1.15865    .19311
1.01636    .58949
    .85023   1.01327
    .73304   1.26966
    .55653   1.52904
    .44040   1.64361
    .30605   1.73567
    .15710   1.79571
  0.00000    1.81560
    .00000  -1.91084
    .16657  -1.90393
    .33200  -1.88289
    .49486  -1.84685
    .65318  -1.79459
    .94511  -1.63698
   1.18125  -1.40776
   1.33723  -1.12207
   1.40551    -.81147
   1.40023    -.50964
   1.34783    -.23766
1.21876    .20313
1.06909    .62007
    .89434   1.06583
    .77107   1.33553
    .58540   1.60837
    .46325   1.72888
    .32192   1.82572
    .16525   1.88887
  0.00000    1.91094
    .00000  -1.99859
    .17422  -1.99136
    .34725  -1.96935
    .51758  -1.93165
    .68317  -1.87700
    .98851  -1.71215
   1.23540  -1.47241
   1.39864  -1.17360
   1.47005    -.84874
   1.46453    -.53304
   1.40972    -.24857
1.27473    .21245
1.11818    .64855
    .93541   1.11478
    .80647   1.39685
    .61228   1.68222
    .48452   1.80826
    .33671   1.90955
    .17284   1.97560
  0.00000    1.99859
    .00000  -2.07983
    .18130  -2.07231
    .36137  -2.04940
    .53862  -2.01017
    .71094  -1.95330
   1.02869  -1.78175
   1.28572  -1.53226
   1.45549  -1.22130
   1.52981    -.88324
   1.52406    -.55471
   1.46703    -.25868
1.32655    .22109
```

(j) Sample Case 10, Continued.

Figure 14.- Continued.

```
1.16364    .67491
   .97343   1.16009
   .83926   1.45364
   .63717   1.75061
   .50422   1.88177
   .35039   1.98718
   .17987   2.05591
  0.00000   2.07983
   .00000  -2.15457
   .18782  -2.14678
   .37435  -2.12305
   .55798  -2.08241
   .73649  -2.02350
  1.06566  -1.84578
  1.33192  -1.58732
  1.50780  -1.26519
  1.58479   -.91498
  1.57883   -.57465
  1.51975   -.26797
1.37422    .22904
1.20545    .69916
  1.00841   1.20178
   .86942   1.50588
   .66007   1.81352
   .52234   1.94940
   .36299   2.05859
   .18633   2.12979
  0.00000   2.15457
   .00000  -2.22282
   .19377  -2.21478
   .38621  -2.19030
   .57565  -2.14837
   .75982  -2.08759
  1.09941  -1.90424
  1.37411  -1.63760
  1.55556  -1.30527
  1.63499   -.94396
  1.62884   -.59285
  1.56789   -.27646
1.41775    .23629
1.24364    .72131
  1.04036   1.23985
   .89696   1.55357
   .68097   1.87096
   .53888   2.01114
   .37448   2.12379
   .19223   2.19725
  0.00000   2.22282
   .00000  -2.28456
   .19915  -2.27630
   .39694  -2.25114
   .59165  -2.20805
   .78093  -2.14558
  1.12995  -1.95714
  1.41228  -1.68309
  1.59877  -1.34153
  1.68040   -.97018
  1.67409   -.60932
  1.61144   -.28414
1.45713    .24285
1.27818    .74135
  1.06925   1.27429
   .92187   1.59673
   .69989   1.92293
   .55385   2.06701
   .38488   2.18279
```

(j) Sample Case 10, Continued.

Figure 14.- Continued.

```
    .19757   2.25829
   0.00000   2.28456
    .00000  -2.33981
    .20397  -2.33135
    .40654  -2.30558
    .60595  -2.26145
    .79981  -2.19746
   1.15728  -2.00447
   1.44643  -1.72379
   1.63743  -1.37397
   1.72104   -.99364
   1.71457   -.62405
   1.65041   -.29101
1.49236    .24873
1.30909    .75927
   1.09511   1.30510
    .94416   1.63534
    .71681   1.96943
    .56725   2.11699
    .39419   2.23557
    .20235   2.31290
   0.00000   2.33981
    .00000  -2.38855
    .20822  -2.37992
    .41501  -2.35361
    .61858  -2.30854
    .81647  -2.24324
   1.18139  -2.04623
   1.47657  -1.75970
   1.67154  -1.40259
   1.75689  -1.01434
   1.75029   -.63705
   1.68479   -.29707
1.52345    .25391
1.33636    .77509
   1.11793   1.33229
    .96383   1.66941
    .73175   2.01046
    .57906   2.16110
    .40240   2.28215
    .20657   2.36108
   0.00000   2.38855
    .00000  -2.43080
    .21190  -2.42201
    .42235  -2.39524
    .62952  -2.34939
    .83091  -2.28292
   1.20228  -2.08242
   1.50268  -1.79083
   1.70111  -1.42740
   1.78797  -1.03228
   1.78125   -.64832
   1.71459   -.30233
1.55040    .25840
1.36000    .78880
   1.13770   1.35586
    .98088   1.69894
    .74469   2.04602
    .58931   2.19932
    .40952   2.32251
    .21022   2.40284
   0.00000   2.43080
    .00000  -2.46655
    .21501  -2.45763
    .42856  -2.43046
    .63877  -2.38394
```

(j) Sample Case 10, Continued.

Figure 14.- Continued.

```
   .84313  -2.31649
  1.21996  -2.11304
  1.52478  -1.81716
  1.72612  -1.44839
  1.81426  -1.04746
  1.80744   -.65786
  1.73981   -.30677
1.57320    .26220
1.38000    .80040
  1.15443   1.37580
   .99531   1.72392
   .75564   2.07611
   .59797   2.23166
   .41554   2.35667
   .21331   2.43818
  0.00000   2.46655
   .00000  -2.49580
   .21756  -2.48677
   .43364  -2.45928
   .64635  -2.41221
   .85313  -2.34396
  1.23443  -2.13810
  1.54286  -1.83871
  1.74659  -1.46556
  1.83577  -1.05988
  1.82887   -.66566
  1.76044   -.31041
1.59185    .26531
1.39636    .80989
  1.16812   1.39211
  1.00711   1.74436
   .76460   2.10073
   .60506   2.25813
   .42047   2.38461
   .21584   2.46709
  0.00000   2.49580
   .00000  -2.51854
   .21955  -2.50944
   .43759  -2.48170
   .65224  -2.43419
   .86091  -2.36532
  1.24568  -2.15758
  1.55692  -1.85547
  1.76251  -1.47892
  1.85251  -1.06955
  1.84554   -.67172
  1.77648   -.31324
1.60636    .26773
1.40909    .81727
  1.17877   1.40480
  1.01629   1.76026
   .77157   2.11987
   .61058   2.27871
   .42430   2.40635
   .21781   2.48958
  0.00000   2.51854
   .00000  -2.53479
   .22096  -2.52563
   .44041  -2.49771
   .65645  -2.44990
   .86646  -2.38058
  1.25372  -2.17150
  1.56697  -1.86744
  1.77388  -1.48846
  1.86446  -1.07645
  1.85745   -.67606
```

(j) Sample Case 10, Continued.

Figure 14.- Continued.

```
   1.78794   -.31526
  1.61673    .26945
  1.41818    .82255
    1.18637   1.41386
    1.02284   1.77162
     .77655   2.13355
     .61452   2.29341
     .42704   2.42187
     .21922   2.50564
    0.00000   2.53479
     .00000  -2.54454
     .22181  -2.53534
     .44211  -2.50732
     .65897  -2.45937
     .86979  -2.38974
    1.25854  -2.17986
    1.57300  -1.87462
    1.78070  -1.49419
    1.87163  -1.08059
    1.86459   -.67866
    1.79482   -.31648
  1.62295    .27049
  1.42364    .82571
    1.19093   1.41930
    1.02678   1.77843
     .77954   2.14176
     .61688   2.30223
     .42868   2.43119
     .22006   2.51529
    0.00000   2.54454
     .00000  -2.54779
     .22210  -2.53858
     .44267  -2.51052
     .65981  -2.46246
     .87091  -2.39279
    1.26015  -2.18264
    1.57500  -1.87702
    1.78298  -1.49610
    1.87402  -1.08197
    1.86698   -.67952
    1.79711   -.31688
  1.62502    .27084
  1.42545    .82676
    1.19245   1.42111
    1.02809   1.78070
     .78053   2.14449
     .61767   2.30517
     .42923   2.43429
     .22034   2.51849
    0.00000   2.54779
 LOBED CROSS SECTION BODY   -  ADDITIONAL PANELING INPUT
   0   0 -1
-18 14
 0.0    5.5      11.     19.5    28.     36.5    45.     53.5    62.     71.
 80.    97.5     115.    145.    154.5   164.    172.    180.
  0.     .5      1.0     1.5      2.0     2.5    3.0     3.5     4.0     4.5
  5.0    6.       7.     8.       9.     10.      12.     14.
```

(j) Sample Case 10, Concluded.

Figure 14.- Continued.

```
  1    0    0    1    0    0    1    1    0    1    0    0    0    0    0    0
  4    1    1    1    3    1    0
 NIELSEN ENGINEERING & RESEARCH, INC.                PROGRAM NOZVTX
 SAMPLE CASE 11
 2:1 ELLIPTICAL CROSS SECTION BODY          REF: AFFDL TR-79-3130 BY GOODWIN
 MACH NO.= 1.5, ALPHAC = 15 DEGREES, PHI = 0 DEGREES
.9636     .5625      6.        10.       1.025
 15.       0.0     1000000.     0.0       1.5
 .4        2.        .4       1.05       0.0       1.0       0.0
 .01       0.0       0.0       0.0       0.0
 14
 0.        .2        .4        .6        .8        1.0       1.2       1.4
 1.6       1.8       2.0       2.2       2.4       2.6
 0.       .0935     .1766     .2500     .3149     .3714     .4200     .4611
 .4949     .5218     .5418     .5550     .5617     .5625
 .4740     .4280     .3856     .3443     .3044     .2659     .2285     .1919
.1561     .1210     .0860     .0515     .01714     0.
0.        .1246     .2354     .3335     .4199     .4952     .5600     .6148
.6599     .6957     .7224     .7400     .7489     .7500
 0.       .0623     .1177     .1668     .2099     .2476     .2800     .3074
.3300     .3479     .3612     .3700     .3744     .3750
 1.6
 2:1 ELLIPTICAL CROSS SECTION BODY - WDYBDY GEOMETRY INPUT
 0  0
-3 -1  8 12
0.       .2      .4      .6       .8      1.     1.2     1.4     1.8     2.2
2.6      6.2
0.       .1246   .2354   .3335   .4200   .4952   .5600   .6148   .6957   .7401
.7500   .7500
 0.       .0623   .1177   .1668   .2100   .2476   .2800   .3074   .3479   .3700
.3750   .3750
 2:1 ELLIPTICAL CROSS SECTION BODY - ADDITIONAL PANELING INPUT
 0  0 -1
-10 11
0.       20.     53.     72.     85.     95.     108.    127.    160.    180.
0.       .2      .4      .6      .8      1.0     1.2     1.4     1.7     2.0
2.5
```

(k) Sample Case 11

Figure 14.- Concluded.

```
NIELSEN ENGINEERING & RESEARCH, INC.                    PROGRAM NDZVTX
SAMPLE CASE 1
3:1 ELLIPTICAL CROSS-SECTION BODY                  REF: NASA TM-74079 BY GRAVES
MACH NO = 2.5, ALPHAC = 20 DEGREES, PHI = 0 DEGREES


        REFERENCE QUANTITIES
          REF. AREA ........   12.57
          REF. LENGTH ......    4.00
          X(MOMENT CENTER) .   16.80
          BODY LENGTH (L)...   28.00
          BASE DIAMETER (D).    4.00


        FLOW CONDITIONS
          MACH NUMBER.......    2.50
          ALPHA C (DEG.) ...   20.00
          PHI (DEG.) .......    0.00
          REYNOLDS NO. (D)..   6.665E+05
          VORTEX FACTOR ....    1.00
          RCORE ............     .03

          ALPHA (DEG.) .....   20.00
          BETA (DEG.) ......    0.00
          U/V ..............     .940
          RE(2-DIM.)........   2.279E+05
          F(RE) CROSSFLOW...   5.699E+04


        INITIAL CONDITIONS       XI        XF        DX       TOL      EMKF      RGAM      FOX
                                2.800     5.600     1.400    .01000    1.050     0.000     0.000


        OPTIONS...

      NCIR     NCF    ISYM   NALSEP  NSEPR NSMOTH  NUFUS  NUPHI   INP   NXFV   NFV   NVP   NVR   NVM   NVA  NASYM
        1       0       0       1       0       0       1       1       0       1      10       0       0       0       0       0

      NPRNTP NPRNTS NPRNTV NPLOTV NPLOTA NPRTVL
        1       1       1       3       2       0

DEFINITIONS OF OUTPUT QUANTITIES ...
     CN(X)      (DCN/DX)/(Q*D) , POSITIVE UP
     CY(X)      (DCY/DX)/(Q*D) , POSITIVE RIGHT
     CN         N/(Q*REFS) , POSITIVE UP
     CY         Y/(Q*REFS) , POSITIVE RIGHT
     CM         M/(Q*REFS*REFL) , POSITIVE NOSE UP
     CR         R/(Q*REFS*REFL) , POSITIVE NOSE LEFT
     CLL        L/(Q*REFS*REFL) , POSITIVE COUNTERCLOCKWISE
```

(a) Page 1

Figure 15.- Output for sample case 1.

INPUT GEOMETRY CHARACTERISTICS
NXR = 30

X	R	DR/DX	A	H
0.0000	0.0000	.2800	0.0000	0.0000
.4200	.1180	.2800	.1760	.0590
.7000	.1960	.2800	.2940	.0980
2.1000	.5870	.2340	.8810	.2940
3.5000	.8500	.1750	1.2750	.4250
4.9000	1.0780	.1580	1.6170	.5390
5.6000	1.1820	.1450	1.7740	.5910
6.3000	1.2810	.1350	1.9220	.6410
7.7000	1.4650	.1280	2.1980	.7330
8.4000	1.5500	.1190	2.3260	.7750
9.1000	1.6310	.1100	2.4470	.8160
10.5000	1.7810	.1020	2.6720	.8910
11.9000	1.9160	.0930	2.8740	.9580
12.6000	1.9770	.0850	2.9650	.9880
13.3000	2.0340	.0760	3.0510	1.0170
14.7000	2.1360	.0690	3.2030	1.0680
15.4000	2.1790	.0550	3.2690	1.0900
16.8000	2.2520	.0470	3.3780	1.1260
17.5000	2.2790	.0340	3.4180	1.1400
18.2000	2.2990	.0200	3.4480	1.1490
19.0400	2.3090	.0040	3.4640	1.1550
19.7000	2.3040	-.0170	3.4560	1.1520
20.3000	2.2880	-.0300	3.4320	1.1440
21.0000	2.2650	-.0410	3.3970	1.1320
22.4000	2.2020	-.0470	3.3030	1.1010
23.1000	2.1650	-.0550	3.2480	1.0830
24.5000	2.0860	-.0570	3.1280	1.0430
25.9000	2.0060	-.0550	3.0090	1.0030
26.6000	1.9700	-.0390	2.9550	.9850
28.0000	1.9230	-.0340	2.8850	.9620

ADDITIONAL OUTPUT PRINTED AT THE FOLLOWING AXIAL STATIONS

XFV = 4.20

FLOW FIELD VELOCITIES ARE CALCULATED AT FIELD POINTS

YFV/R	ZFV/R
.250	.750
.250	1.000
.500	.750
.500	1.000
.750	.500
.750	1.000
1.000	.500
1.000	1.000
1.250	.500
1.250	1.000

(b) Page 2

Figure 15.- Continued.

3:1 ELLIPTICAL CROSS-SECTION BODY - WDYBDY GEOMETRY INPUT ** GEOM **

PRINT OPTIONS AND PANEL SYMMETRY

IPRT(1)	IXZSYM	ITHSYM
1	0	0

GEOMETRY OPTION INFORMATION

J2	J6	NFUS	NRAUX	NFORX
-3	-1	1	10	30

VEHICLE GEOMETRY DEFINTION ** CONFIG **

NFU	XFUS - FUSELAGE X-STATIONS									
1	0.00000	.42000	.70000	2.10000	3.50000	4.90000	5.60000	6.30000	7.70000	8.40000
1	9.10000	10.50000	11.90000	12.60000	13.30000	14.70000	15.40000	16.80000	17.50000	18.20000
1	19.04000	19.70000	20.30000	21.00000	22.40000	23.10000	24.50000	25.90000	26.60000	28.00000

NFU	FUSBY - ELLIPTIC FUSELAGE SEMI-MAJOR AXES									
1	0.00000	.17600	.29400	.88100	1.27500	1.61700	1.77400	1.92200	2.19800	2.32600
1	2.44700	2.67200	2.87400	2.96500	3.05100	3.20300	3.26900	3.37800	3.41800	3.44800
1	3.46400	3.45600	3.43200	3.39700	3.30300	3.24800	3.12800	3.00900	2.95500	2.88500

NFU	FUSAZ - ELLIPTIC FUSELAGE SEMI-MINOR AXES									
1	0.00000	.05900	.09800	.29400	.42500	.53900	.59100	.64100	.73300	.77500
1	.81600	.89100	.95800	.98800	1.01700	1.06800	1.09000	1.12600	1.14000	1.14900
1	1.15500	1.15200	1.14400	1.13200	1.10100	1.08300	1.04300	1.00300	.98500	.96200

(c) Page 3

Figure 15.- Continued.

3:1 ELLIPTICAL CROSS-SECTION BODY - ADDITIONAL PANELING INPUT ** GEOM **

OUTPUT OPTION, IPRINT = -1

ADDITIONAL PANELING INFORMATION

K2	KFUS	KRADX	KFORX
1	1	0	8

XFUSK= 0. .42000 .70000 2.1000 3.5000 4.9000 5.6000 6.3000

(d) Page 4

Figure 15.- Continued.

BODY PANEL CORNER POINT COORDINATES ** BODPAN **

1 AND 3 INDICATE BODY PANEL LEADING-EDGE POINTS, 2 AND 4 INDICATE TRAILING-EDGE POINTS

PANEL	X 1	Y 1	Z 1	X 2	Y 2	Z 2	X 3	Y 3	Z 3	X 4	Y 4	Z 4
1	0.00000	0.00000	0.00000	.42000	.00000	-.05900	0.00000	0.00000	0.00000	.42000	.02132	-.05857
2	0.00000	0.00000	0.00000	.42000	.02132	-.05857	0.00000	0.00000	0.00000	.42000	.04766	-.05680
3	0.00000	0.00000	0.00000	.42000	.04766	-.05680	0.00000	0.00000	0.00000	.42000	.08837	-.05102
4	0.00000	0.00000	0.00000	.42000	.08837	-.05102	0.00000	0.00000	0.00000	.42000	.15577	-.02747
5	0.00000	0.00000	0.00000	.42000	.15577	-.02747	0.00000	0.00000	0.00000	.42000	.15577	.02747
6	0.00000	0.00000	0.00000	.42000	.15577	.02747	0.00000	0.00000	0.00000	.42000	.08837	.05102
7	0.00000	0.00000	0.00000	.42000	.08837	.05102	0.00000	0.00000	0.00000	.42000	.04766	.05680
8	0.00000	0.00000	0.00000	.42000	.04766	.05680	0.00000	0.00000	0.00000	.42000	.02132	.05857
9	0.00000	0.00000	0.00000	.42000	.02132	.05857	0.00000	0.00000	0.00000	.42000	-.00000	.05900
10	0.00000	0.00000	0.00000	.42000	-.00000	.05900	0.00000	0.00000	0.00000	.42000	-.02132	.05857
11	0.00000	0.00000	0.00000	.42000	-.02132	.05857	0.00000	0.00000	0.00000	.42000	-.04766	.05680
12	0.00000	0.00000	0.00000	.42000	-.04766	.05680	0.00000	0.00000	0.00000	.42000	-.08837	.05102
13	0.00000	0.00000	0.00000	.42000	-.08837	.05102	0.00000	0.00000	0.00000	.42000	-.15577	.02747
14	0.00000	0.00000	0.00000	.42000	-.15577	.02747	0.00000	0.00000	0.00000	.42000	-.15577	-.02747
15	0.00000	0.00000	0.00000	.42000	-.15577	-.02747	0.00000	0.00000	0.00000	.42000	-.08837	-.05102
16	0.00000	0.00000	0.00000	.42000	-.08837	-.05102	0.00000	0.00000	0.00000	.42000	-.04766	-.05680
17	0.00000	0.00000	0.00000	.42000	-.04766	-.05680	0.00000	0.00000	0.00000	.42000	-.02132	-.05857
18	0.00000	0.00000	0.00000	.42000	-.02132	-.05857	0.00000	0.00000	0.00000	.42000	-.00000	-.05900
19	.42000	.00000	-.05900	.70000	.00000	-.09800	.42000	.02132	-.05857	.70000	.03541	-.09729
20	.42000	.02132	-.05857	.70000	.03541	-.09729	.42000	.04766	-.05680	.70000	.07919	-.09438
21	.42000	.04766	-.05680	.70000	.07919	-.09438	.42000	.08837	-.05102	.70000	.14700	-.08487
22	.42000	.08837	-.05102	.70000	.14700	-.08487	.42000	.15577	-.02747	.70000	.25988	-.04582
23	.42000	.15577	-.02747	.70000	.25988	-.04582	.42000	.15577	.02747	.70000	.25988	.04582
24	.42000	.15577	.02747	.70000	.25988	.04582	.42000	.08837	.05102	.70000	.14700	.08487
25	.42000	.08837	.05102	.70000	.14700	.08487	.42000	.04766	.05680	.70000	.07919	.09438
26	.42000	.04766	.05680	.70000	.07919	.09438	.42000	.02132	.05857	.70000	.03541	.09729
27	.42000	.02132	.05857	.70000	.03541	.09729	.42000	-.00000	.05900	.70000	-.00000	.09800
28	.42000	-.00000	.05900	.70000	-.00000	.09800	.42000	-.02132	.05857	.70000	-.03541	.09729
29	.42000	-.02132	.05857	.70000	-.03541	.09729	.42000	-.04766	.05680	.70000	-.07919	.09438
30	.42000	-.04766	.05680	.70000	-.07919	.09438	.42000	-.08837	.05102	.70000	-.14700	.08487
31	.42000	-.08837	.05102	.70000	-.14700	.08487	.42000	-.15577	.02747	.70000	-.25988	.04582
32	.42000	-.15577	.02747	.70000	-.25988	.04582	.42000	-.15577	-.02747	.70000	-.25988	-.04582
33	.42000	-.15577	-.02747	.70000	-.25988	-.04582	.42000	-.08837	-.05102	.70000	-.14700	-.08487
34	.42000	-.08837	-.05102	.70000	-.14700	-.08487	.42000	-.04766	-.05680	.70000	-.07919	-.09438
35	.42000	-.04766	-.05680	.70000	-.07919	-.09438	.42000	-.02132	-.05857	.70000	-.03541	-.09729
36	.42000	-.02132	-.05857	.70000	-.03541	-.09729	.42000	-.00000	-.05900	.70000	-.00000	-.09800
37	.70000	.00000	-.09800	2.10000	.00000	-.29400	.70000	.03541	-.09729	2.10000	.10623	-.29186
38	.70000	.03541	-.09729	2.10000	.10623	-.29186	.70000	.07919	-.09438	2.10000	.23756	-.28311
39	.70000	.07919	-.09438	2.10000	.23756	-.28311	.70000	.14700	-.08487	2.10000	.44087	-.25454
40	.70000	.14700	-.08487	2.10000	.44087	-.25454	.70000	.25988	-.04582	2.10000	.77895	-.13735
41	.70000	.25988	-.04582	2.10000	.77895	-.13735	.70000	.25988	.04582	2.10000	.77895	.13735
42	.70000	.25988	.04582	2.10000	.77895	.13735	.70000	.14700	.08487	2.10000	.44087	.25454
43	.70000	.14700	.08487	2.10000	.44087	.25454	.70000	.07919	.09438	2.10000	.23756	.28311
44	.70000	.07919	.09438	2.10000	.23756	.28311	.70000	.03541	.09729	2.10000	.10623	.29186
45	.70000	.03541	.09729	2.10000	.10623	.29186	.70000	-.00000	.09800	2.10000	-.00000	.29400
46	.70000	-.00000	.09800	2.10000	-.00000	.29400	.70000	-.03541	.09729	2.10000	-.10623	.29186
47	.70000	-.03541	.09729	2.10000	-.10623	.29186	.70000	-.07919	.09438	2.10000	-.23756	.28311
48	.70000	-.07919	.09438	2.10000	-.23756	.28311	.70000	-.14700	.08487	2.10000	-.44087	.25454
49	.70000	-.14700	.08487	2.10000	-.44087	.25454	.70000	-.25988	.04582	2.10000	-.77895	.13735
50	.70000	-.25988	.04582	2.10000	-.77895	.13735	.70000	-.25988	-.04582	2.10000	-.77895	-.13735
51	.70000	-.25988	-.04582	2.10000	-.77895	-.13735	.70000	-.14700	-.08487	2.10000	-.44087	-.25454
52	.70000	-.14700	-.08487	2.10000	-.44087	-.25454	.70000	-.07919	-.09438	2.10000	-.23756	-.28311
53	.70000	-.07919	-.09438	2.10000	-.23756	-.28311	.70000	-.03541	-.09729	2.10000	-.10623	-.29186

(e) Page 5

Figure 15.- Continued.

54	.70000	-.03541	-.09729	2.10000	-.10623	-.29186	.70000	-.00000	-.09800	2.10000	-.00000	-.29400
55	2.10000	.00000	-.29400	3.50000	.00000	-.42500	2.10000	.10623	-.29186	3.50000	.15356	-.42191
56	2.10000	.10623	-.29186	3.50000	.15356	-.42191	2.10000	.23756	-.28311	3.50000	.34344	-.40929
57	2.10000	.23756	-.28311	3.50000	.34344	-.40929	2.10000	.44087	-.25454	3.50000	.63750	-.36806
58	2.10000	.44087	-.25454	3.50000	.63750	-.36806	2.10000	.77895	-.13735	3.50000	1.12703	-.19873
59	2.10000	.77895	-.13735	3.50000	1.12703	-.19873	2.10000	.77895	.13735	3.50000	1.12703	.19873
60	2.10000	.77895	.13735	3.50000	1.12703	.19873	2.10000	.44087	.25454	3.50000	.63750	.36806
61	2.10000	.44087	.25454	3.50000	.63750	.36806	2.10000	.23756	.28311	3.50000	.34344	.40929
62	2.10000	.23756	.28311	3.50000	.34344	.40929	2.10000	.10623	.29186	3.50000	.15356	.42191
63	2.10000	.10623	.29186	3.50000	.15356	.42191	2.10000	-.00000	.29400	3.50000	-.00000	.42500
64	2.10000	-.00000	.29400	3.50000	-.00000	.42500	2.10000	-.10623	.29186	3.50000	-.15356	.42191
65	2.10000	-.10623	.29186	3.50000	-.15356	.42191	2.10000	-.23756	.28311	3.50000	-.34344	.40929
66	2.10000	-.23756	.28311	3.50000	-.34344	.40929	2.10000	-.44087	.25454	3.50000	-.63750	.36806
67	2.10000	-.44087	.25454	3.50000	-.63750	.36806	2.10000	-.77895	.13735	3.50000	-1.12703	.19873
68	2.10000	-.77895	.13735	3.50000	-1.12703	.19873	2.10000	-.77895	-.13735	3.50000	-1.12703	-.19873
69	2.10000	-.77895	-.13735	3.50000	-1.12703	-.19873	2.10000	-.44087	-.25454	3.50000	-.63750	-.36806
70	2.10000	-.44087	-.25454	3.50000	-.63750	-.36806	2.10000	-.23756	-.28311	3.50000	-.34344	-.40929
71	2.10000	-.23756	-.28311	3.50000	-.34344	-.40929	2.10000	-.10623	-.29186	3.50000	-.15356	-.42191
72	2.10000	-.10623	-.29186	3.50000	-.15356	-.42191	2.10000	-.00000	-.29400	3.50000	-.00000	-.42500
73	3.50000	.00000	-.42500	4.90000	.00000	-.53900	3.50000	.15356	-.42191	4.90000	.19475	-.53508
74	3.50000	.15356	-.42191	4.90000	.19475	-.53508	3.50000	.34344	-.40929	4.90000	.43556	-.51908
75	3.50000	.34344	-.40929	4.90000	.43556	-.51908	3.50000	.63750	-.36806	4.90000	.80850	-.46679
76	3.50000	.63750	-.36806	4.90000	.80850	-.46679	3.50000	1.12703	-.19873	4.90000	1.42934	-.25203
77	3.50000	1.12703	-.19873	4.90000	1.42934	-.25203	3.50000	1.12703	.19873	4.90000	1.42934	.25203
78	3.50000	1.12703	.19873	4.90000	1.42934	.25203	3.50000	.63750	.36806	4.90000	.80850	.46679
79	3.50000	.63750	.36806	4.90000	.80850	.46679	3.50000	.34344	.40929	4.90000	.43556	.51908
80	3.50000	.34344	.40929	4.90000	.43556	.51908	3.50000	.15356	.42191	4.90000	.19475	.53508
81	3.50000	.15356	.42191	4.90000	.19475	.53508	3.50000	-.00000	.42500	4.90000	-.00000	.53900
82	3.50000	-.00000	.42500	4.90000	-.00000	.53900	3.50000	-.15356	.42191	4.90000	-.19475	.53508
83	3.50000	-.15356	.42191	4.90000	-.19475	.53508	3.50000	-.34344	.40929	4.90000	-.43556	.51908
84	3.50000	-.34344	.40929	4.90000	-.43556	.51908	3.50000	-.63750	.36806	4.90000	-.80850	.46679
85	3.50000	-.63750	.36806	4.90000	-.80850	.46679	3.50000	-1.12703	.19873	4.90000	-1.42934	.25203
86	3.50000	-1.12703	.19873	4.90000	-1.42934	.25203	3.50000	-1.12703	-.19873	4.90000	-1.42934	-.25203
87	3.50000	-1.12703	-.19873	4.90000	-1.42934	-.25203	3.50000	-.63750	-.36806	4.90000	-.80850	-.46679
88	3.50000	-.63750	-.36806	4.90000	-.80850	-.46679	3.50000	-.34344	-.40929	4.90000	-.43556	-.51908
89	3.50000	-.34344	-.40929	4.90000	-.43556	-.51908	3.50000	-.15356	-.42191	4.90000	-.19475	-.53508
90	3.50000	-.15356	-.42191	4.90000	-.19475	-.53508	3.50000	-.00000	-.42500	4.90000	-.00000	-.53900
91	4.90000	.00000	-.53900	5.60000	.00000	-.59100	4.90000	.19475	-.53508	5.60000	.21354	-.58670
92	4.90000	.19475	-.53508	5.60000	.21354	-.58670	4.90000	.43556	-.51908	5.60000	.47760	-.56918
93	4.90000	.43556	-.51908	5.60000	.47760	-.56918	4.90000	.80850	-.46679	5.60000	.88662	-.51189
94	4.90000	.80850	-.46679	5.60000	.88662	-.51189	4.90000	1.42934	-.25203	5.60000	1.56793	-.27647
95	4.90000	1.42934	-.25203	5.60000	1.56793	-.27647	4.90000	1.42934	.25203	5.60000	1.56793	.27647
96	4.90000	1.42934	.25203	5.60000	1.56793	.27647	4.90000	.80850	.46679	5.60000	.88662	.51189
97	4.90000	.80850	.46679	5.60000	.88662	.51189	4.90000	.43556	.51908	5.60000	.47760	.56918
98	4.90000	.43556	.51908	5.60000	.47760	.56918	4.90000	.19475	.53508	5.60000	.21354	.58670
99	4.90000	.19475	.53508	5.60000	.21354	.58670	4.90000	-.00000	.53900	5.60000	-.00000	.59100
100	4.90000	-.00000	.53900	5.60000	-.00000	.59100	4.90000	-.19475	.53508	5.60000	-.21354	.58670
101	4.90000	-.19475	.53508	5.60000	-.21354	.58670	4.90000	-.43556	.51908	5.60000	-.47760	.56918
102	4.90000	-.43556	.51908	5.60000	-.47760	.56918	4.90000	-.80850	.46679	5.60000	-.88662	.51189
103	4.90000	-.80850	.46679	5.60000	-.88662	.51189	4.90000	-1.42934	.25203	5.60000	-1.56793	.27647
104	4.90000	-1.42934	.25203	5.60000	-1.56793	.27647	4.90000	-1.42934	-.25203	5.60000	-1.56793	-.27647
105	4.90000	-1.42934	-.25203	5.60000	-1.56793	-.27647	4.90000	-.80850	-.46679	5.60000	-.88662	-.51189
106	4.90000	-.80850	-.46679	5.60000	-.88662	-.51189	4.90000	-.43556	-.51908	5.60000	-.47760	-.56918
107	4.90000	-.43556	-.51908	5.60000	-.47760	-.56918	4.90000	-.19475	-.53508	5.60000	-.21354	-.58670
108	4.90000	-.19475	-.53508	5.60000	-.21354	-.58670	4.90000	-.00000	-.53900	5.60000	-.00000	-.59100
109	5.60000	.00000	-.59100	6.30000	.00000	-.64100	5.60000	.21354	-.58670	6.30000	.23160	-.63633
110	5.60000	.21354	-.58670	6.30000	.23160	-.63633	5.60000	.47760	-.56918	6.30000	.51796	-.61728
111	5.60000	.47760	-.56918	6.30000	.51796	-.61728	5.60000	.88662	-.51189	6.30000	.96137	-.55505
112	5.60000	.88662	-.51189	6.30000	.96137	-.55505	5.60000	1.56793	-.27647	6.30000	1.69914	-.29960
113	5.60000	1.56793	-.27647	6.30000	1.69914	-.29960	5.60000	1.56793	.27647	6.30000	1.69914	.29960

(f) Page 6

Figure 15.- Continued.

114	5.60000	1.56793	.27647	6.30000	1.69914	.29960	5.60000	.88662	.51189	6.30000	.96137	.55505
115	5.60000	.88662	.51189	6.30000	.96137	.55505	5.60000	.47760	.56918	6.30000	.51796	.61728
116	5.60000	.47760	.56918	6.30000	.51796	.61728	5.60000	.21354	.58670	6.30000	.23160	.63633
117	5.60000	.21354	.58670	6.30000	.23160	.63633	5.60000	-.00000	.59100	6.30000	-.00000	.64100
118	5.60000	-.00000	.59100	6.30000	-.00000	.64100	5.60000	-.21354	.58670	6.30000	-.23160	.63633
119	5.60000	-.21354	.58670	6.30000	-.23160	.63633	5.60000	-.47760	.56918	6.30000	-.51796	.61728
120	5.60000	-.47760	.56918	6.30000	-.51796	.61728	5.60000	-.88662	.51189	6.30000	-.96137	.55505
121	5.60000	-.88662	.51189	6.30000	-.96137	.55505	5.60000	-1.56793	.27647	6.30000	-1.69914	.29960
122	5.60000	-1.56793	.27647	6.30000	-1.69914	.29960	5.60000	-1.56793	-.27647	6.30000	-1.69914	-.29960
123	5.60000	-1.56793	-.27647	6.30000	-1.69914	-.29960	5.60000	-.88662	-.51189	6.30000	-.96137	-.55505
124	5.60000	-.88662	-.51189	6.30000	-.96137	-.55505	5.60000	-.47760	-.56918	6.30000	-.51796	-.61728
125	5.60000	-.47760	-.56918	6.30000	-.51796	-.61728	5.60000	-.21354	-.58670	6.30000	-.23160	-.63633
126	5.60000	-.21354	-.58670	6.30000	-.23160	-.63633	5.60000	-.00000	-.59100	6.30000	-.00000	-.64100

(g) Page 7

Figure 15.- Continued.

BODY PANEL CENTROID POINT COORDINATES

POINT	X CP	Y CP	Z CP
1	.28000	.00711	-.03919
2	.28000	.02299	-.03845
3	.28000	.04534	-.03594
4	.28000	.08138	-.02616
5	.28000	.10384	.00000
6	.28000	.08138	.02616
7	.28000	.04534	.03594
8	.28000	.02299	.03845
9	.28000	.00711	.03919
10	.28000	-.00711	.03919
11	.28000	-.02299	.03845
12	.28000	-.04534	.03594
13	.28000	-.08138	.02616
14	.28000	-.10384	.00000
15	.28000	-.08138	-.02616
16	.28000	-.04534	-.03594
17	.28000	-.02299	-.03845
18	.28000	-.00711	-.03919
19	.57159	.01447	-.07982
20	.57161	.04684	-.07834
21	.57164	.09243	-.07325
22	.57175	.16617	-.05339
23	.57169	.21217	.00000
24	.57175	.16617	.05339
25	.57164	.09243	.07325
26	.57161	.04684	.07834
27	.57159	.01447	.07982
28	.57159	-.01447	.07982
29	.57161	-.04684	.07834
30	.57164	-.09243	.07325
31	.57175	-.16617	.05339
32	.57169	-.21217	.00000
33	.57175	-.16617	-.05339
34	.57164	-.09243	-.07325
35	.57161	-.04684	-.07834
36	.57159	-.01447	-.07982
37	1.51667	.03836	-.21156
38	1.51666	.12414	-.20763
39	1.51663	.24499	-.19415
40	1.51654	.44051	-.14152
41	1.51659	.56264	.00000
42	1.51654	.44051	.14152
43	1.51663	.24499	.19415
44	1.51666	.12414	.20763
45	1.51667	.03836	.21156
46	1.51667	-.03836	.21156
47	1.51666	-.12414	.20763
48	1.51663	-.24499	.19415
49	1.51654	-.44051	.14152
50	1.51659	-.56264	.00000
51	1.51654	-.44051	-.14152
52	1.51663	-.24499	-.19415
53	1.51666	-.12414	-.20763
54	1.51667	-.03836	-.21156
55	2.84251	.06567	-.16215

(h) Page 8

Figure 15.- Continued.

56	2.84253	.21252	-.35543
57	2.84257	.41944	-.33239
58	2.84267	.75439	-.24233
59	2.84261	.96358	.00000
60	2.84267	.75439	.24233
61	2.84257	.41944	.33239
62	2.84253	.21252	.35543
63	2.84251	.06567	.36215
64	2.84251	-.06567	.36215
65	2.84253	-.21252	.35543
66	2.84257	-.41944	.33239
67	2.84267	-.75439	.24233
68	2.84261	-.96358	.00000
69	2.84267	-.75439	-.24233
70	2.84257	-.41944	-.33239
71	2.84253	-.21252	-.35543
72	2.84251	-.06567	-.36215
73	4.22759	.08748	-.48248
74	4.22759	.28314	-.47354
75	4.22759	.55884	-.44286
76	4.22759	1.00526	-.32290
77	4.22759	1.28414	.00000
78	4.22759	1.00526	.32290
79	4.22759	.55884	.44286
80	4.22759	.28314	.47354
81	4.22759	.08748	.48248
82	4.22759	-.08748	.48248
83	4.22759	-.28314	.47354
84	4.22759	-.55884	.44286
85	4.22759	-1.00526	.32290
86	4.22759	-1.28414	.00000
87	4.22759	-1.00526	-.32290
88	4.22759	-.55884	-.44286
89	4.22759	-.28314	-.47354
90	4.22759	-.08748	-.48248
91	5.25537	.10215	-.56334
92	5.25537	.33060	-.55290
93	5.25538	.65253	-.51710
94	5.25541	1.17394	-.37706
95	5.25539	1.49970	.00000
96	5.25541	1.17394	.37706
97	5.25538	.65253	.51710
98	5.25537	.33060	.55290
99	5.25537	.10215	.56334
100	5.25537	-.10215	.56334
101	5.25537	-.33060	.55290
102	5.25538	-.65253	.51710
103	5.25541	-1.17394	.37706
104	5.25539	-1.49970	.00000
105	5.25541	-1.17394	-.37706
106	5.25538	-.65253	-.51710
107	5.25537	-.33060	-.55290
108	5.25537	-.10215	-.56334
109	5.95473	.11135	-.61409
110	5.95473	.36037	-.60270
111	5.95471	.71128	-.56366
112	5.95465	1.27945	-.41098
113	5.95469	1.63441	.00000
114	5.95465	1.27945	.41098
115	5.95471	.71128	.56366

(i) Page 9

Figure 15.- Continued.

116	5.95473	.36037	.60270
117	5.95473	.11135	.61409
118	5.95473	-.11135	.61409
119	5.95473	-.36037	.60270
120	5.95471	-.71128	.56366
121	5.95465	-1.27945	.41098
122	5.95469	-1.63441	.00000
123	5.95465	-1.27945	-.41098
124	5.95471	-.71128	-.56366
125	5.95473	-.36037	-.60270
126	5.95473	-.11135	-.61409

(j) Page 10

Figure 15.- Continued.

BODY PANEL AREAS AND INCLINATION ANGLES

BODY PANEL	PANEL AREA	DELTA RAD	THETA RAD	DELTA DEG	THETA DEG
1	.00452	.13953	-3.12122	7.99473	-178.833
2	.00560	.14158	-3.07450	8.11178	-176.156
3	.00873	.14871	-3.00075	8.52056	-171.930
4	.01524	.18207	-2.80532	10.43191	-160.733
5	.01230	.35515	-1.57080	20.34842	-90.000
6	.01524	.18207	-.33628	10.43191	-19.267
7	.00873	.14871	-.14084	8.52056	-8.070
8	.00560	.14158	-.06709	8.11178	-3.844
9	.00452	.13953	-.02037	7.99473	-1.167
10	.00452	.13953	.02037	7.99473	1.167
11	.00560	.14158	.06709	8.11178	3.844
12	.00873	.14871	.14084	8.52056	8.070
13	.01524	.18207	.33628	10.43191	19.267
14	.01230	.35515	1.57080	20.34842	90.000
15	.01524	.18207	2.80532	10.43191	160.733
16	.00873	.14871	3.00075	8.52056	171.930
17	.00560	.14158	3.07450	8.11178	176.156
18	.00452	.13953	3.12122	7.99473	178.833
19	.00802	.13838	-3.12136	7.92848	-178.841
20	.00994	.14045	-3.07497	8.04698	-176.183
21	.01551	.14767	-3.00171	8.46097	-171.985
22	.02716	.18138	-2.80735	10.39255	-160.849
23	.02189	.35599	-1.57080	20.39685	-90.000
24	.02716	.18138	-.33424	10.39255	-19.151
25	.01551	.14767	-.13988	8.46097	-8.015
26	.00994	.14045	-.06662	8.04698	-3.817
27	.00802	.13838	-.02023	7.92848	-1.159
28	.00802	.13838	.02023	7.92848	1.159
29	.00994	.14045	.06662	8.04698	3.817
30	.01551	.14767	.13988	8.46097	8.015
31	.02716	.18138	.33424	10.39255	19.151
32	.02189	.35599	1.57080	20.39685	90.000
33	.02716	.18138	2.80735	10.39255	160.849
34	.01551	.14767	3.00171	8.46097	171.985
35	.00994	.14045	3.07497	8.04698	176.183
36	.00802	.13838	3.12136	7.92848	178.841
37	.10013	.13907	-3.12141	7.96796	-178.844
38	.12408	.14108	-3.07514	8.08343	-176.193
39	.19377	.14813	-3.00206	8.48704	-172.005
40	.33964	.18118	-2.80808	10.38092	-160.891
41	.27350	.35505	-1.57080	20.34294	-90.000
42	.33964	.18118	-.33351	10.38092	-19.109
43	.19377	.14813	-.13953	8.48704	-7.995
44	.12408	.14108	-.06645	8.08343	-3.807
45	.10013	.13907	-.02018	7.96796	-1.156
46	.10013	.13907	.02018	7.96796	1.156
47	.12408	.14108	.06645	8.08343	3.807
48	.19377	.14813	.13953	8.48704	7.995
49	.33964	.18118	.33351	10.38092	19.109
50	.27350	.35505	1.57080	20.34294	90.000
51	.33964	.18118	2.80808	10.38092	160.891
52	.19377	.14813	3.00206	8.48704	172.005
53	.12408	.14108	3.07514	8.08343	176.193
54	.10013	.13907	3.12141	7.96796	178.844
55	.18268	.09328	-3.12143	5.34472	-178.845

(k) Page 11

Figure 15.- Continued.

56	.22635	.09466	-3.07519	5.42344	-176.196
57	.35332	.09946	-3.00216	5.69880	-172.011
58	.61766	.12206	-2.80830	6.99357	-160.904
59	.48483	.24369	-1.57080	13.96232	-90.000
60	.61766	.12206	-.33329	6.99357	-19.096
61	.35332	.09946	-.13943	5.69880	-7.989
62	.22635	.09466	-.06640	5.42344	-3.804
63	.18268	.09328	-.02016	5.34472	-1.155
64	.18268	.09328	.02016	5.34472	1.155
65	.22635	.09466	.06640	5.42344	3.804
66	.35332	.09946	.13943	5.69880	7.989
67	.61766	.12206	.33329	6.99357	19.096
68	.48483	.24369	1.57080	13.96232	90.000
69	.61766	.12206	2.80830	6.99357	160.904
70	.35332	.09946	3.00216	5.69880	172.011
71	.22635	.09466	3.07519	5.42344	176.196
72	.18268	.09328	3.12143	5.34472	178.845
73	.24468	.08123	-3.12145	4.65430	-178.846
74	.30317	.08242	-3.07525	4.72239	-176.199
75	.47324	.08658	-3.00229	4.96061	-172.019
76	.82710	.10617	-2.80856	6.08328	-160.919
77	.64560	.21267	-1.57080	12.18509	-90.000
78	.82710	.10617	-.33303	6.08328	-19.081
79	.47324	.08658	-.13930	4.96061	-7.981
80	.30317	.08242	-.06634	4.72239	-3.801
81	.24468	.08123	-.02014	4.65430	-1.154
82	.24468	.08123	.02014	4.65430	1.154
83	.30317	.08242	.06634	4.72239	3.801
84	.47324	.08658	.13930	4.96061	7.981
85	.82710	.10617	.33303	6.08328	19.081
86	.64560	.21267	1.57080	12.18509	90.000
87	.82710	.10617	2.80856	6.08328	160.919
88	.47324	.08658	3.00229	4.96061	172.019
89	.30317	.08242	3.07525	4.72239	176.199
90	.24468	.08123	3.12145	4.65430	178.846
91	.14333	.07414	-3.12146	4.24778	-178.847
92	.17759	.07524	-3.07529	4.31089	-176.201
93	.27723	.07909	-3.00237	4.53168	-172.023
94	.48451	.09722	-2.80873	5.57015	-160.928
95	.37713	.19545	-1.57080	11.19861	-90.000
96	.48451	.09722	-.33286	5.57015	-19.072
97	.27723	.07909	-.13922	4.53168	-7.977
98	.17759	.07524	-.06630	4.31089	-3.799
99	.14333	.07414	-.02013	4.24778	-1.153
100	.14333	.07414	.02013	4.24778	1.153
101	.17759	.07524	.06630	4.31089	3.799
102	.27723	.07909	.13922	4.53168	7.977
103	.48451	.09722	.33286	5.57015	19.072
104	.37713	.19545	1.57080	11.19861	90.000
105	.48451	.09722	2.80873	5.57015	160.928
106	.27723	.07909	3.00237	4.53168	172.023
107	.17759	.07524	3.07529	4.31089	176.201
108	.14333	.07414	3.12146	4.24778	178.847
109	.15623	.07129	-3.12145	4.08440	-178.846
110	.19358	.07230	-3.07525	4.14221	-176.199
111	.30214	.07583	-3.00229	4.34459	-172.019
112	.52781	.09258	-2.80856	5.30432	-160.919
113	.41027	.18529	-1.57080	10.61653	-90.000
114	.52781	.09258	-.33303	5.30432	-19.081
115	.30214	.07583	-.13930	4.34459	-7.981

(ℓ) Page 12

Figure 15.- Continued.

116	.19358	.07230	-.06634	4.14221	-3.801
117	.15623	.07129	-.02014	4.08440	-1.154
118	.15623	.07129	.02014	4.08440	1.154
119	.19358	.07230	.06634	4.14221	3.801
120	.30214	.07583	.13930	4.34459	7.981
121	.52781	.09258	.33303	5.30432	19.081
122	.41027	.18529	1.57080	10.61653	90.000
123	.52781	.09258	2.80856	5.30432	160.919
124	.30214	.07583	3.00229	4.34459	172.019
125	.19358	.07230	3.07525	4.14221	176.199
126	.15623	.07129	3.12145	4.08440	178.846

THE ITERATION CONVERGED AFTER 7 ITERATIONS WITH A TEST CRITERION OF .0010000

THE SOLUTION AT THE PRESENT ITERATION IS
GA(N),N=1,126

.80241	.79565	.77233	.67589	.06642	-.39400	-.51046	-.54133	-.55058	-.55058
-.54133	-.51046	-.39400	.06642	.67589	.77233	.79565	.80241	.80419	.79739
.77416	.67765	.06567	-.39600	-.51378	-.54488	-.55415	-.55415	-.54488	-.51378
-.39600	.06567	.67765	.77416	.79739	.80419	.80482	.79781	.77506	.67972
.06656	-.39827	-.51395	-.54429	-.55391	-.55391	-.54429	-.51395	-.39827	.06656
.67972	.77506	.79781	.80482	.80241	.85563	.83553	.77728	.14278	-.62026
-.65849	-.68931	-.70081	-.70081	-.68931	-.65849	-.62026	.14278	.77728	.83553
.85563	.86241	1.02724	.97313	.94478	.89829	.16287	-.72356	-.77963	-.80390
-.84862	-.84862	-.80390	-.77963	-.72356	.16287	.89829	.94478	.97313	1.02724
.96977	.96182	.95095	.95388	.16070	-.79751	-.80588	-.82348	-.83027	-.83027
-.82348	-.80588	-.79751	.16070	.95388	.95095	.96182	.96977	1.07997	1.07133
1.01466	.97510	.15957	-.82606	-.88788	-.95696	-.95850	-.95850	-.95696	-.88788
-.82606	.15957	.97510	1.01466	1.07133	1.07997				

VELOCITY ON BODY ** SOLVE **

MACH= 2.500 ALPHA= 20.000 PHIR= 0.000

PANEL NO.	SOURCE STRENGTH	AXIAL VELOCITY	LATERAL VELOCITY	VERTICAL VELOCITY	NORMAL
1	.80241	-.14646	.24943E-01	-.45294	.46932
2	.79565	-.14894	.81658E-01	-.44949	.47043
3	.77233	-.15728	.16714	-.43671	.47412
4	.67589	-.18722	.34247	-.36907	.48767
5	.06642	-.12455	.30231	.19606	.32676
6	-.39400	.63560E-01	-.13474	-.99253E-01	-.14738
7	-.51046	.65624E-01	-.91372E-01	-.17694	-.19567
8	-.54133	.63186E-01	-.47469E-01	-.19557	-.20524
9	-.55058	.62272E-01	-.14741E-01	-.20097	-.20793
10	-.55058	.62272E-01	.14741E-01	-.20097	-.20793
11	-.54133	.63186E-01	.47469E-01	-.19557	-.20524
12	-.51046	.65624E-01	.91372E-01	-.17694	-.19567
13	-.39400	.63560E-01	.13474	-.99253E-01	-.14738
14	.06642	-.12455	-.30231	.19606	.32676
15	.67589	-.18722	-.34247	-.36907	.48767
16	.77233	-.15728	-.16714	-.43671	.47412
17	.79565	-.14894	-.81658E-01	-.44949	.47043
18	.80241	-.14646	-.24943E-01	-.45294	.46932
19	.80419	-.14602	.24808E-01	-.45207	.46830
20	.79739	-.14850	.81264E-01	-.44870	.46944
21	.77416	-.15690	.16634	-.43619	.47326

(m) Page 13

Figure 15.- Continued.

22	.67765	-.18712	.34166	-.36948	.48730
23	.06567	-.12490	.30297	.19556	.32750
24	-.39600	.63905E-01	-.13464	-.10042	-.14828
25	-.51378	.66003E-01	-.91522E-01	-.17806	-.19673
26	-.54488	.63563E-01	-.47560E-01	-.19669	-.20636
27	-.55415	.62698E-01	-.14738E-01	-.20209	-.20906
28	-.55415	.62698E-01	.14738E-01	-.20209	-.20906
29	-.54488	.63563E-01	.47560E-01	-.19669	-.20636
30	-.51378	.66003E-01	.91522E-01	-.17806	-.19673
31	-.39600	.63905E-01	.13464	-.10042	-.14828
32	.06567	-.12490	-.30297	.19556	.32750
33	.67765	-.18712	-.34166	-.36948	.48730
34	.77416	-.15690	-.16634	-.43619	.47326
35	.79739	-.14850	-.81264E-01	-.44870	.46944
36	.80419	-.14602	-.24808E-01	-.45207	.46830
37	.80482	-.14631	.24879E-01	-.45259	.46891
38	.79781	-.14882	.81226E-01	-.44919	.47001
39	.77506	-.15700	.16597	-.43665	.47367
40	.67972	-.18690	.34118	-.36976	.48721
41	.06656	-.12451	.30224	.19731	.32667
42	-.39827	.63930E-01	-.13510	-.10064	-.14856
43	-.51395	.65742E-01	-.91010E-01	-.17773	-.19630
44	-.54429	.63364E-01	-.47442E-01	-.19609	-.20574
45	-.55391	.62348E-01	-.14782E-01	-.20144	-.20839
46	-.55391	.62348E-01	.14782E-01	-.20144	-.20839
47	-.54429	.63364E-01	.47442E-01	-.19609	-.20574
48	-.51395	.65742E-01	.91010E-01	-.17773	-.19630
49	-.39827	.63930E-01	.13510	-.10064	-.14856
50	.06656	-.12451	-.30224	.19731	.32667
51	.67972	-.18690	-.34118	-.36976	.48721
52	.77506	-.15700	-.16597	-.43665	.47367
53	.79781	-.14882	-.81226E-01	-.44919	.47001
54	.80482	-.14631	-.24879E-01	-.45259	.46891
55	.86241	-.12745	.23036E-01	-.41756	.42799
56	.85563	-.13008	.72666E-01	-.41422	.42855
57	.83553	-.13644	.14646	-.40241	.43034
58	.77728	-.15450	.33059	-.32950	.43521
59	.14278	-.75017E-01	.21498	.30876	.22673
60	-.62026	.77030E-01	-.21546	-.13544	-.20638
61	-.65849	.85055E-01	-.78792E-01	-.22770	-.24372
62	-.68931	.81513E-01	-.44625E-01	-.24188	-.25092
63	-.70081	.78468E-01	-.15991E-01	-.24642	-.25293
64	-.70081	.78468E-01	.15991E-01	-.24642	-.25293
65	-.68931	.81513E-01	.44625E-01	-.24188	-.25092
66	-.65849	.85055E-01	.78792E-01	-.22770	-.24372
67	-.62026	.77030E-01	.21546	-.13544	-.20638
68	.14278	-.75017E-01	-.21498	.30876	.22673
69	.77728	-.15450	-.33059	-.32950	.43521
70	.83553	-.13644	-.14646	-.40241	.43034
71	.85563	-.13008	-.72666E-01	-.41422	.42855
72	.86241	-.12745	-.23036E-01	-.41756	.42799
73	1.02724	-.10821	.46019E-01	-.40880	.41707
74	.97313	-.12104	.99873E-01	-.40316	.41747
75	.94478	-.12462	.15861	-.39122	.41869
76	.89829	-.13980	.33876	-.31504	.42099
77	.16297	-.60400E-01	.18987	.37329	.19834
78	-.72356	.77763E-01	-.24376	-.14296	-.22183
79	-.77963	.78902E-01	-.11940	-.23600	-.25618
80	-.80390	.80473E-01	-.80406E-01	-.25222	-.26275
81	-.84862	.70287E-01	-.51325E-01	-.25874	-.26457

(n) Page 14

Figure 15.- Continued.

82	-.84862	.70287E-01	.51325E-01	-.25874	-.26457
83	-.80390	.80473E-01	.80406E-01	-.25222	-.26275
84	-.77963	.78902E-01	.11940	-.23600	-.25518
85	-.72356	.77763E-01	.24376	-.14296	-.22183
86	.16287	-.40400E-01	-.14987	.37429	.19834
87	.89829	-.13980	-.33875	-.31504	.42099
88	.94478	-.12462	-.15861	-.39122	.41869
89	.97313	-.12104	-.99873E-01	-.40116	.41747
90	1.02724	-.10821	-.46019E-01	-.40880	.41707
91	.96977	-.10504	.23383E-01	-.40355	.41061
92	.96182	-.11207	.78695E-01	-.39932	.41094
93	.95095	-.11818	.16662	-.38442	.41190
94	.95388	-.13275	.34718	-.30526	.41293
95	.16070	-.52266E-01	.17569	.39736	.18250
96	-.79751	.82607E-01	-.26597	-.14458	-.23051
97	-.80588	.78576E-01	-.14122	-.24074	-.26341
98	-.82348	.74416E-01	-.60892E-01	-.26136	-.26967
99	-.83027	.70240E-01	-.19168E-01	-.26661	-.27141
100	-.83027	.70240E-01	.19168E-01	-.26661	-.27141
101	-.82348	.74416E-01	.60892E-01	-.26136	-.26967
102	-.80588	.78576E-01	.14122	-.24074	-.26341
103	-.79751	.82607E-01	.26597	-.14458	-.23051
104	.16070	-.52266E-01	-.17569	.39736	.18250
105	.95388	-.13275	-.34718	-.30526	.41293
106	.95095	-.11818	-.16662	-.38442	.41190
107	.96182	-.11207	-.78695E-01	-.39932	.41094
108	.96977	-.10504	-.23383E-01	-.40355	.41061
109	1.07997	-.10574	.24497E-01	-.40109	.40801
110	1.07133	-.10274	.94353E-01	-.39650	.40825
111	1.01466	-.11463	.15721	-.38327	.40892
112	.97510	-.12734	.35431	-.29927	.40871
113	.15957	-.47255E-01	.16728	.42864	.17312
114	-.82606	.81214E-01	-.27990	-.14491	-.23497
115	-.88788	.76794E-01	-.12548	-.24645	-.26655
116	-.95696	.66279E-01	-.87827E-01	-.26317	-.27250
117	-.95850	.71729E-01	-.19117E-01	-.26940	-.27415
118	-.95850	.71729E-01	.19117E-01	-.26940	-.27415
119	-.95696	.66279E-01	.87827E-01	-.26317	-.27250
120	-.88788	.76794E-01	.12548	-.24645	-.26655
121	-.82606	.81214E-01	.27990	-.14491	-.23497
122	.15957	-.47255E-01	-.16728	.42864	.17312
123	.97510	-.12734	-.35431	-.29927	.40871
124	1.01466	-.11463	-.15721	-.38327	.40892
125	1.07133	-.10274	-.94353E-01	-.39650	.40825
126	1.07997	-.10574	-.24497E-01	-.40109	.40801

MODIFIED SOURCE STRENGTH

1	18	.12591	.12716	.13093	.14095	.06642	.14095	.13093	.12716	.12591	.12591
		.12716	.13093	.14095	.06642	.14095	.13093	.12716	.12591		
19	36	.12502	.12626	.13019	.14083	.06567	.14083	.13019	.12626	.12502	.12502
		.12626	.13019	.14083	.06567	.14083	.13019	.12626	.12502		
37	54	.12546	.12676	.13056	.14072	.06656	.14072	.13056	.12676	.12546	.12546
		.12676	.13056	.14072	.06656	.14072	.13056	.12676	.12546		
55	72	.08080	.08316	.08852	.07851	.14278	.07851	.08852	.08316	.08080	.08080
		.08316	.08852	.07851	.14278	.07851	.08852	.08316	.08080		
73	90	.08931	.08461	.08258	.08737	.16287	.08737	.08258	.08461	.08931	.08931
		.08461	.08258	.08737	.16287	.08737	.08258	.08461	.08931		
91	108	.06975	.06917	.07254	.07818	.16070	.07818	.07254	.06917	.06975	.06975
		.06917	.07254	.07818	.16070	.07818	.07254	.06917	.06975		

(o) Page 15

Figure 15.- Continued.

109	126	.06073	.05719	.06339	.07452	.15957	.07452	.06339	.05719	.06073	.06073
		.05719	.06339	.07452	.15957	.07452	.06339	.05719	.06073		

(p) Page 16

Figure 15.- Continued.

X	R	DR/DX	A	B	M
2.8000	.7185	.2045	1.0780	.3595	2.5000

BODY SURFACE PRESSURE DISTRIBUTION

J	Y	Z	BETA	U/V0	V/V0	W/V0	VT/V0	CP(M)	DPHI/DT	CPZ	CP(I)	VCP/V0
1	0.0000	-.3591	0.000	.8116	.0000	-.1907	.1907	.4791	0.0000	.3049	.3049	0.0000
2	.0939	-.3578	14.713	.8111	.0471	-.1896	.1954	.4771	0.0000	.3040	.3040	.0399
3	.1872	-.3537	27.889	.8094	.0924	-.1863	.2079	.4718	0.0000	.3016	.3016	.0803
4	.2790	-.3469	38.807	.8066	.1417	-.1792	.2285	.4621	0.0000	.2973	.2973	.1217
5	.3687	-.3375	47.529	.8039	.1870	-.1712	.2536	.4452	0.0000	.2895	.2895	.1648
6	.4555	-.3255	54.454	.8000	.2418	-.1547	.2870	.4197	0.0000	.2775	.2775	.2101
7	.5389	-.3110	60.012	.7951	.3068	-.1295	.3330	.3773	0.0000	.2570	.2570	.2585
8	.6182	-.2942	64.554	.7910	.3637	-.1062	.3789	.3264	0.0000	.2308	.2308	.3109
9	.6928	-.2751	68.344	.7876	.4149	-.0833	.4232	.2716	0.0000	.2006	.2006	.3685
10	.7622	-.2539	71.573	.7847	.4623	-.0594	.4661	.2153	0.0000	.1670	.1670	.4326
11	.8257	-.2308	74.381	.7939	.4735	.0376	.4750	.1796	0.0000	.1442	.1442	.5051
12	.8829	-.2060	76.868	.8049	.4782	.1485	.5008	.1185	0.0000	.1014	.1014	.5880
13	.9335	-.1796	79.112	.8148	.4845	.2584	.5491	.0365	0.0000	.0346	.0346	.6840
14	.9769	-.1518	81.169	.8239	.4897	.3720	.6150	-.0522	0.0000	-.0571	-.0571	.7956
15	1.0129	-.1228	83.086	.8324	.4890	.4943	.6953	-.1330	0.0000	-.1764	-.1764	.9241
16	1.0411	-.0929	84.898	.8405	.4730	.6281	.7863	-.1916	0.0000	-.3247	-.3247	1.0665
17	1.0615	-.0624	86.638	.8482	.4278	.7696	.8805	-.2207	0.0000	-.4947	-.4947	1.2096
18	1.0738	-.0313	88.330	.8557	.3405	.9004	.9626	-.2280	0.0000	-.6589	-.6589	1.3237
19	1.0779	-.0000	90.000	.8631	.2178	.9895	1.0132	-.2286	0.0000	-.7714	-.7714	1.3686
20	1.0738	.0313	91.670	.8775	.0653	.9188	.9212	-.2273	0.0000	-.6184	-.6184	1.3237
21	1.0615	.0624	93.362	.8920	-.0522	.8067	.8083	-.2158	0.0000	-.4491	-.4491	1.2096
22	1.0411	.0929	95.102	.9070	-.1284	.6844	.6963	-.1867	0.0000	-.3074	-.3074	1.0665
23	1.0129	.1228	96.914	.9226	-.1767	.5706	.5973	-.1489	0.0000	-.2079	-.2079	.9241
24	.9769	.1518	98.831	.9391	-.2116	.4695	.5149	-.1163	0.0000	-.1470	-.1470	.7956
25	.9335	.1796	100.888	.9568	-.2430	.3785	.4498	-.0976	0.0000	-.1177	-.1177	.6840
26	.8829	.2060	103.132	.9761	-.2768	.2933	.4033	-.0960	0.0000	-.1154	-.1154	.5880
27	.8257	.2308	105.619	.9975	-.3164	.2099	.3797	-.1114	0.0000	-.1391	-.1391	.5051
28	.7622	.2539	108.427	1.0165	-.3457	.1365	.3717	-.1303	0.0000	-.1715	-.1715	.4326
29	.6928	.2751	111.656	1.0178	-.3062	.1096	.3252	-.1130	0.0000	-.1416	-.1416	.3685
30	.6182	.2942	115.446	1.0192	-.2642	.0832	.2770	-.0961	0.0000	-.1155	-.1155	.3109
31	.5389	.3110	119.988	1.0209	-.2184	.0557	.2254	-.0803	0.0000	-.0931	-.0931	.2585
32	.4555	.3255	125.546	1.0230	-.1669	.0254	.1688	-.0667	0.0000	-.0751	-.0751	.2101
33	.3687	.3375	132.471	1.0234	-.1269	.0057	.1271	-.0575	0.0000	-.0636	-.0636	.1648
34	.2790	.3469	141.193	1.0220	-.0983	-.0033	.0984	-.0497	0.0000	-.0541	-.0541	.1217
35	.1872	.3537	152.111	1.0202	-.0673	-.0115	.0682	-.0423	0.0000	-.0454	-.0454	.0803
36	.0939	.3578	165.287	1.0183	-.0354	-.0156	.0387	-.0362	0.0000	-.0384	-.0384	.0399
37	.0000	.3591	180.000	1.0176	.0000	-.0170	.0170	-.0339	0.0000	-.0359	-.0359	.0000
38	-.0939	.3578	194.713	1.0183	.0354	-.0156	-.0387	-.0362	0.0000	-.0384	-.0384	-.0399
39	-.1872	.3537	207.889	1.0202	.0673	-.0115	-.0682	-.0423	0.0000	-.0454	-.0454	-.0803
40	-.2790	.3469	218.807	1.0220	.0983	-.0033	-.0984	-.0497	0.0000	-.0541	-.0541	-.1217
41	-.3687	.3375	227.529	1.0234	.1269	.0057	-.1271	-.0575	0.0000	-.0636	-.0636	-.1648
42	-.4555	.3255	234.454	1.0230	.1669	.0254	-.1688	-.0667	0.0000	-.0751	-.0751	-.2101
43	-.5389	.3110	240.012	1.0209	.2184	.0557	-.2254	-.0803	0.0000	-.0931	-.0931	-.2585
44	-.6182	.2942	244.554	1.0192	.2642	.0832	-.2770	-.0961	0.0000	-.1155	-.1155	-.3109
45	-.6928	.2751	248.344	1.0178	.3062	.1096	-.3252	-.1130	0.0000	-.1416	-.1416	-.3685
46	-.7622	.2539	251.573	1.0165	.3457	.1365	-.3717	-.1303	0.0000	-.1715	-.1715	-.4326
47	-.8257	.2308	254.381	.9975	.3164	.2099	-.3797	-.1114	0.0000	-.1391	-.1391	-.5051
48	-.8829	.2060	256.868	.9761	.2768	.2933	-.4033	-.0960	0.0000	-.1154	-.1154	-.5880
49	-.9335	.1796	259.112	.9568	.2430	.3785	-.4498	-.0976	0.0000	-.1177	-.1177	-.6840
50	-.9769	.1518	261.169	.9391	.2116	.4695	-.5149	-.1163	0.0000	-.1470	-.1470	-.7956
51	-1.0129	.1228	263.086	.9226	.1767	.5706	-.5973	-.1489	0.0000	-.2079	-.2079	-.9241
52	-1.0411	.0929	264.898	.9070	.1284	.6844	-.6963	-.1867	0.0000	-.3074	-.3074	-1.0665
53	-1.0615	.0624	266.638	.8920	.0522	.8067	-.8083	-.2158	0.0000	-.4491	-.4491	-1.2096

(q) Page 17

Figure 15.- Continued.

54	-1.0738	.0313	268.330	.8775	-.0653	.9188	-.9212	-.2273	0.0000	-.6184	-.6184	-1.3237
55	-1.0779	.0000	270.000	.8631	-.2178	.9895	-1.0132	-.2286	0.0000	-.7714	-.7714	-1.3686
56	-1.0738	-.0313	271.670	.8557	-.3405	.9004	-.9626	-.2280	0.0000	-.6589	-.6589	-1.3237
57	-1.0615	-.0624	273.362	.8482	-.4278	.7696	-.8805	-.2207	0.0000	-.4947	-.4947	-1.2096
58	-1.0411	-.0929	275.102	.8405	-.4730	.6281	-.7863	-.1916	0.0000	-.3247	-.3247	-1.0665
59	-1.0129	-.1228	276.914	.8324	-.4890	.4943	-.6953	-.1330	0.0000	-.1764	-.1764	-.9241
60	-.9769	-.1518	278.831	.8239	-.4897	.3720	-.6150	-.0522	0.0000	-.0571	-.0571	-.7956
61	-.9335	-.1796	280.888	.8148	-.4845	.2584	-.5491	.0365	0.0000	.0346	.0346	-.6840
62	-.8829	-.2060	283.132	.8049	-.4782	.1485	-.5008	.1185	0.0000	.1014	.1014	-.5880
63	-.8257	-.2309	285.619	.7939	-.4735	.0376	-.4750	.1796	0.0000	.1442	.1442	-.5051
64	-.7622	-.2539	288.427	.7847	-.4623	-.0594	-.4661	.2153	0.0000	.1670	.1670	-.4326
65	-.6928	-.2751	291.656	.7876	-.4149	-.0833	-.4232	.2716	0.0000	.2006	.2006	-.3685
66	-.6182	-.2942	295.446	.7910	-.3637	-.1062	-.3789	.3264	0.0000	.2308	.2308	-.3109
67	-.5389	-.3110	299.988	.7951	-.3068	-.1295	-.3330	.3773	0.0000	.2570	.2570	-.2585
68	-.4555	-.3255	305.546	.8000	-.2418	-.1547	-.2870	.4197	0.0000	.2775	.2775	-.2101
69	-.3687	-.3375	312.471	.8039	-.1870	-.1712	-.2536	.4452	0.0000	.2895	.2895	-.1648
70	-.2790	-.3469	321.193	.8066	-.1417	-.1792	-.2285	.4621	0.0000	.2973	.2973	-.1217
71	-.1872	-.3537	332.111	.8094	-.0924	-.1863	-.2079	.4718	0.0000	.3016	.3016	-.0803
72	-.0939	-.3578	345.287	.8111	-.0471	-.1896	-.1954	.4771	0.0000	.3040	.3040	-.0399
73	-.0000	-.3591	360.000	.8116	.0000	-.1907	-.1907	.4791	0.0000	.3049	.3049	-.0000

FORCE AND MOMENT COFFFICIENTS - PRESSURE INTEGRATION

X	CN(X)	CY(X)	CN	CY	CM	CR	CSL	XCPN	XCPY
2.80000	2.0530E-01	8.6935E-11	8.8286E-02	0.	3.2960E-01	0.	2.6207E-12	1.867	1.867

(r) Page 18

Figure 15.- Continued.

STRATFORD SEPARATION CRITERION (LAMINAR) F(S) = .02976

SUMMARY OF PRESSURE DISTRIBUTION AND SEPARATION POINTS ON BODY ... X = 2.80

+Y SIDE:		Y	Z	BETA	ARC	CP	CP'	DCP'/DX
	STAGNATION PT.	0.000	-.359	0.000	.305	.479		
	MIN. PRESSURE	1.078	-.000	90.000	1.200	-.229	0.000	0.000
	SEPARATION	1.056	.070	93.825	1.275	-.208	.017	.525

-Y SIDE:		Y	Z	BETA	ARC	CP	CP'	DCP'/DX
	STAGNATION PT.	.000	.359	180.000	.305	-.034		
	MIN. PRESSURE	-1.078	.000	270.000	1.200	-.229	0.000	0.000
	SEPARATION	-1.056	.070	266.175	1.275	-.208	.017	.525

INITIAL POSITIONS AND STRENGTHS OF SHED VORTICITY AT X = 2.800

	NV	GAM/V	M(K)	Y	Z	BETA	VT/V	YC	ZC	RG/R
+Y SIDE:	1	.4503	.2115	1.2672	.0847	93.8249	.7775	1.0162	.1125	1.4229
-Y SIDE:	2	-.4503	.2115	-1.2672	.0847	266.1751	.7775	-1.0162	.1125	1.4229

(s) Page 19

Figure 15.- Continued.

SUMMARY OF VORTEX FIELD AT X = 4.200 H = 1.40000

	NV	GAM/V	Y	Z	ASHED	BETA	YC	ZC	RG	RG/R
1	1	.45032	1.16962	.69202	2.80000	120.611	.92345	.94354	1.32024	1.36954
1	2	-.45032	-1.16962	.69202	2.80000	239.389	-.92345	.94354	1.32024	1.36954

CENTROID OF VORTICITY

	GAM/V	Y	Z
+Y BODY:	.45032	1.16962	.69202
-Y BODY:	-.45032	-1.16962	.69202

(t) Page 20

Figure 15.- Continued.

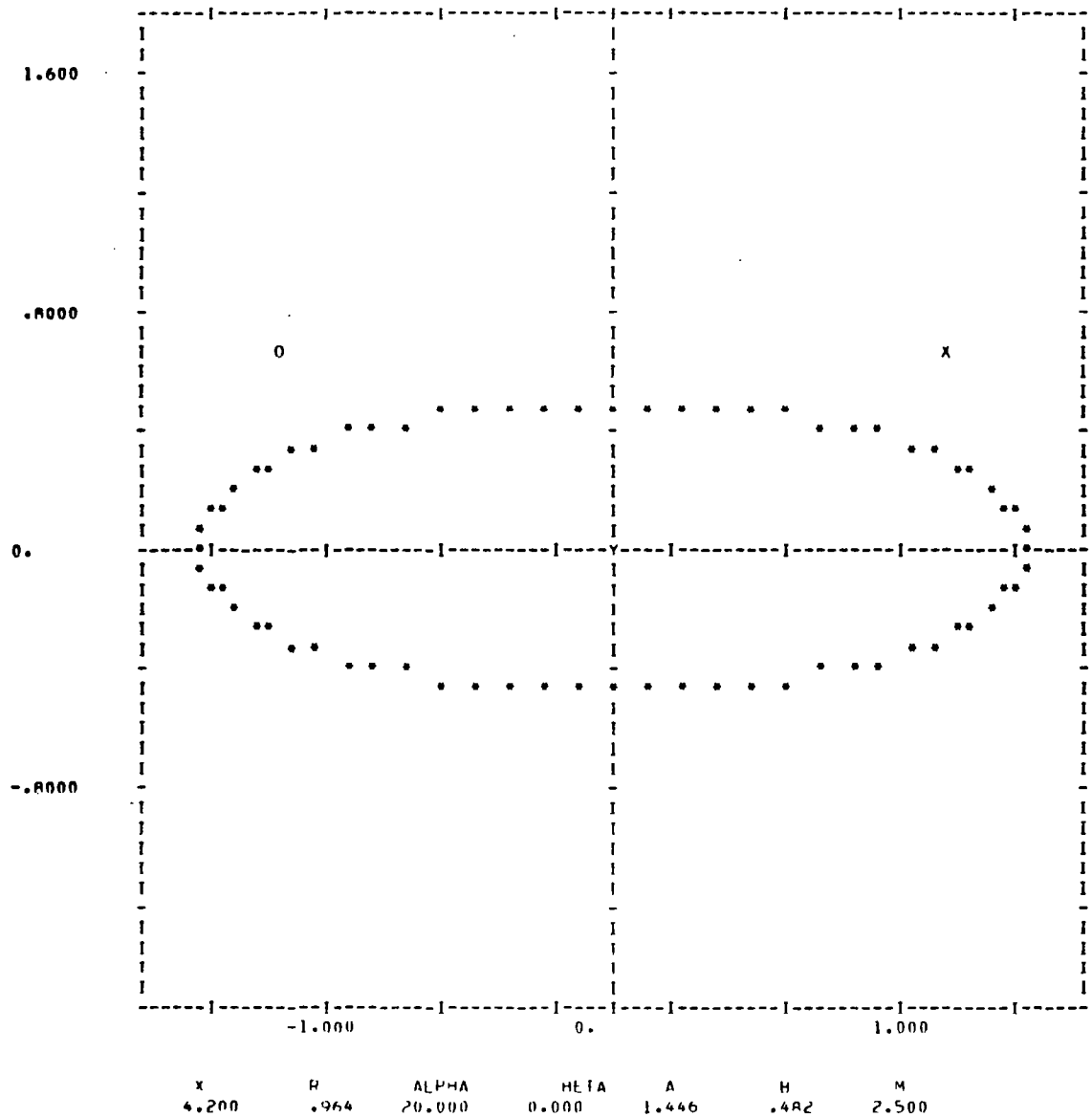

(u) Page 23

Figure 15.- Continued.

VELOCITY COMPONENTS AT SPECIFIED FIELD POINTS AT X = 4.20

J	Y	Z	U/V0	V/V0	W/V0	VT/V0	Y/D	Z/D
1	.2410	.7230	9.1365E-01	-3.4614E-02	1.2126E-01	1.2610E-01	.1250	.3750
2	.2410	.9640	9.1947E-01	-3.0524E-02	1.4284E-01	1.4606E-01	.1250	.5000
3	.4820	.7230	9.1585E-01	-5.7109E-02	1.0825E-01	1.2239E-01	.2500	.3750
4	.4820	.9640	9.1689E-01	-6.8524E-02	1.4337E-01	1.5891E-01	.2500	.5000
5	.7230	.4820	9.1481E-01	-3.5174E-02	8.1534E-02	8.8797E-02	.3750	.2500
6	.7230	.9640	9.1474E-01	-1.2153E-01	1.3785E-01	1.8377E-01	.3750	.5000
7	.9640	.4820	9.1022E-01	5.2814E-02	5.2321E-02	7.4343E-02	.5000	.2500
8	.9640	.9640	9.1417E-01	-2.3093E-01	1.4919E-01	2.7493E-01	.5000	.5000
9	1.2050	.4820	9.0519E-01	1.5568E-01	3.4164E-01	3.7544E-01	.6250	.2500
10	1.2050	.9640	8.9854E-01	-3.0922E-01	3.6347E-01	4.7720E-01	.6250	.5000

(v) Page 24

Figure 15.- Continued.

STRATFORD SEPARATION CRITERION (LAMINAR) F(S) = .02976

SUMMARY OF PRESSURE DISTRIBUTION AND SEPARATION POINTS ON BODY ... X = 5.60

+Y SIDE:		Y	Z	BETA	ARC	CP	CP'	DCP'/DX
	STAGNATION PT.	0.000	-.590	0.000	.274	.401		
	MIN. PRESSURE	1.774	-.000	90.000	1.974	-.229	0.000	0.000
	SEPARATION	1.753	.088	92.862	2.065	-.210	.015	.343

-Y SIDE:		Y	Z	BETA	ARC	CP	CP'	DCP'/DX
	STAGNATION PT.	-.155	.588	194.730	.274	-.158		
	MIN. PRESSURE	-1.774	.000	270.000	1.974	-.229	0.000	0.000
	SEPARATION	-1.753	.088	267.138	2.065	-.210	.015	.343

INITIAL POSITIONS AND STRENGTHS OF SHED VORTICITY AT X = 5.600

	NV	GAM/V	M(K)	Y	Z	BETA	VT/V	YC	ZC	RG/R
+Y SIDE:	5	.4035	.1884	1.9411	.0970	92.8623	.7359	1.4696	.1429	1.2491
-Y SIDE:	6	-.4035	.1884	-1.9411	.0970	267.1377	.7359	-1.4696	.1429	1.2491

CENTROID OF VORTICITY

	GAM/V	Y	Z
+Y BODY:	1.27609	1.50176	.63474
-Y BODY:	-1.27609	-1.50176	.63474

********** CONTRIBUTION OF NOSE SECTION TO TOTAL LOADS **********

STRENGTHS AND POSITIONS OF VORTICES AT END OF NOSE SECTION

A = 2.0000

I	GAMMA/2PIVA	YO/A	ZO/A
1	.10155	.7509	.3174
2	-.10155	-.7509	.3174

FORCE AND MOMENT COEFFICIENTS IN UNROLLED BODY COORDINATES

CZO	CMYO	CYO	CMZO	CMXO
.38251	1.20011	.00000	-.00000	-.00000

CL = .359
CD = .131

(w) Page 30

Figure 15.- Concluded.

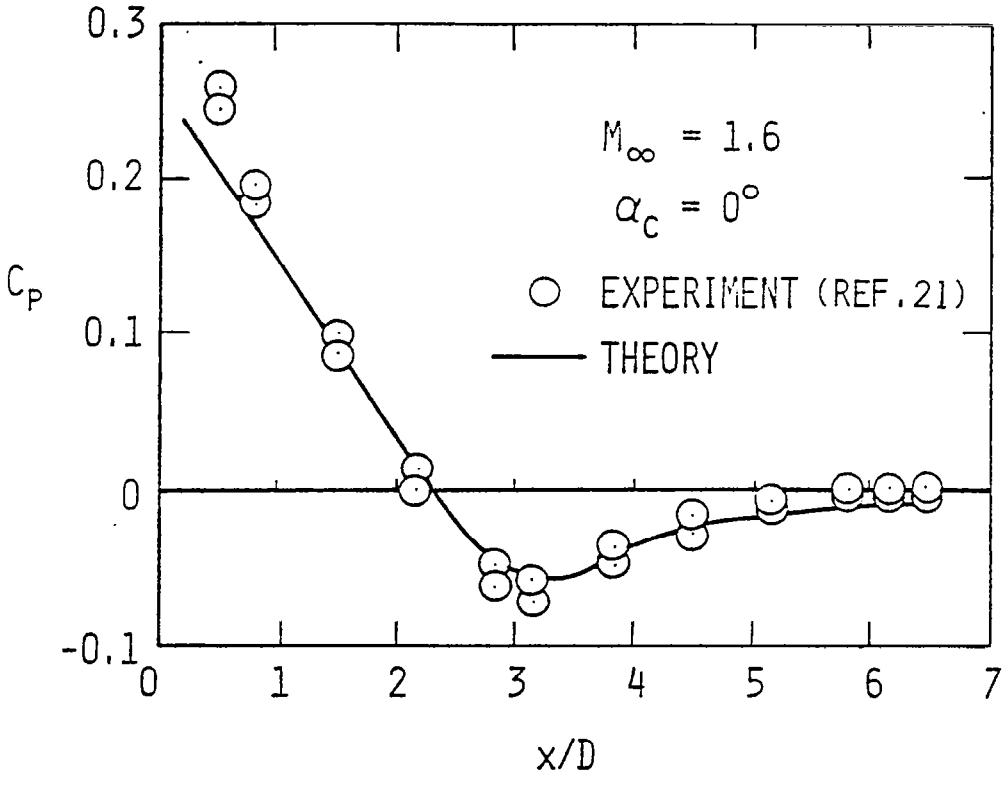

(a) $M_\infty = 1.6$

Figure 16. - Measured and predicted pressure distribution on an ogive-cylinder at $\alpha=0°$.

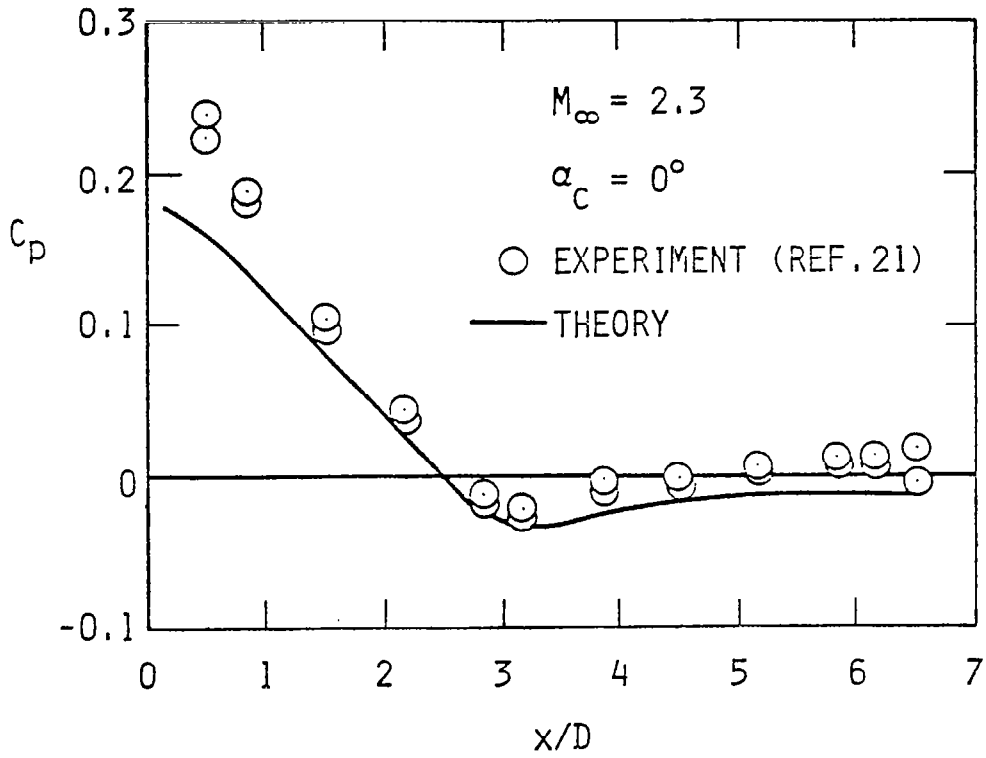

(b) $M_\infty = 2.3$

Figure 16. - Continued.

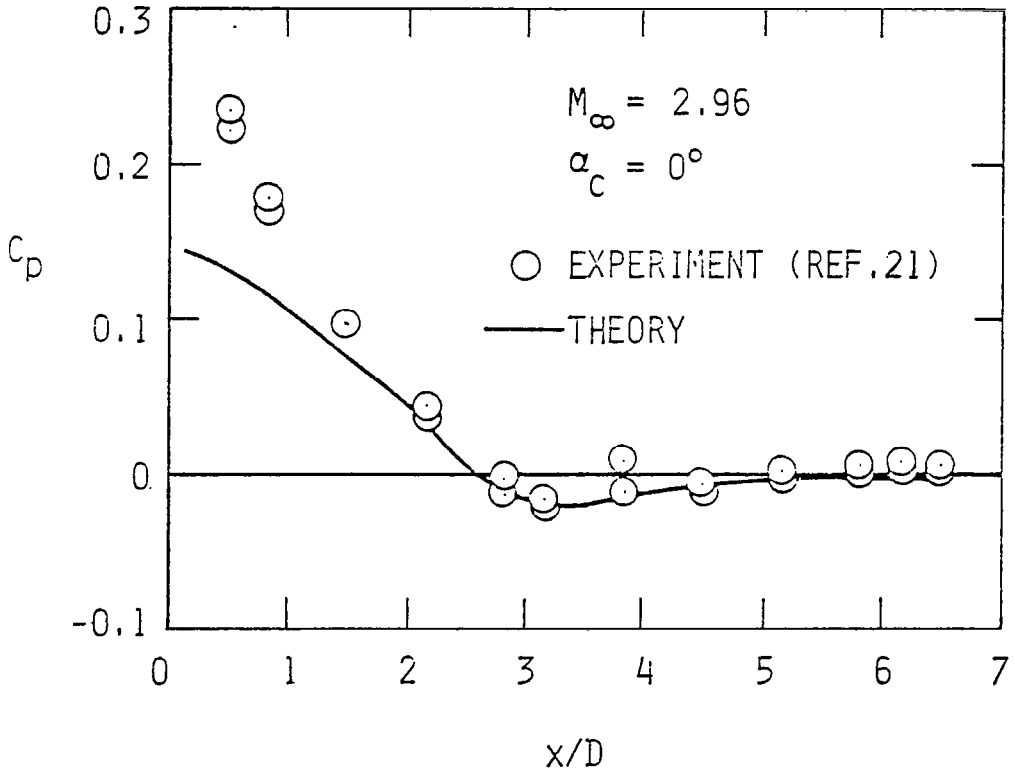

(c) $M_\infty = 2.96$

Figure 16. - Concluded.

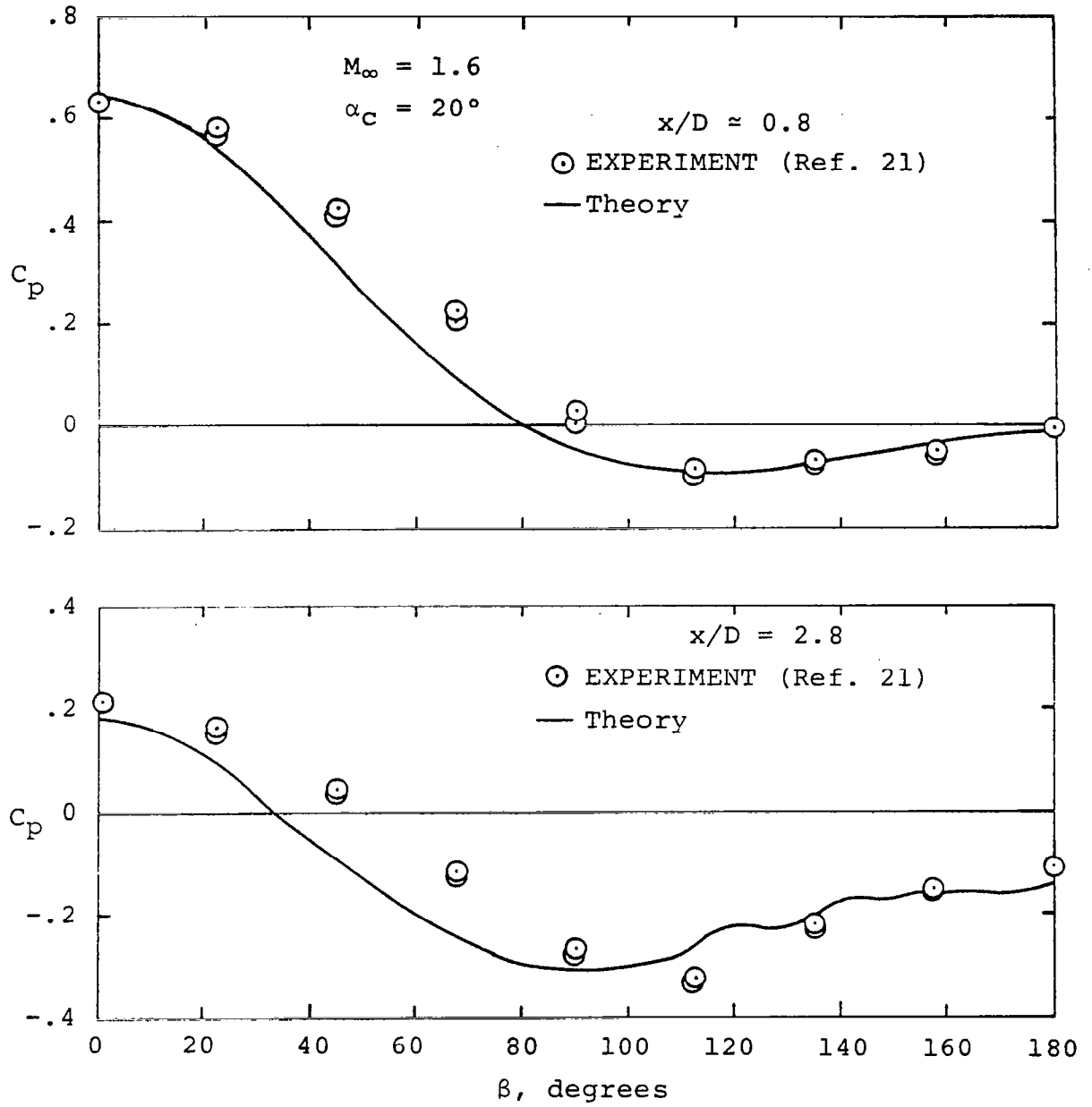

(a) x/D = 0.8 and 2.8

Figure 17.- Measured and predicted circumferential pressure distribution on an ogive-cylinder body at M_∞ = 1.6, α_c = 20°.

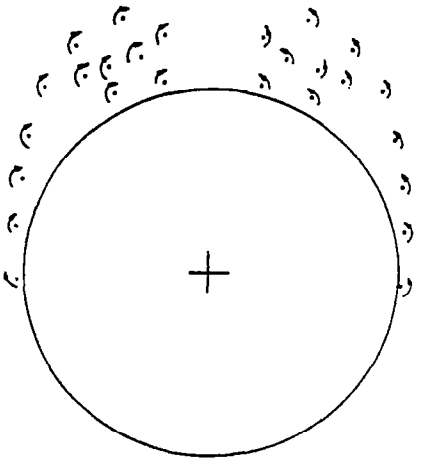

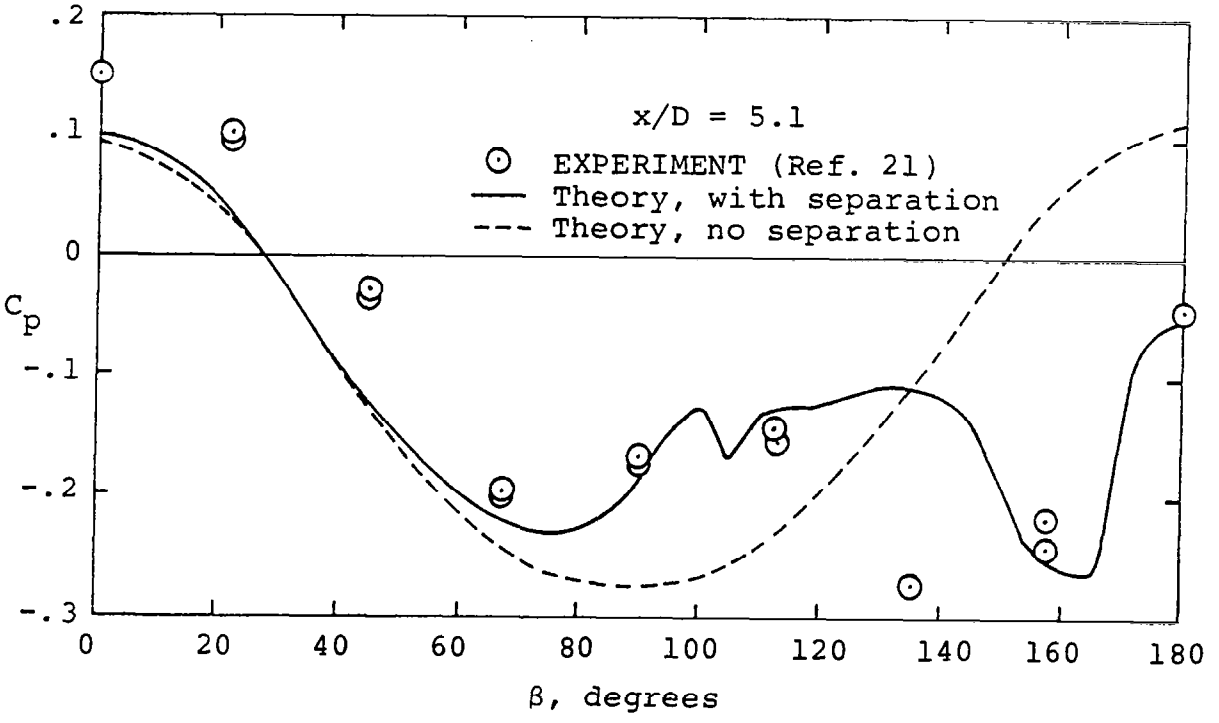

(b) x/D = 5.1

Figure 17.- Concluded.

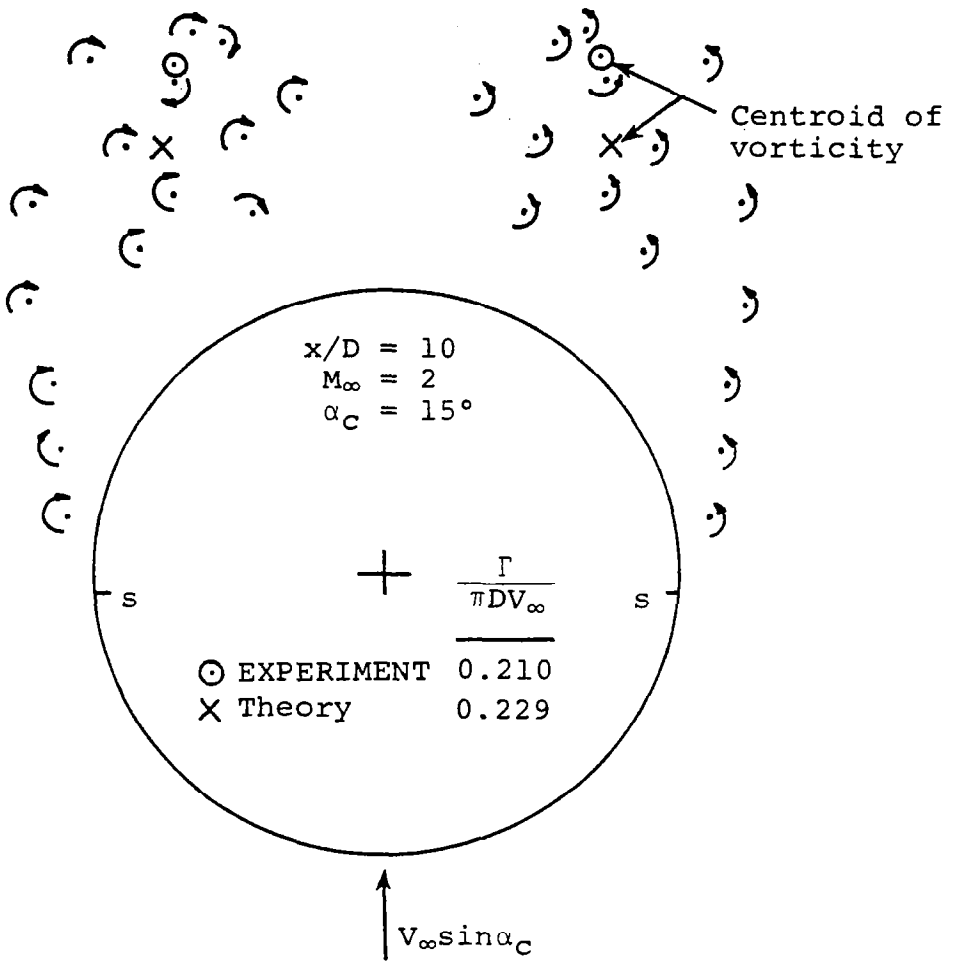

Figure 18.- Predicted vortex wake on the lee side of an ogive cylinder.

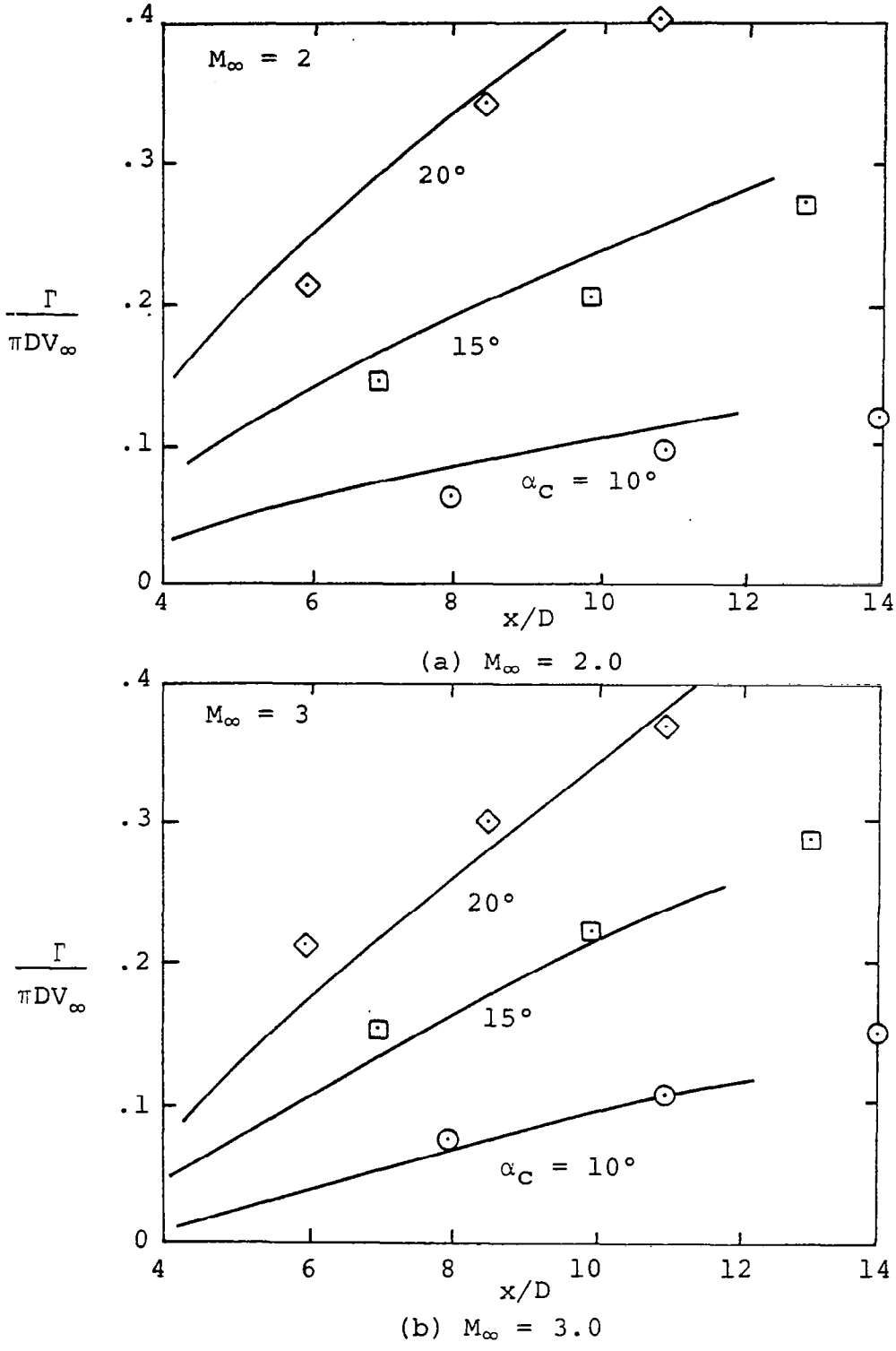

Figure 19.- Measured and predicted body vortex strength on an ogive cylinder.

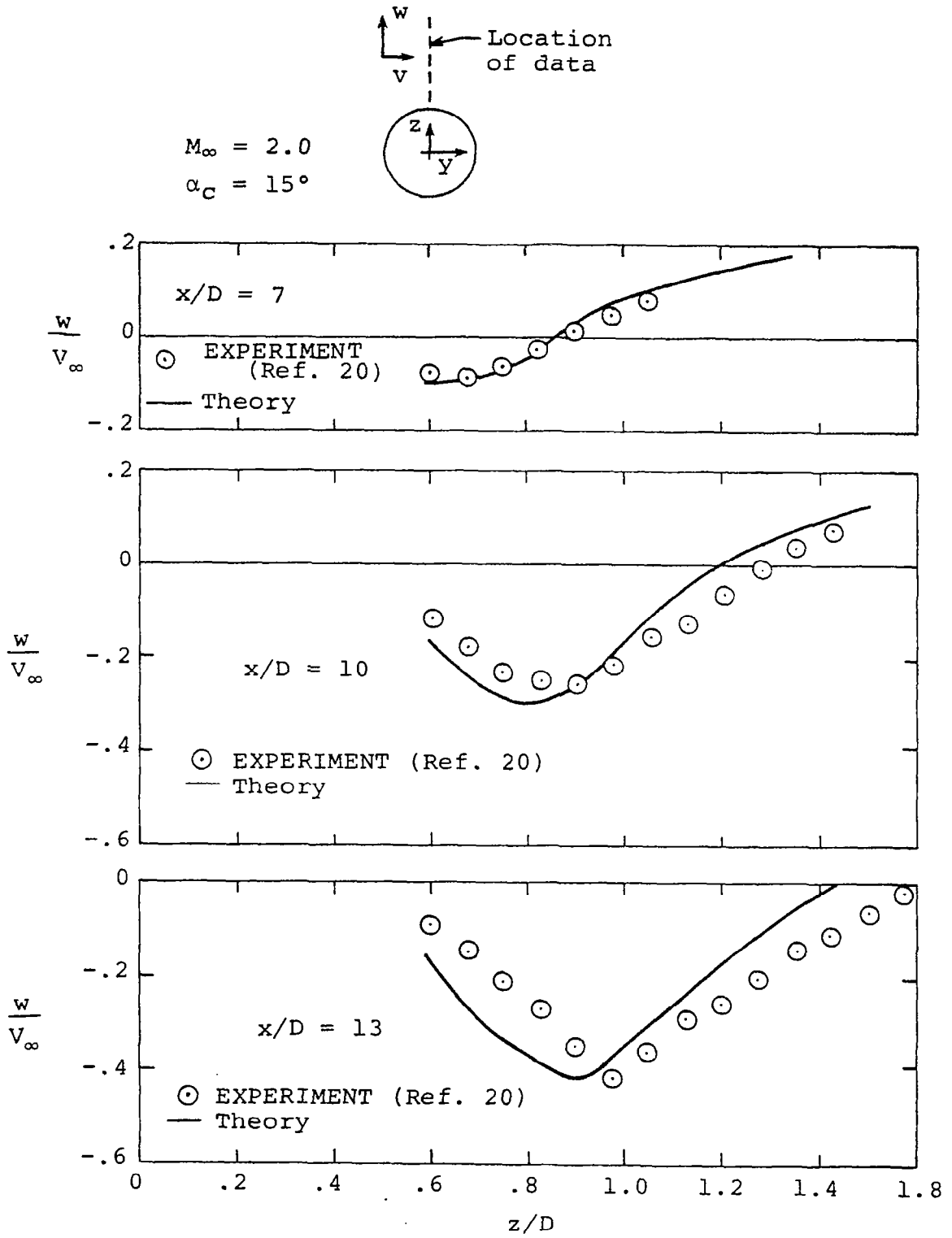

Figure 20.- Measured and predicted downwash distribution on the lee side of an ogive cylinder at M_∞ = 2, α_c = 15°.

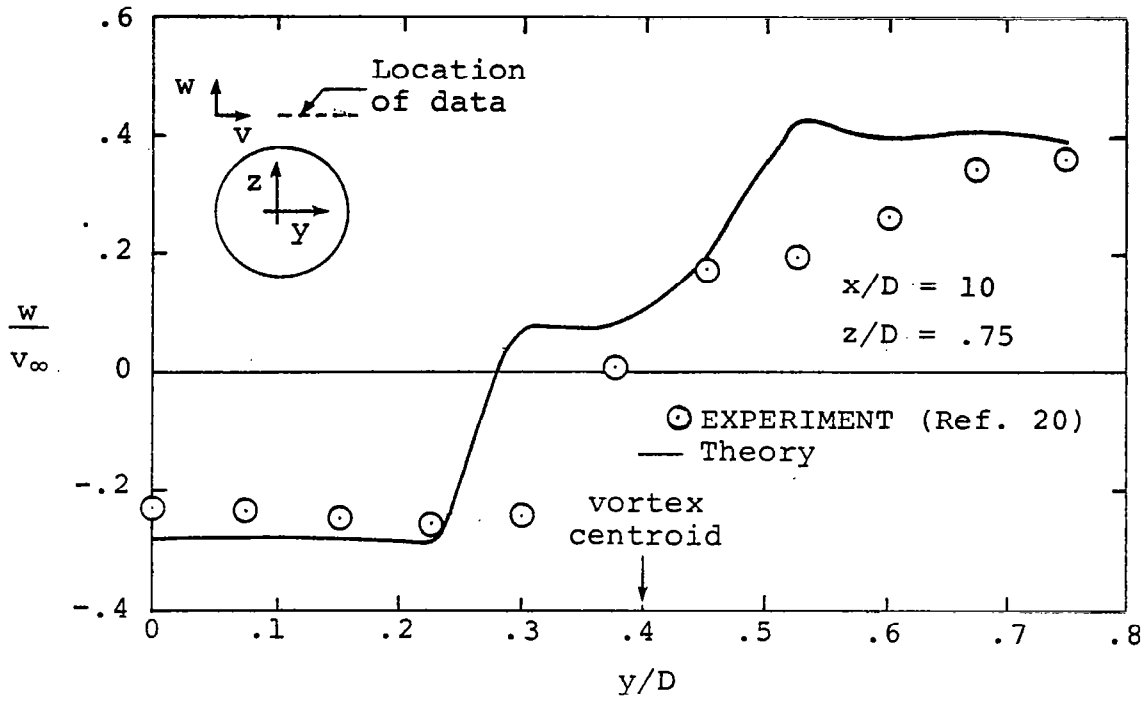

(a) z/D = .75

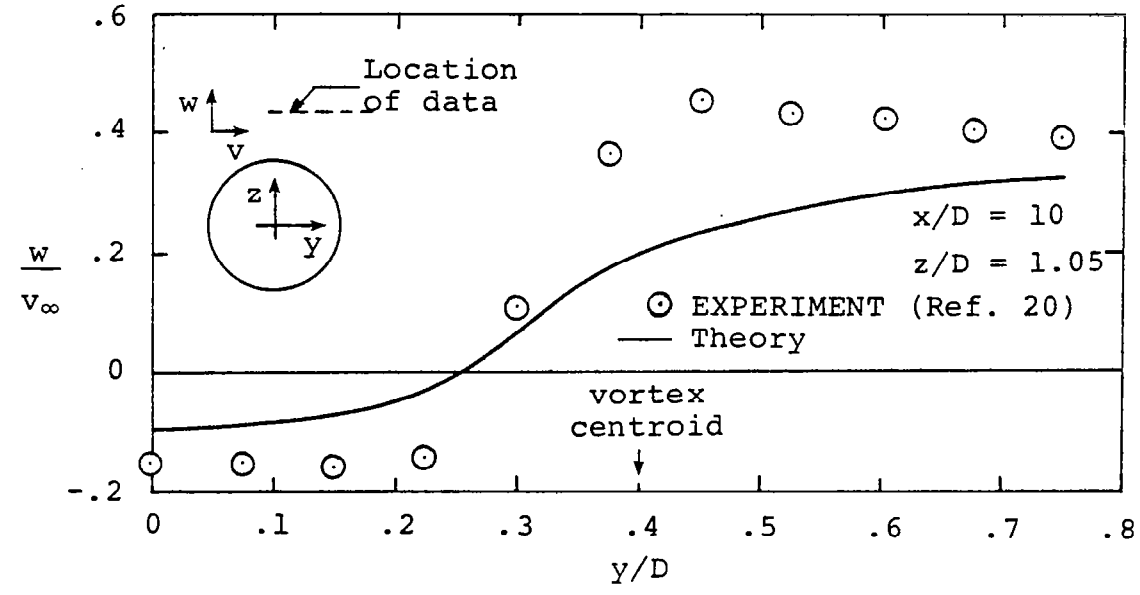

(b) z/D = 1.05

Figure 21.- Measured and predicted downwash distribution on the lee side of an ogive cylinder at $M_\infty = 2$, $\alpha_c = 15°$, x/D = 10.

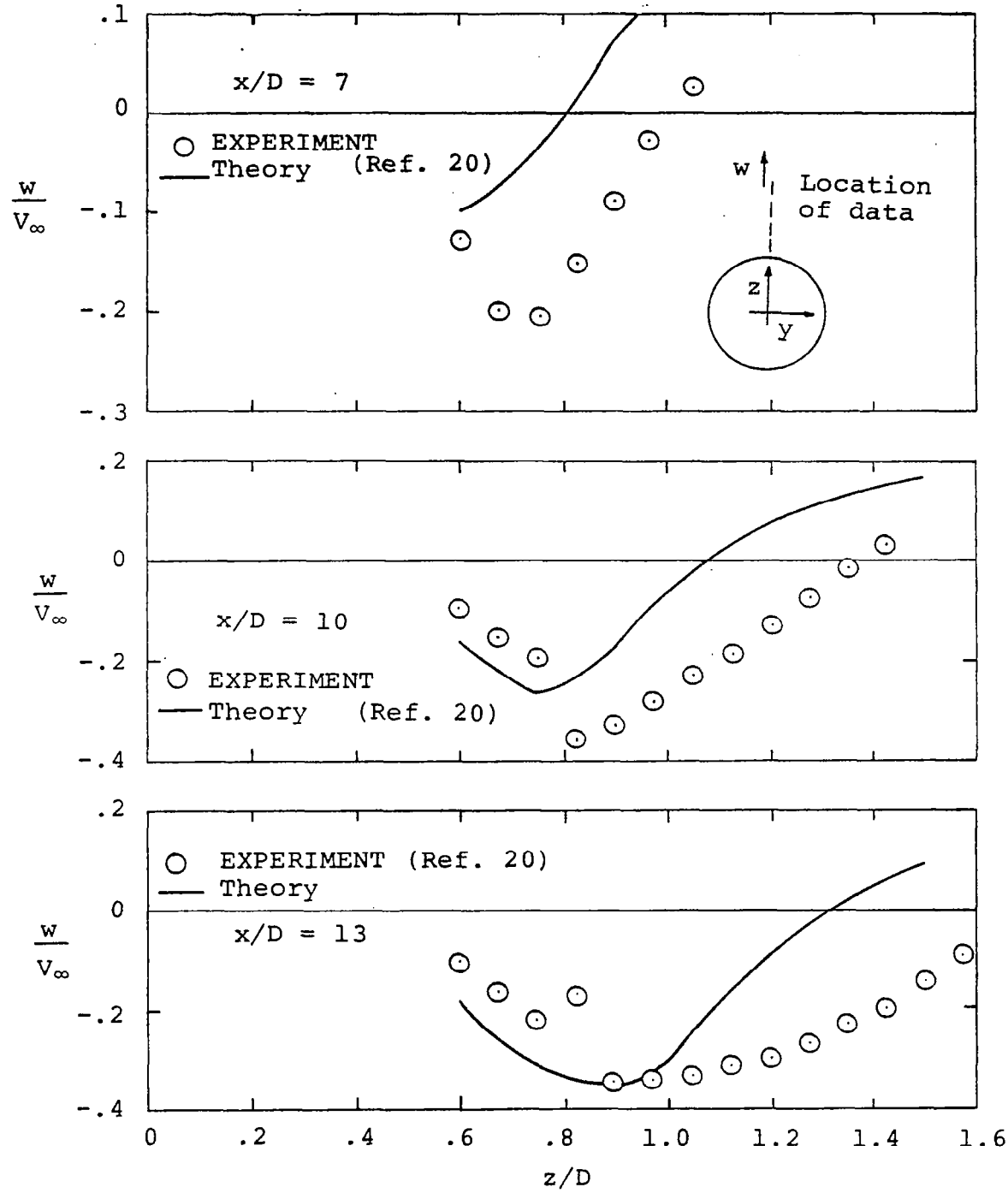

Figure 22.- Measured and predicted downwash distribution on the lee side of an ogive cylinder at $M_\infty = 3$, $\alpha_c = 15°$.

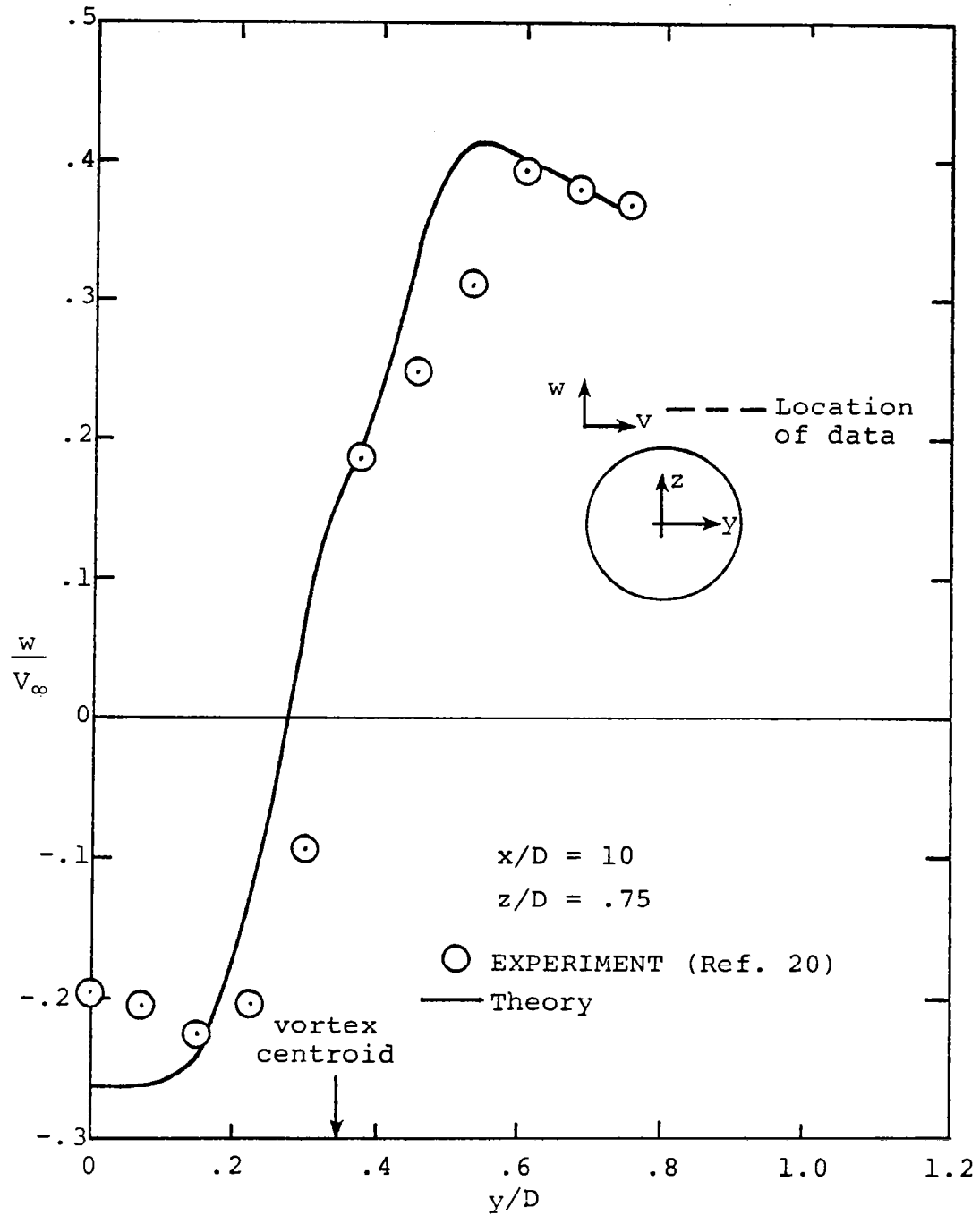

(a) z/D = .75

Figure 23.- Measured and predicted downwash distribution on the lee side of an ogive cylinder at $M_\infty = 3$, $\alpha_c = 15°$, x/D = 10.

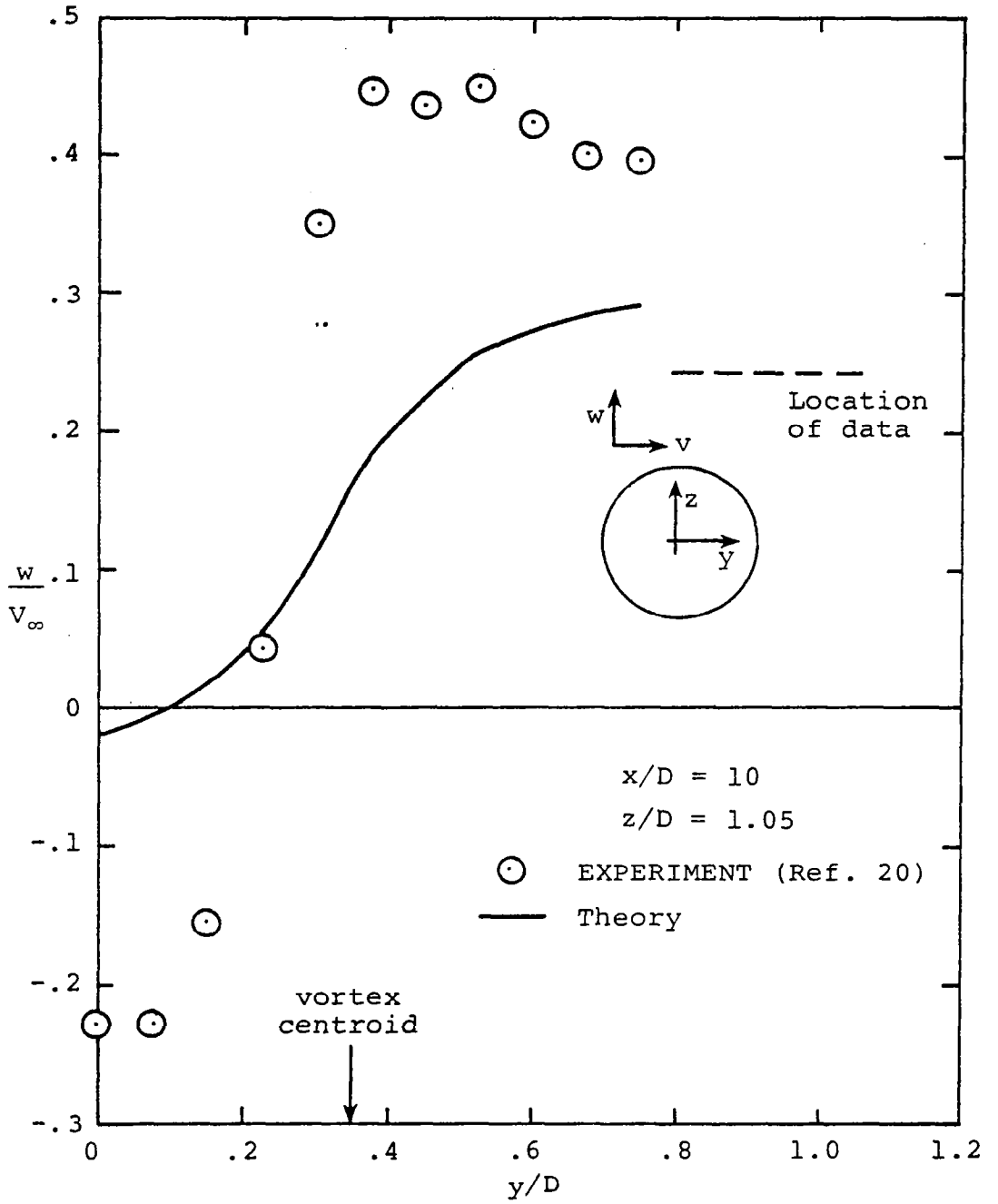

(b) z/D = 1.05

Figure 23.- Concluded.

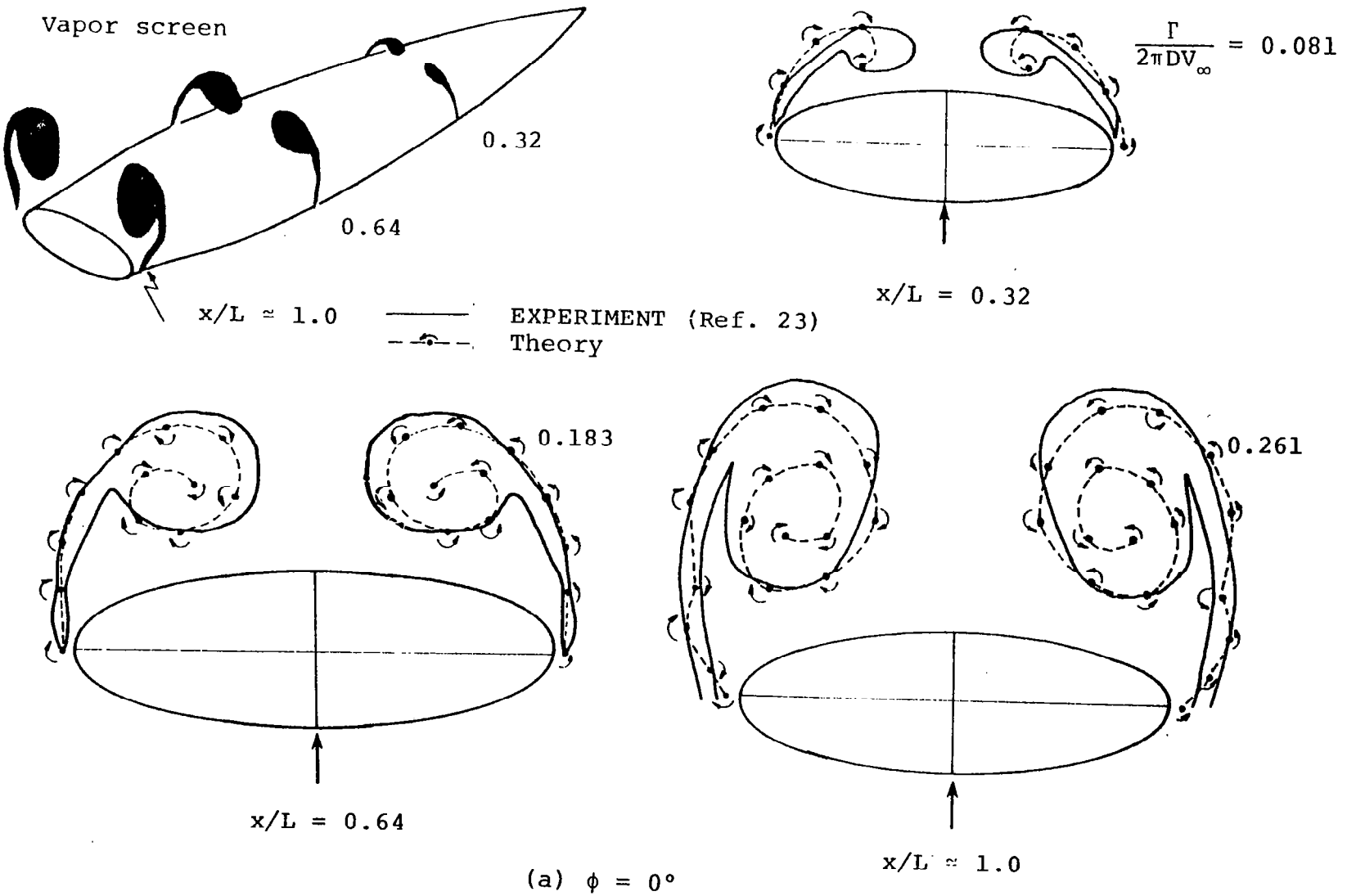

(a) $\phi = 0°$

Figure 24.- Measured and predicted vortex patterns on a 3:1 elliptic cross section body at $M_\infty = 2.5$ and $\alpha_c = 20°$.

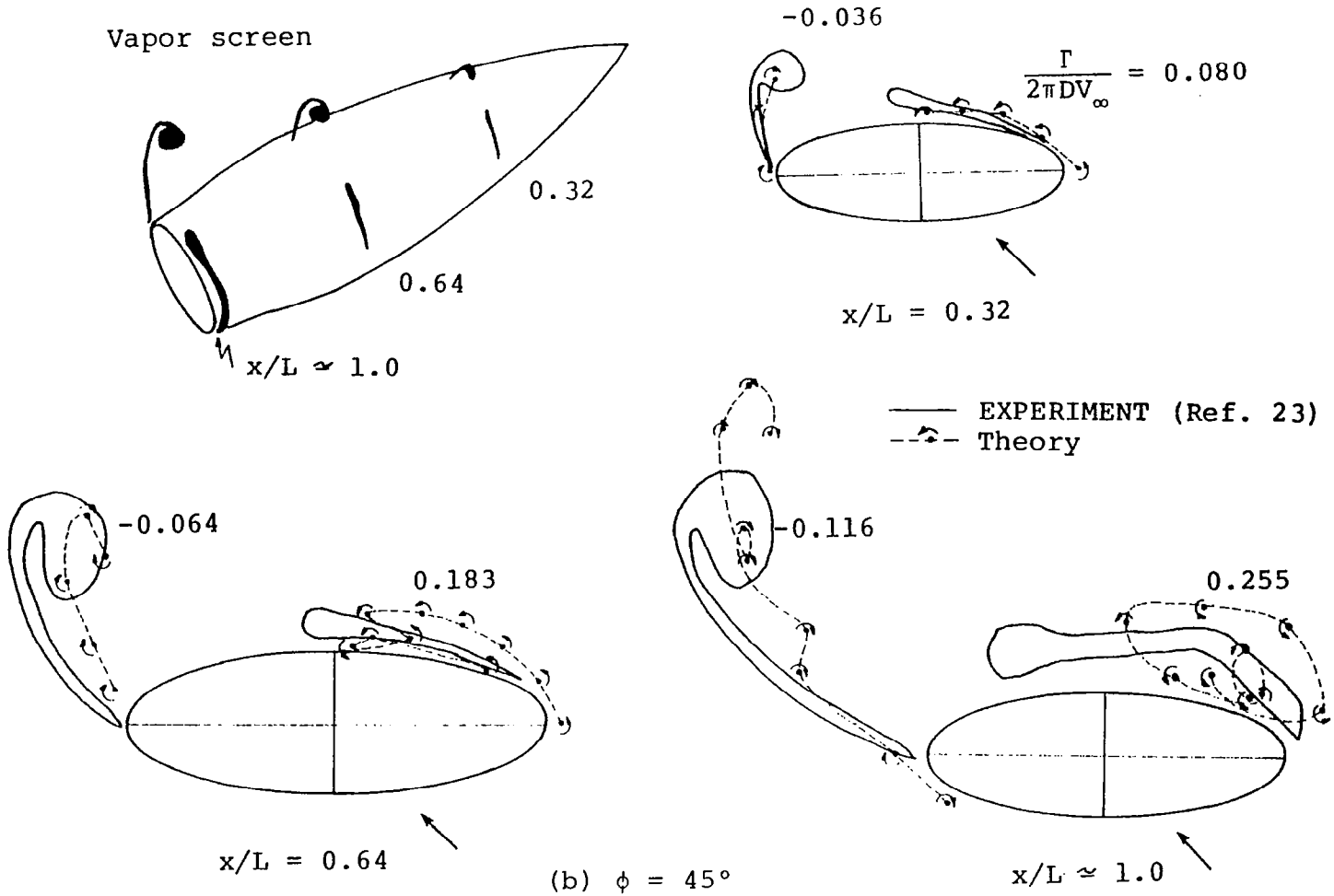

Figure 24.-Concluded.

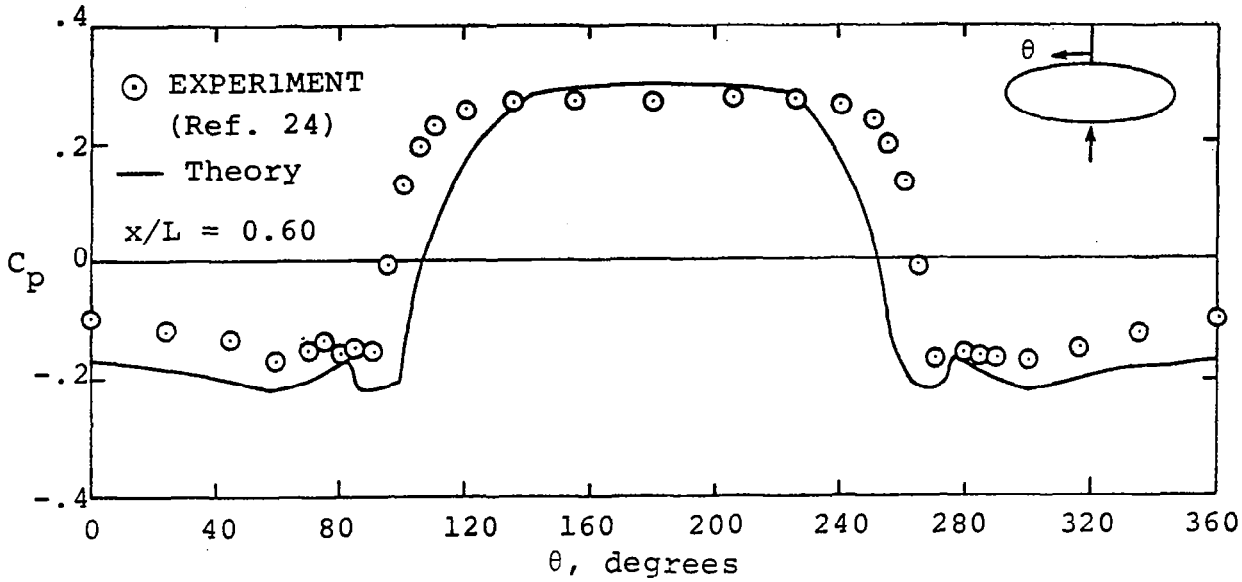

(a) $\phi = 0°$

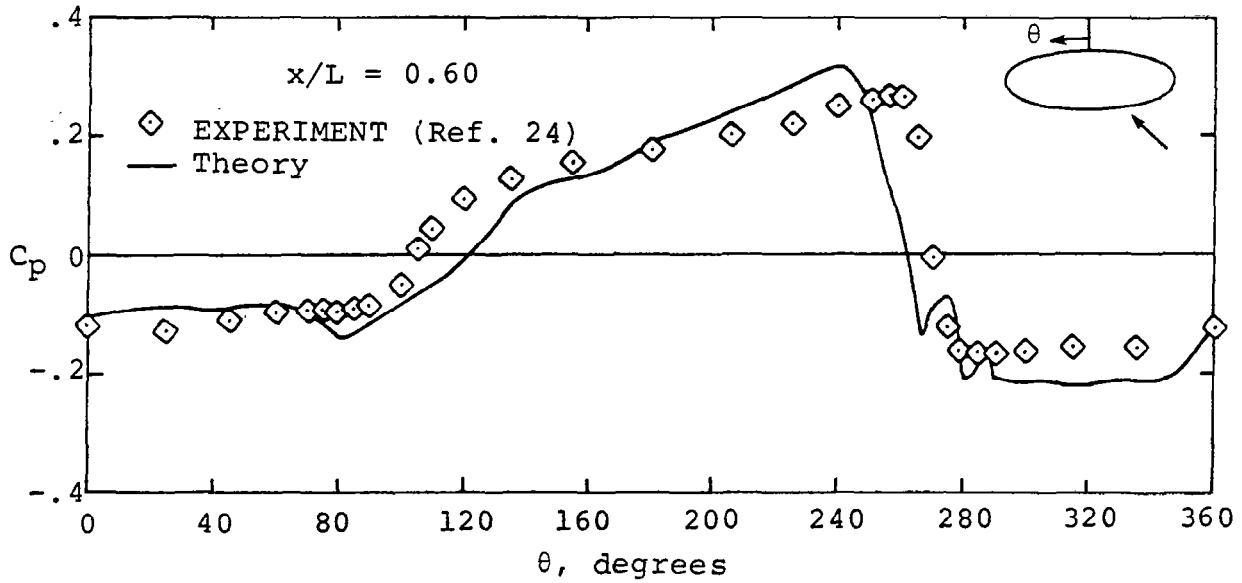

(b) $\phi = 45°$

Figure 25.- Measured and predicted circumferential distribution on a 3:1 elliptic cross section missle at $M_\infty = 2.5$, $\alpha_c = 20°$, x/L = 0.60.

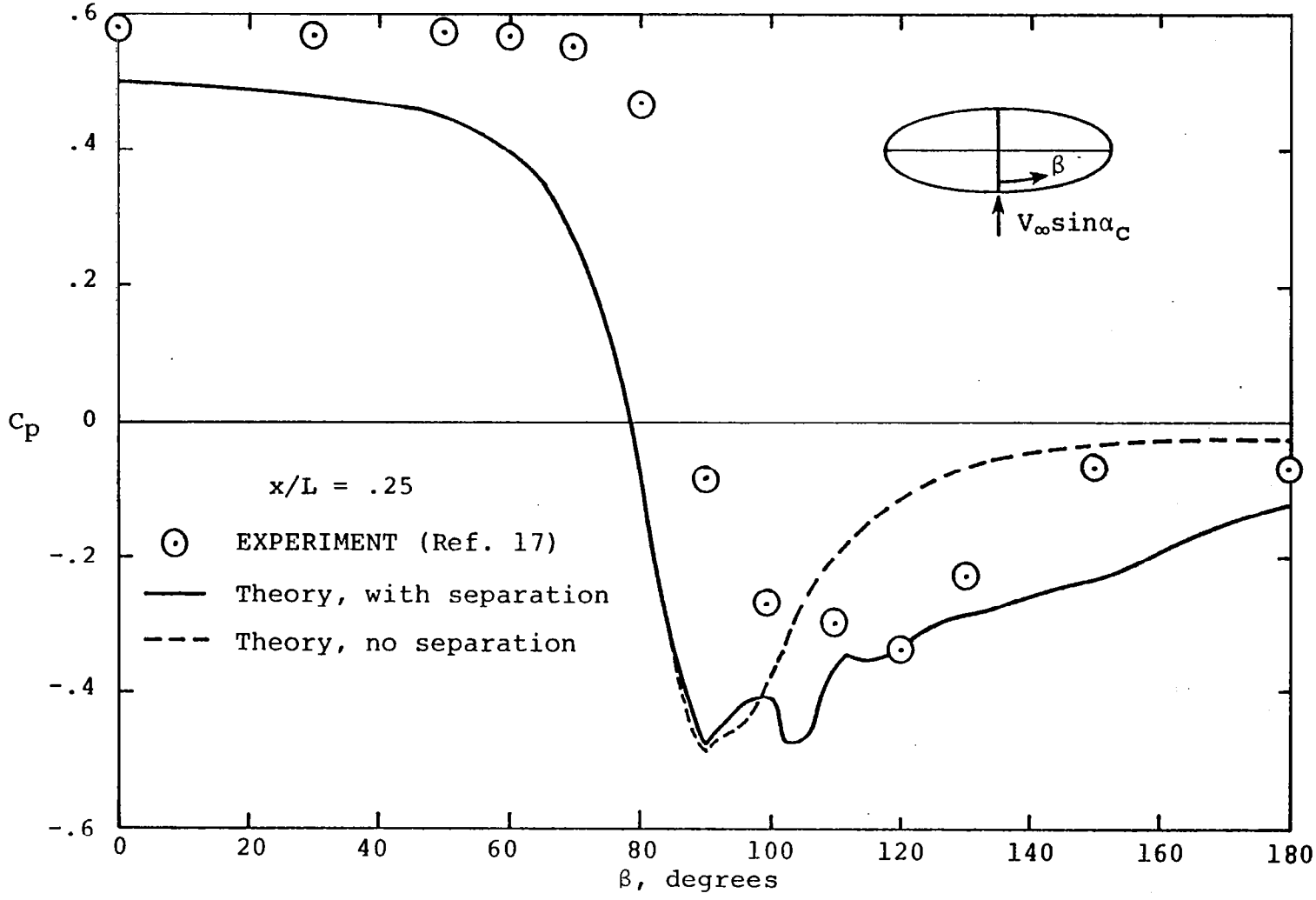

(a) x/L = 0.25

Figure 26.- Measured and predicted circumferential pressure distribution on a 3:1 elliptic cone forebody at $M_\infty = 1.7$, $\alpha_c = 20.35°$.

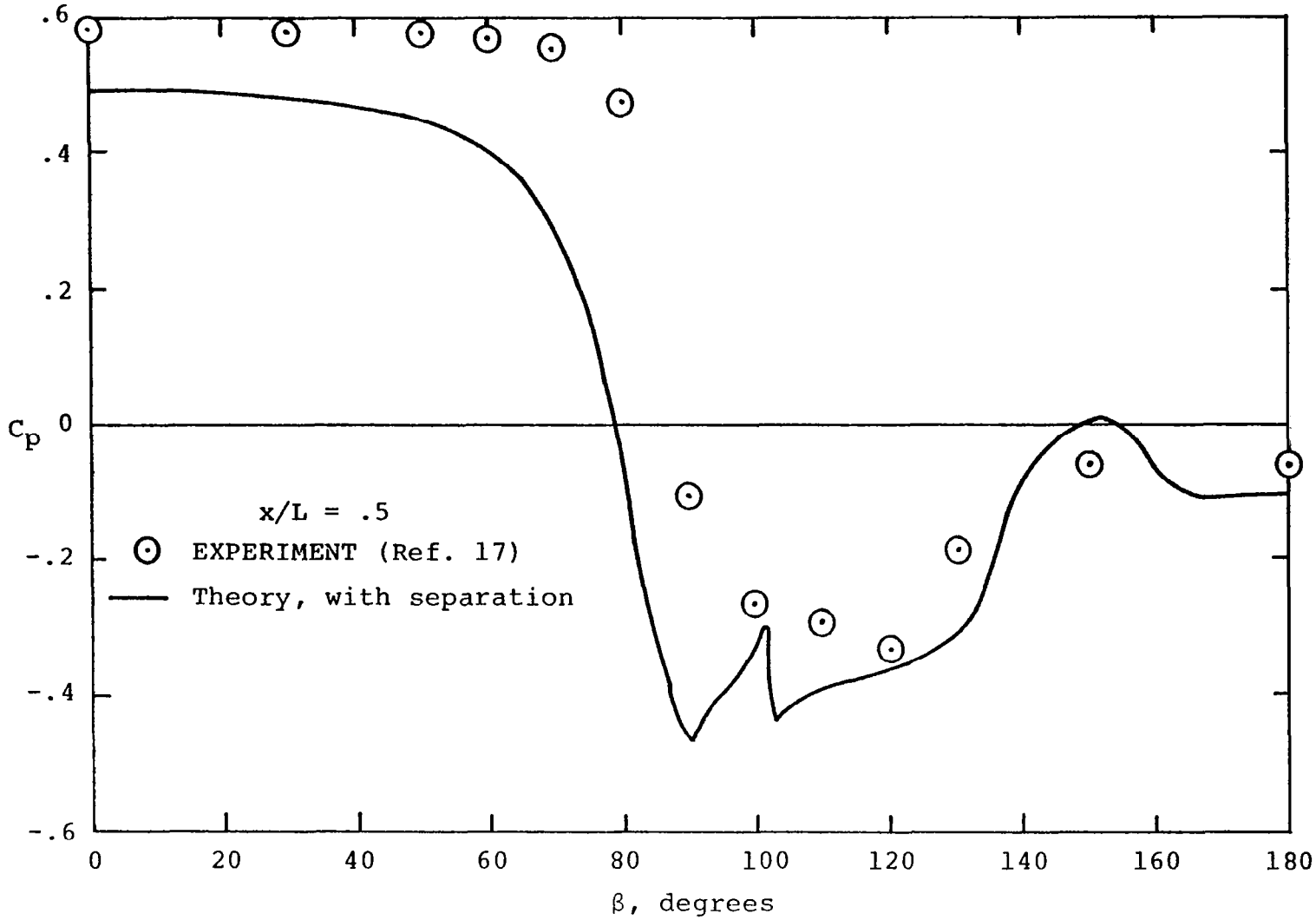

(b) x/L = 0.50

Figure 26.- Concluded.

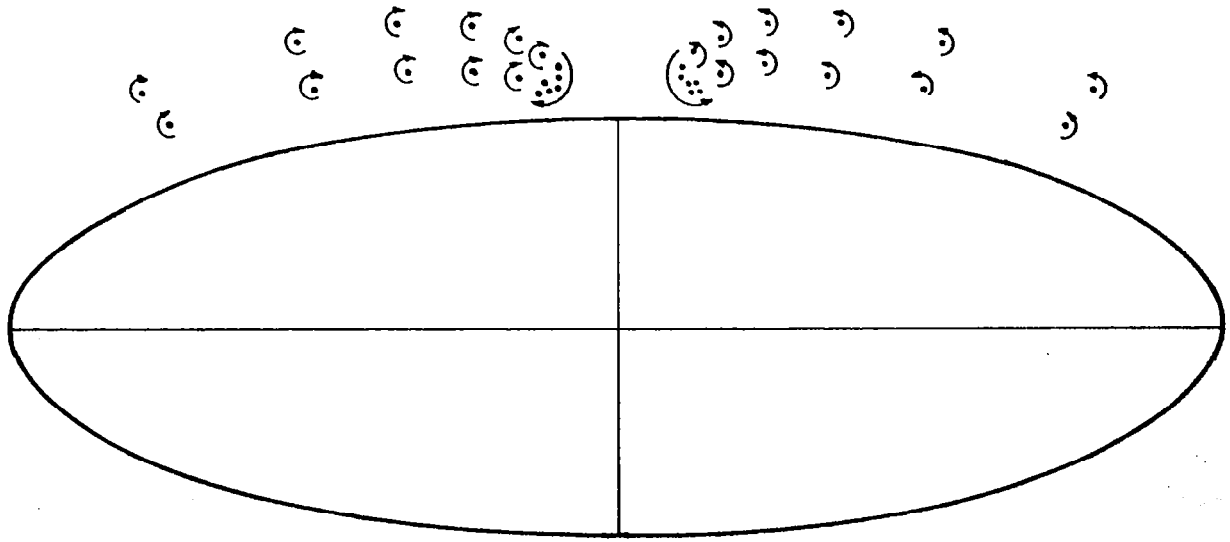

Figure 27.- Predicted vortex patterns on a 3:1 elliptic cone forebody at $M_\infty = 1.7$, $\alpha_c = 20.35°$, X/L = 0.25.

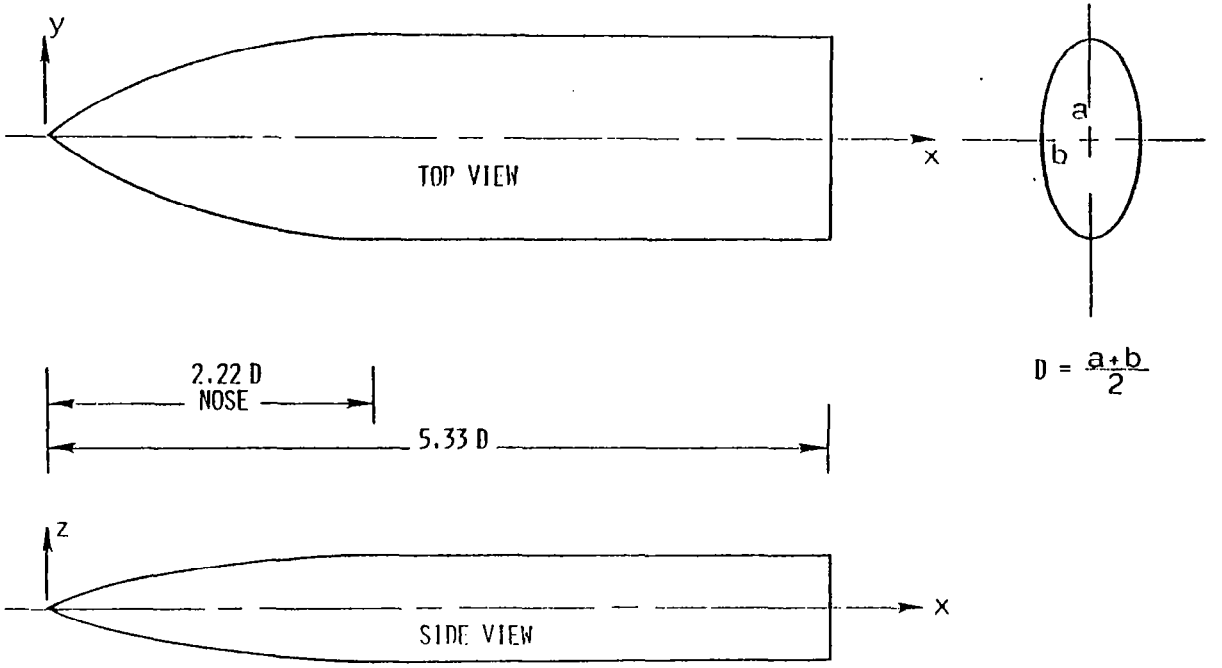

Figure 28. - 2:1 elliptic cross section body.(Reference 22)

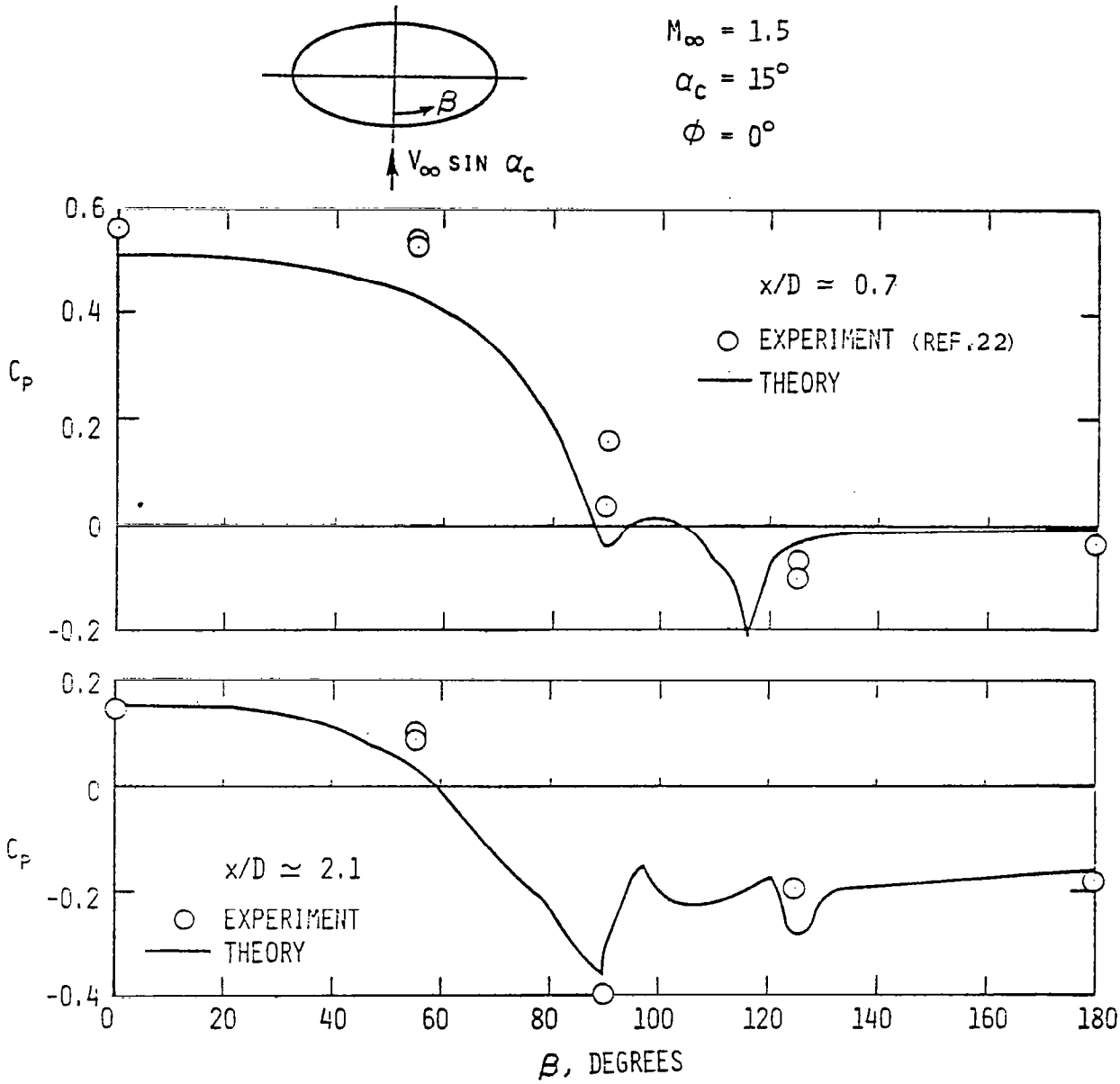

(a) ϕ = 0°

Figure 29.- Measured and predicted circumferential pressure distribution on a 2:1 elliptic cross section body at M_∞ = 1.5, α_c = 15°.

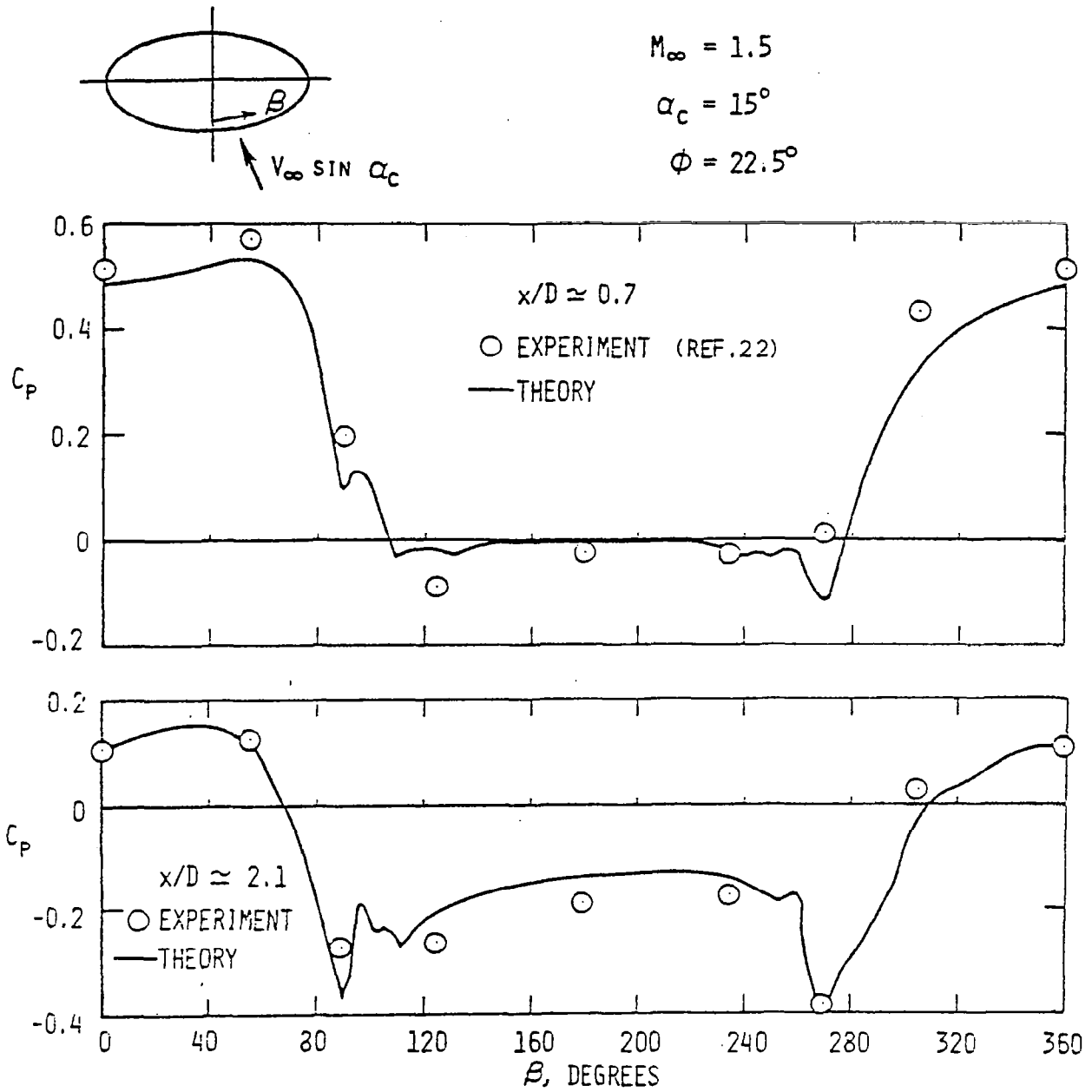

(b) $\phi = 22.5°$

Figure 29.- Continued.

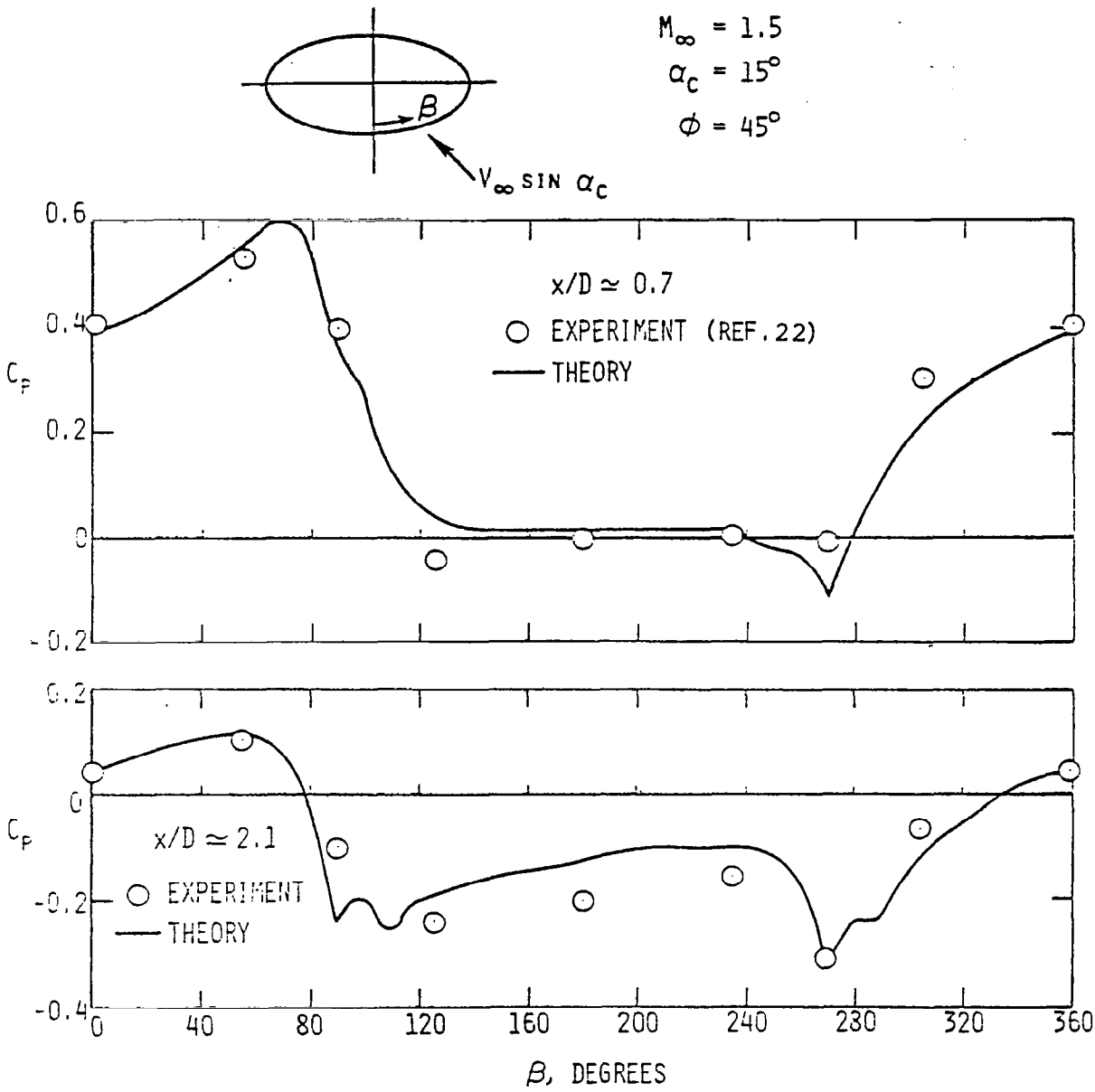

(c) ϕ = 45°

Figure 29.- Concluded.

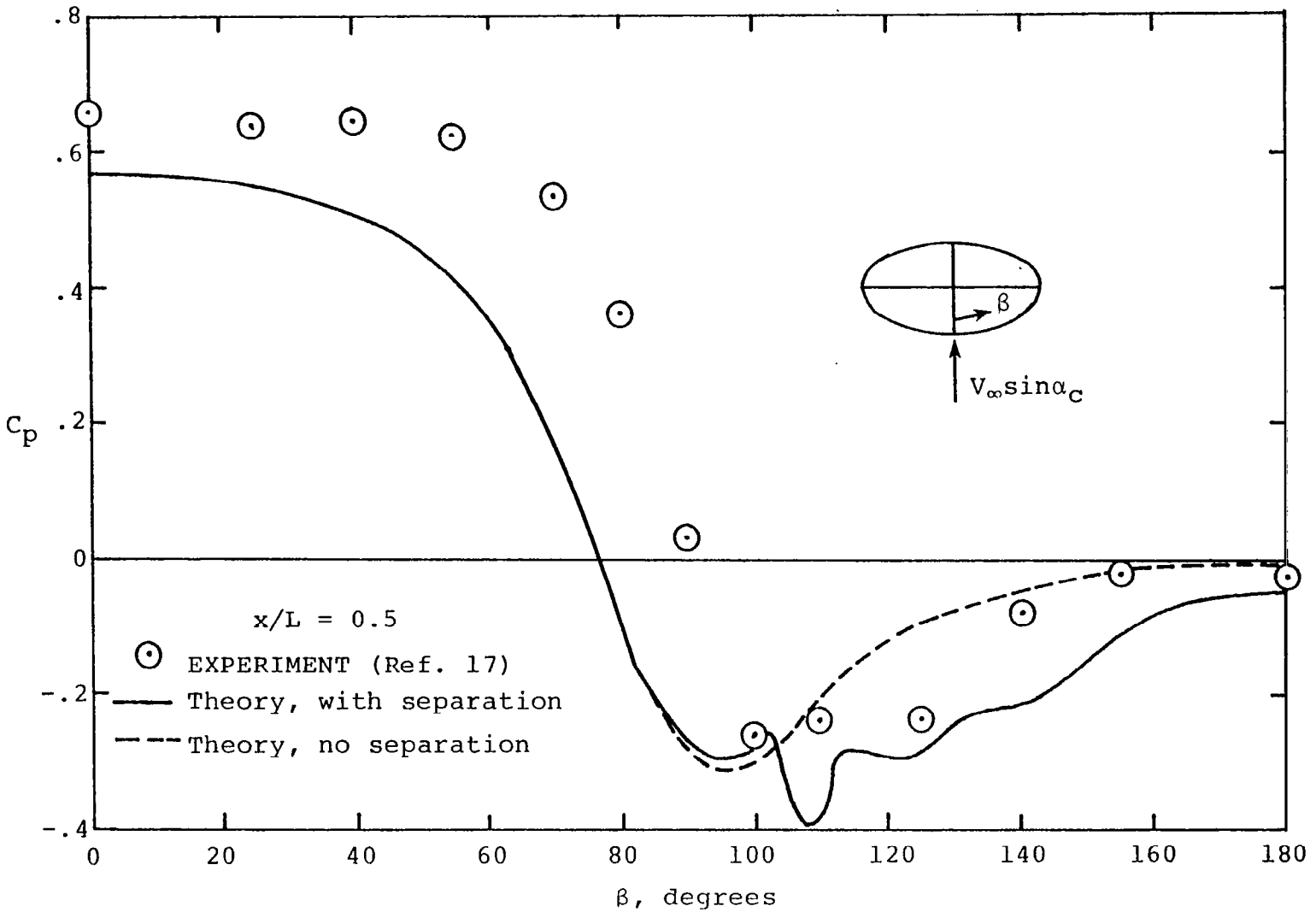

Figure 30.- Measured and predicted circumferential pressure distribution on a 2:1 elliptic cone forebody at $M_\infty = 1.7$, $\alpha_c = 20.35°$, x/L = 0.5.

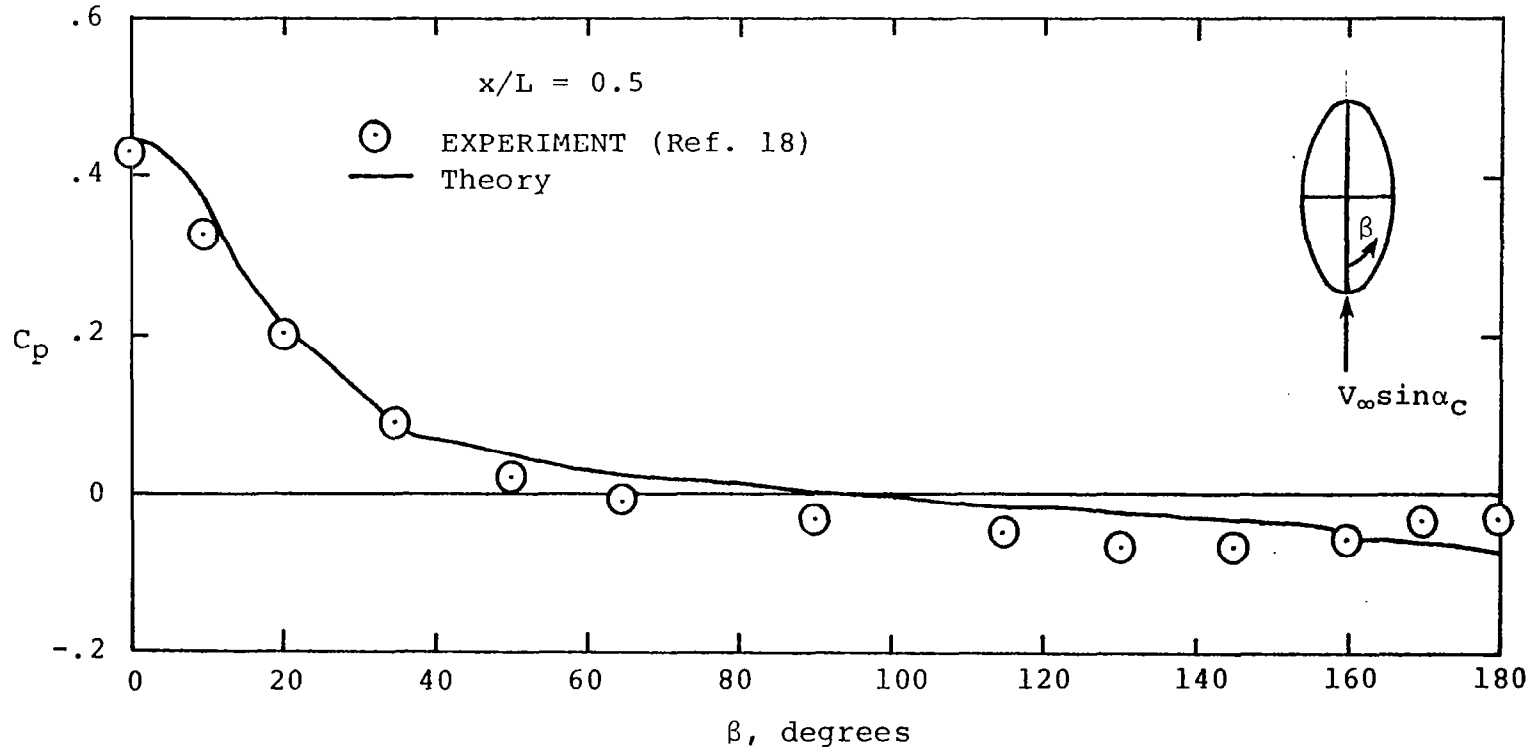

Figure 31.- Measured and predicted circumferential pressure distribution on a 2:1 elliptic forebody at $M_\infty = 1.7$, $\alpha_c = 20.36°$, x/L = 0.5.

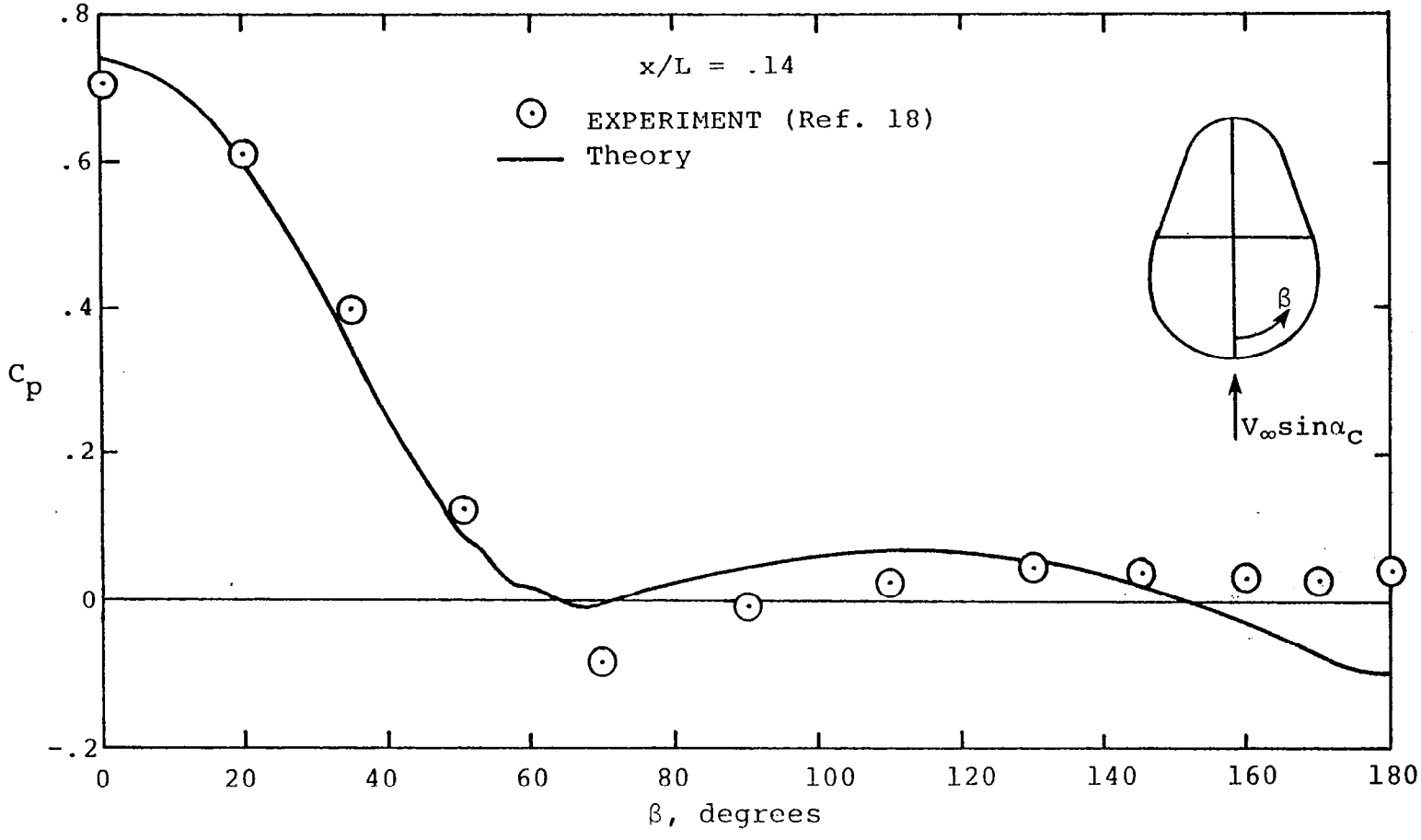

(a) x/L = .14

Figure 32.- Measured and predicted pressure distribution on a lobed cross section body at $M_\infty = 1.7$, $\alpha_c = 20.36°$.

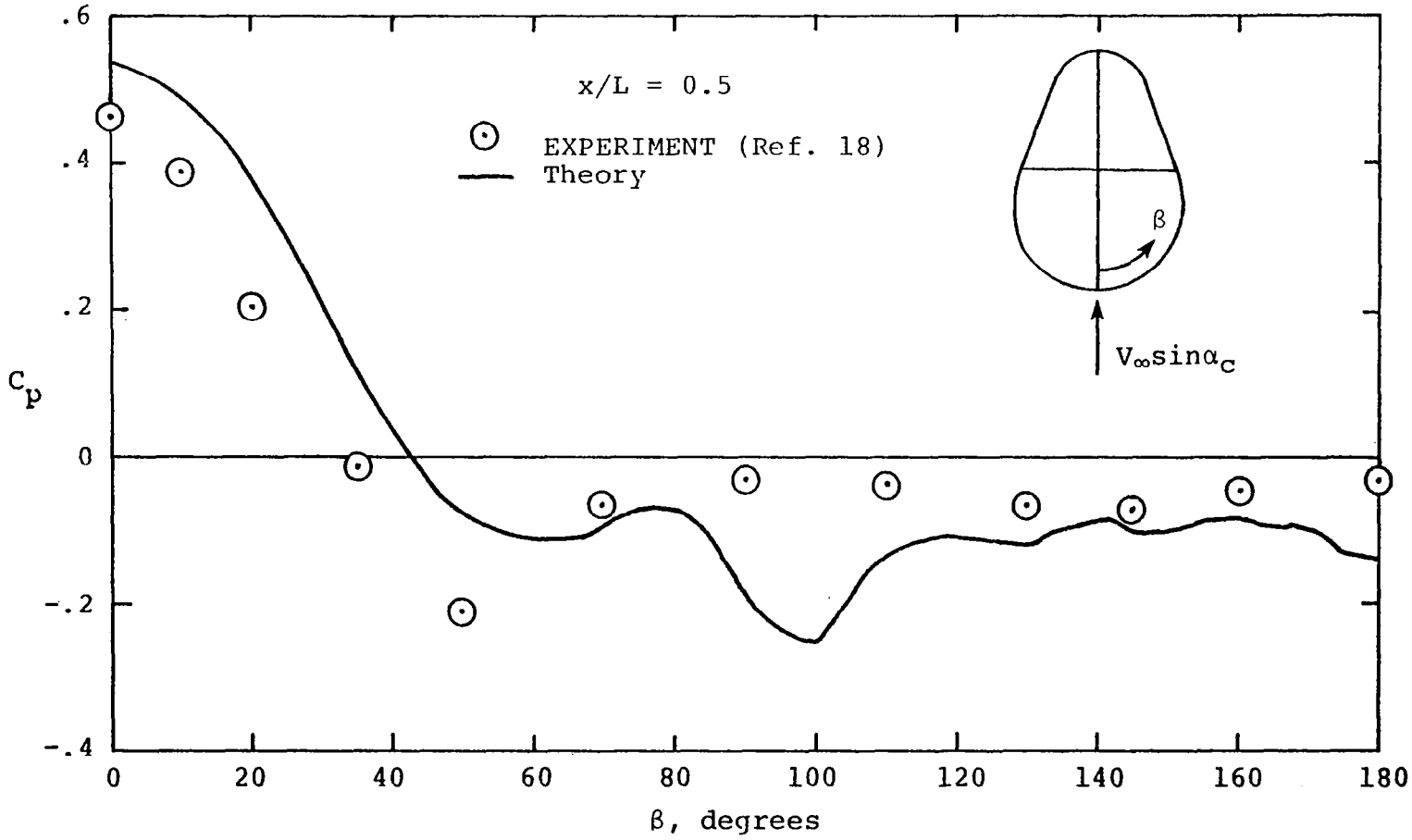

(b) x/L = .5

Figure 32.- Concluded.

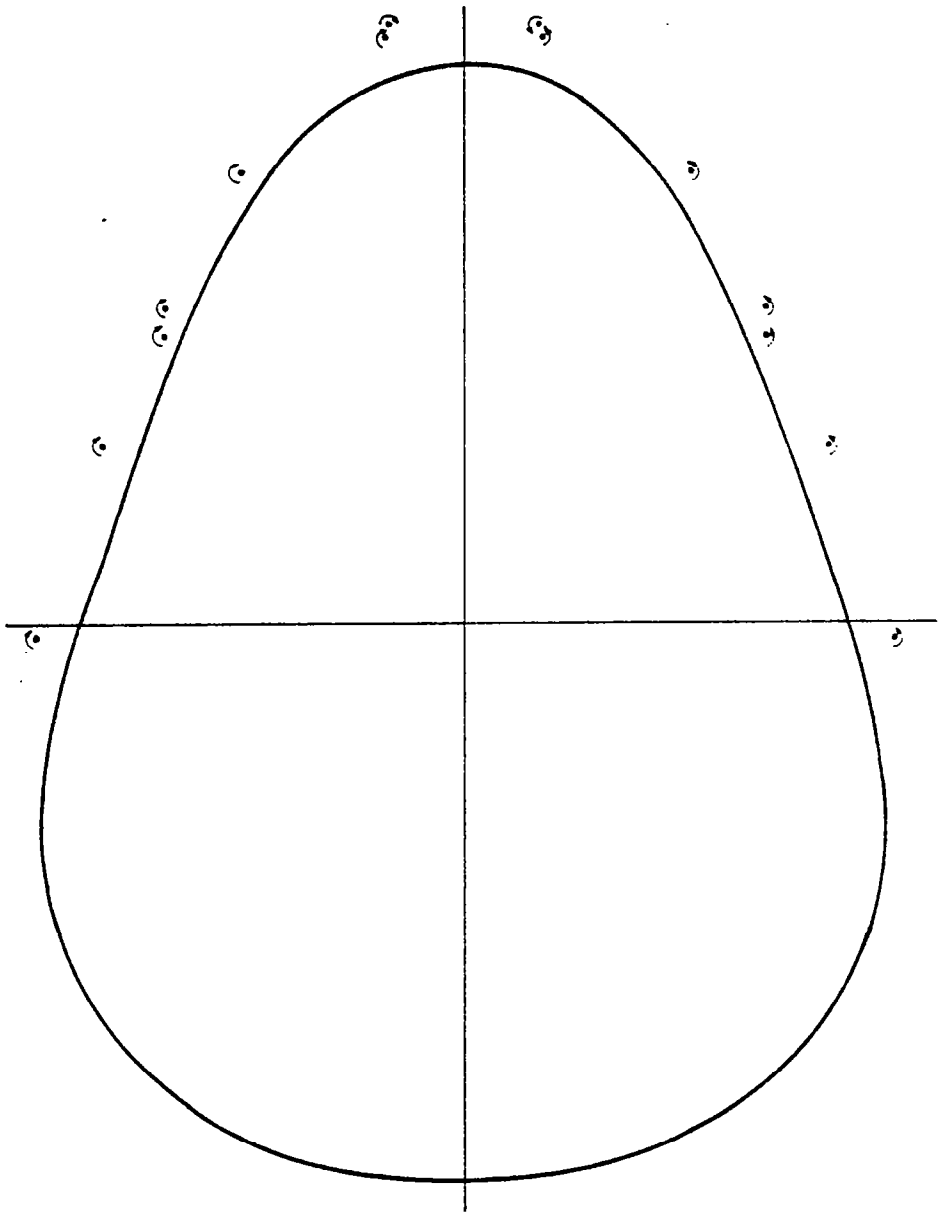

Figure 33.- Predicted vortex wake on a lobed body at $M_\infty = 1.7$, $\alpha_c = 20.36°$, $x/L = 0.50$.

1. Report No.	2. Government Accession No.	3. Recipient's Catalog No.
NASA CR-3754		

4. Title and Subtitle	5. Report Date
PREDICTION OF VORTEX SHEDDING FROM CIRCULAR AND NONCIRCULAR BODIES IN SUPERSONIC FLOW	January 1984
	6. Performing Organization Code: 815/C
7. Author(s): M. R. Mendenhall and S. C. Perkins, Jr.	8. Performing Organization Report No.: NEAR TR 307
	10. Work Unit No.
9. Performing Organization Name and Address: Nielsen Engineering & Research, Inc., 510 Clyde Avenue, Mountain View, CA 94043	11. Contract or Grant No.: NAS1-17027
	13. Type of Report and Period Covered: Contractor Report
12. Sponsoring Agency Name and Address: National Aeronautics and Space Administration, Washington, DC 20546	14. Sponsoring Agency Code

15. Supplementary Notes

Langley Technical Monitor: Jerry M. Allen
Final Report

15. Abstract

An engineering prediction method and associated computer code NOZVTX to predict nose vortex shedding from circular and noncircular bodies in supersonic flow at angles of attack and roll are presented. The body is represented by either a supersonic panel method for noncircular cross sections or line sources and doublets for circular cross sections, and the lee side vortex wake is modeled by discrete vortices in crossflow planes. The three-dimensional steady flow problem is reduced to a two-dimensional, unsteady, separated flow problem for solution. Comparison of measured and predicted surface pressure distributions, flow field surveys, and aerodynamic chararacteristics are presented for bodies with circular and noncircular cross-sectional shapes.

17. Key Words (Suggested by Author(s))	18. Distribution Statement
Supersonic Flow Vortex Shedding Elliptic Bodies Missile Aerodynamics	Unclassified - Unlimited Subject Category 02

19. Security Classif. (of this report)	20. Security Classif. (of this page)	21. No. of Pages	22. Price
Unclassified	Unclassified	200	A09

For sale by the National Technical Information Service, Springfield, Virginia 22161

☆U.S. GOVERNMENT PRINTING OFFICE:1984-739-010/47 REGION NO. 4